2016

Effect of GNSS Receiver Signal Tracking Parameters on Earthquake Monitoring Performance

Clare, Adam

UNIVERSITY OF CALGARY

Effect of GNSS Receiver Signal Tracking Parameters on Earthquake Monitoring Performance

by

Adam Clare

A THESIS

SUBMITTED TO THE FACULTY OF GRADUATE STUDIES

IN PARTIAL FULFILMENT OF THE REQUIREMENTS FOR THE

DEGREE OF MASTER OF SCIENCE

GRADUATE PROGRAM IN GEOMATICS ENGINEERING

CALGARY, ALBERTA

JULY, 2016

Abstract

This research focuses on the performance of GNSS receiver carrier phase tracking loops for earthquake monitoring systems. An earthquake was simulated using a hardware simulator; position, velocity and acceleration displacements were obtained to recreate the dynamics of the 2011 Tohoku earthquake, Japan. Using a software defined receiver, various tracking bandwidths and integration times were tested. Using the phase lock indicator and carrier-to-noise ratio as metrics, an adaptive carrier tracking loop was successfully designed and tested to maximize performance for this application. Four different simulations were done to assess the performance of the adaptive carrier tracking loop. Two simulations with carrier-to-noise ratios greater and less than 35 dB-Hz were done using the original dynamics of the 2011 Tohoku earthquake. The other two simulations tested were the dynamics of the same earthquake scaled by a factor of 10, with carrier-to-noise ratios greater and less than 35 dB-Hz.

Acknowledgements

I would like to acknowledge the following people; without whom it would not be possible to complete this work:

1. My supervisor, Gérard Lachapelle. Thank you for taking a chance and accepting me as a graduate student. Without your knowledge, advice and guidance this work would not have been possible. The opportunities you have provided, both academic and professionally are something I will always appreciate and I am truly honored being one of your graduate students.
2. My co-supervisor Tao Lin. Your knowledge and expertise in many areas have provided me with a range of skills I never thought possible.
3. My school friends: Bernhard, Kent, Laura, Jeremy, Sergey, Erin, Tori and Ivan. Thank you for all the lunch and coffee discussions. You have all helped me throughout my degree in one way or another.
4. My parents and my sister. You have supported me throughout everything I have done and I am eternally grateful for everything you have done for me.
5. My wife Michelle. You have always been by my side supporting me and with words of encouragement. Without you nothing I have done would have been possible.

Table of Contents

List of Tables

List of Figures and Illustrations

List of Symbols, Abbreviations and Nomenclature

Symbol	Definition
ACTL	Adaptive Carrier Tracking Loop
CL	Costas Loop
C/N_0	Carrier-to-Noise Ratio
DLL	Delay Lock Loop
EMS	Earthquake Monitoring Systems
FLI	Frequency Lock Indicator
FLL	Frequency Lock Loop
GNSS	Global Navigation Satellite System
GPS	Global Positioning System
LOS	Line of Sight
IMU	Inertial Measurement Unit
NCO	Numerical Controlled Oscillator
PLAN	Position Location And Navigation
PLI	Phase Lock Indicator
PLL	Phase Lock Loop
SDR	Software Defined Receiver (Radio)
SNR	Signal to Noise Ratio

Chapter One: INTRODUCTION

Research and development on the use of GNSS receivers for earthquake monitoring systems (EMS) and other high dynamic applications have been gathering much interest for the last decade. The advent of software defined receivers (SDR) is allowing for in-depth and focused research on receiver's performance in these types of application. Carrier phase measurements, which are generated using a phase lock loop (PLL), are essential for achieving the highest accuracy possible from a receiver. PLLs however suffer degradation under dynamic stress, thus maintaining high levels of accuracy during high dynamics becomes problematic. As well, PLLs usually aid delay lock loops (DLLs), which generate pseudoranges, making them one of the most important part of a GNSS receiver. This thesis focuses on the performance of PLLs for EMS and other high dynamic environments and proposes an adaptive carrier tracking loop (ACTL) for otherwise unaided receivers to maintain tracking and high levels of accuracy during high dynamics.

1.1 Background

A GNSS receiver must first replicate the incoming signals by generating a local replica of the pseudo random noise (PRN) code and carrier frequency (plus Doppler frequency) for each satellite in view. The receiver must then synchronize the local PRN and carrier frequency with the incoming signals. Synchronization of PRN codes is done using a DLL and the carrier frequency using a carrier tracking loop, typically a PLL. Synchronization accuracy depends on the design (parameters) of the tracking loops, signal characteristics and Doppler frequency. The Doppler frequency is a function of the

satellite and receiver dynamics and changes rapidly when the receiver is subject to high dynamics. In order for carrier tracking loops to be tolerant of dynamic stress, wider tracking bandwidths and short integration times are ideal. However, for better tracking performance and higher accuracy, narrower tracking bandwidths and longer integration times are preferred. This creates a conflict in the design of carrier tracking loops to be used in high dynamic applications. This research looks at adapting the carrier tracking loops to overcome this design contradiction. Difficulty arises in adapting the carrier tracking loops as an unaided receiver has little or no information of whether dynamics are being experienced or will be experienced. In this research the well-established and commonly used signal metrics phase lock indicator (PLI), frequency lock indicator (FLI) and carrier-to-noise (C/N_0) ratio are used in the decision making process on adapting the tracking loops. In most receivers, the carrier tracking loops aid the DLLs. This makes the carrier tracking loops the weakest link, making their performance of prime importance.

Using a SDR provides the flexibility of testing and evaluating various carrier tracking loop designs and easy implementation of the proposed adaptive carrier tracking loop. This research uses GSNRx (Petovello et al 2008, Lin et al 2014), a software receiver developed by the PLAN Group of the University of Calgary. Along with GSNRx, a hardware simulator (SPIRENT GSS7700) is used to simulate the required high dynamic environments.

To provide the dynamics of an earthquake, 100 Hz acceleration data was obtained for the 2011 M9.0 Tohoku earthquake, Japan (National Research Institute for Earth Science and Disaster Prevention 2015). This event was selected for the high

accelerations experienced and provides an upper limit, worst case scenario that an EMS receiver may experience. Figure 1.1 shows the map of Japan's GNSS/Seismograph earthquake monitoring system and the epicentre of the 2011 earthquake. The Fukushima nuclear disaster was a direct result of the earthquake, which had a depth of 2400 metres and peak acceleration, velocity and position displacements of 2.7 g, 91 cm/s and 3.5 m, respectively.

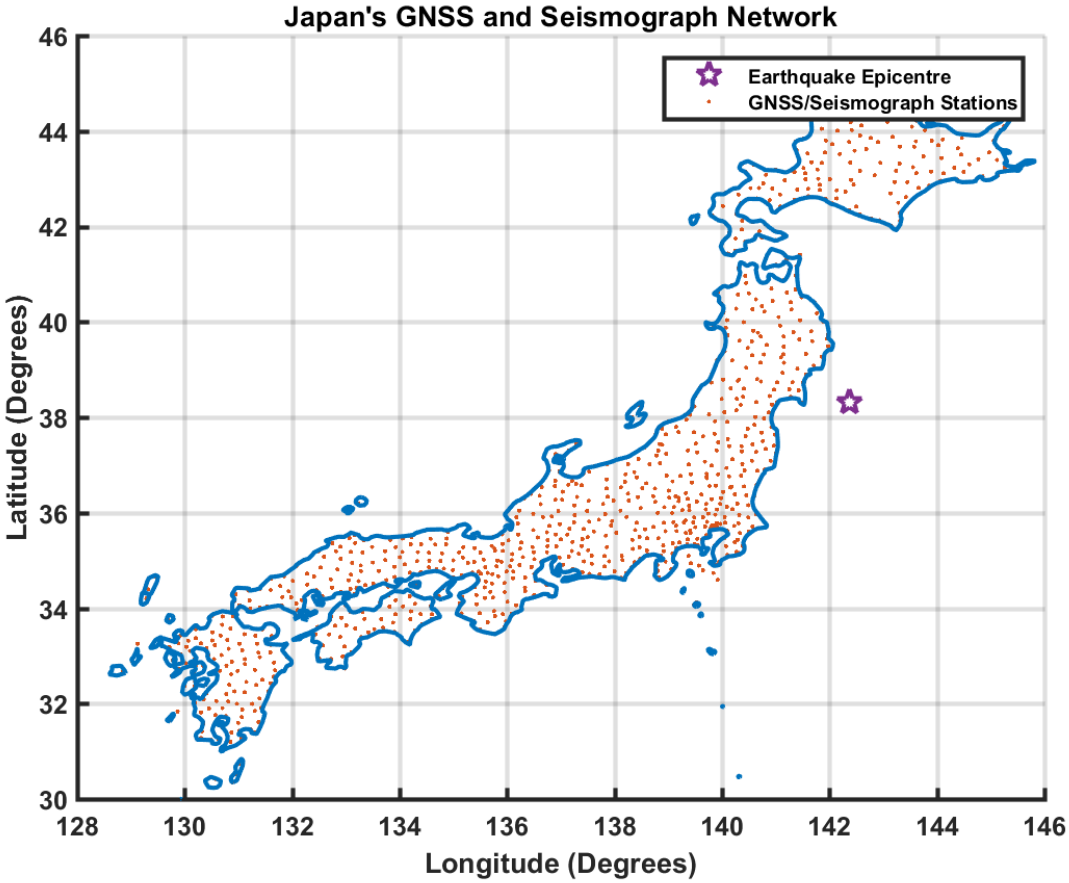

Figure 1.1 Japan's GNSS/Seismograph network

The acceleration data was integrated once to obtain the velocity changes, and integrated again to obtain the position changes. Integration was done using the software

SeismoSpect (SeismoSoft.com 2015) to correct for any integration biases and remove any drift caused by the integration. The true changes of position, velocity and acceleration in the East, North and Up directions are shown in Figure 1.2. The earthquake lasted for a total of five minutes and there is a ten-minute static period before the start. Although other derived data sets and experiments will be used throughout this research, this earthquake simulation will provide the benchmark for evaluating performance of a GNSS receiver and the proposed ACTL implemented in this research.

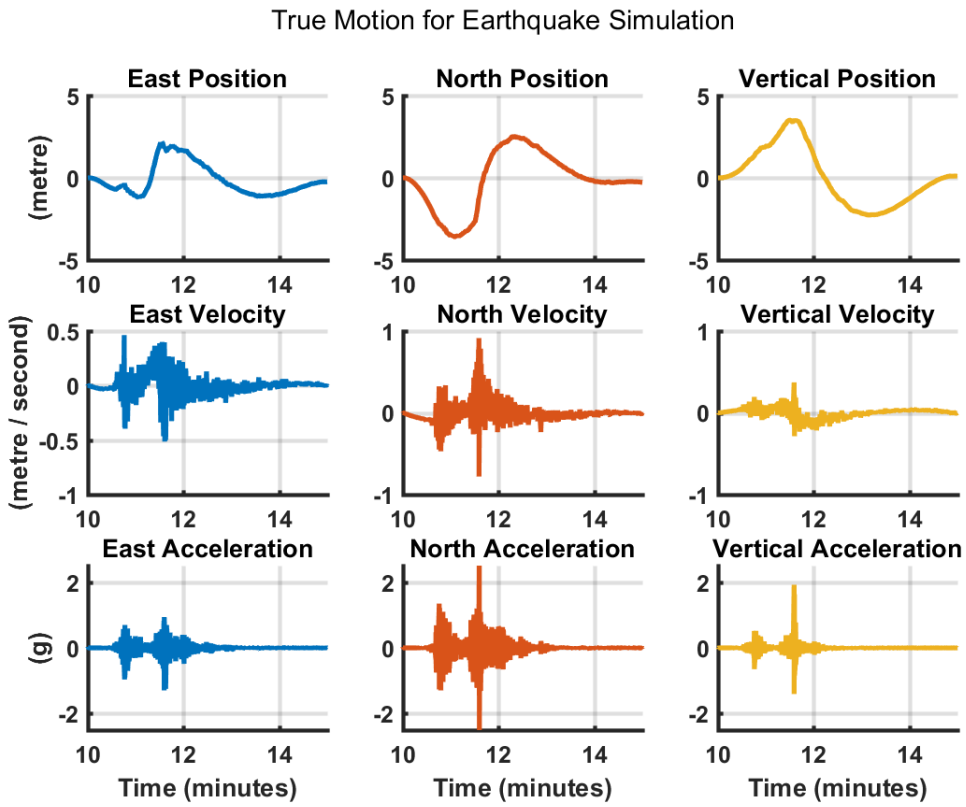

Figure 1.2 Dynamics of simulated earthquake. Obtained from integration of acceleration data during the 2011 Tohoku earthquake

Figure 1.3 shows the power spectral density of the acceleration data obtained. The power spectral density of acceleration data is useful for understanding the range of frequencies in a signal. For example, this figure shows that majority of the acceleration in the North direction is in the range of 3 to 8 Hz.

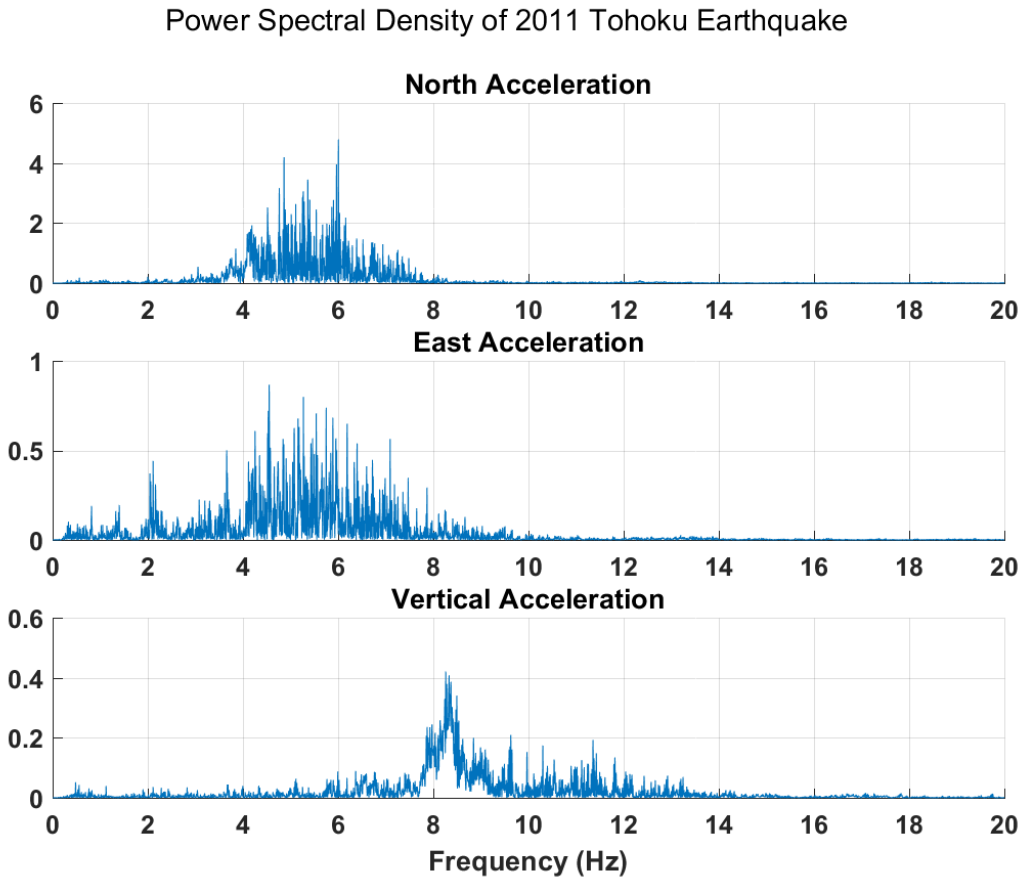

Figure 1.3 Power spectral density of acceleration data from 2011 Tohoku Earthquake

1.2 Limitations of Previous Work

The benefits and use of GNSS receivers for earthquake monitoring has been well documented during the last decade (e.g. Crowell et al 2009, 2012; Grenrich & Bock 2006, Wright et al 2012); however there has been little research focusing on the

performance of a receiver in these types of applications. Most research has been limited to the use of hardware receivers and limited testing dynamics (e.g. Haberling et al 2015; Moschas and Stiros 2015; Ebinuma and Kato 2012)

A standard approach for carrier tracking loops being used in dynamic applications is to choose a tracking bandwidth based on the worst case SNR and the largest expected dynamics. Since the carrier-to-noise ratio is inversely proportional to the tracking loop bandwidth, this method can produce sub-optimal results, especially during low dynamics.

It is well established that a frequency lock loop (FLL) or even an FLL-assisted-PLL is one way to overcome the dynamic limitations of a pure PLL (Lin et al 2014, Ward 1998). Due to the narrow FLL bandwidth of a FLL-assisted-PLL, under low dynamics the performance is comparable to a PLL. Under higher dynamics however, it switches to FLL in which case the accuracy will degrade.

External Doppler aiding from other sensors, typically an inertial measurement unit (IMU), is another method to deal with dynamic stress (e.g. Gao & Lachapelle 2008, Petovello & Lachapelle 2006). Providing the tracking loops with estimates of the dynamics, commonly referred to as ultra-tight integration, allows the tracking bandwidths to be narrower as dynamic stress information is being externally provided. However, there are some problems with this technique. Firstly, any error in estimating the dynamics will affect all tracking loops. Secondly ultra-tight methods require direct access to the receivers tracking loops. Typically, only receiver manufacturers have access to the tracking loops, making implementation reserved for manufacturers only. Lastly this method is dependent on the quality of the oscillator and additional sensor

used, higher quality sensors are typically required which increases cost significantly (Watson et al 2008).

Adapting the tracking loops using optimal techniques has also been investigated (Lian et al 2005, Wang & Song 2015). Optimal techniques attempt to estimate the signal dynamics from the phase error and then compute the optimal bandwidth based on the estimated dynamics. There are also drawbacks to these types of methods. Firstly, the phase errors from the discriminator output fluctuate due to thermal noise. This makes it difficult to obtain reliable estimates of the true phase errors, which in turn affects the estimation of signal dynamics, which then affects the bandwidth selection. Secondly, these methods assume that the cause of the phase errors is only due to noise and dynamic stress which, for most applications, is not always true. Lastly, these methods require phase error estimates over time and are iterative processes, which increases the time latency of the process.

Machine learning algorithms (fuzzy controllers or neural networks) have also been used for adapting carrier tracking loops (Kamel et al 2010, Simon & El-Sherief 1995). The disadvantages of these methods are that they are complex to implement. As well they are known as black box techniques with little information known about implementation except by the developers. These methods require much greater computational resources and typically require training sets and supervised learning techniques, adding to the implementation and application complexity.

In the majority of the research done on receiver performance for EMS and high dynamic applications, thermal noise and dynamic stress are considered the only error sources. However, carrier phase multipath is always an issue. As multipath is location

dependent, it is nearly impossible to remove its effect. It affects receiver tracking performance and, hence, position accuracy and should be considered for high accuracy applications.

1.3 Objectives and Contributions

Due to the absence of receiver performance research, specifically on carrier tracking loops, for EMS and other high dynamic applications, this thesis has the following objectives:

1. Demonstrate the strengths and limitations of carrier tracking loops for high dynamic applications and the need for adaptive tracking loops.
2. Design and implement an adaptive carrier phase tracking loop in GSNRx and analyse its merit.
3. Test and evaluate the performance of both fixed carrier tracking loops and the proposed adaptive tracking loop.
4. Compare all results from GSNRx to a commercial hardware receiver.

Several contributions are made in this research, namely:

- Demonstration of the usefulness and power of using a software defined receiver for testing and analysing the use of GNSS in real world applications.
- Analysis of the effect of carrier tracking loop design on EMS and other high dynamic applications.
- The practicality of adapting the carrier tracking loops using selected signal metrics and advantages for unaided receivers.

- Analysis of the effect of thermal noise, dynamic stress and carrier phase multipath on receiver tracking performance.

1.4 Thesis Outline

Chapter 2 reviews the fundamentals of carrier tracking loops. The major design parameters, discriminator, tracking loop bandwidth and pre-detection integration time are described. The major errors affecting carrier tracking loops, thermal noise, multipath and dynamic stress are also discussed.

Chapter 3 presents the design and implementation details, reasoning, advantages and limitations of the proposed adaptive tracking loop used in this research.

Chapter 4 presents the results and findings of carrier tracking loop performance in simulated high dynamic environments. Two different tests will be presented. First a test that recreates an earthquake and demonstrates related carrier tracking loop performance. The second test creates a trajectory with large accelerations and jerks. This test is useful for understanding the upper limit of tracking performance.

Chapter 5 presents a brief analysis of multipath effects on carrier tracking loop performance. Two tests were conducted, one in open sky conditions and a second in a high multipath environment. These tests are useful for understanding the performance of carrier tracking loops under actual multipath conditions before high dynamics are experienced, for example before an earthquake.

Chapter 6 presents the conclusions and recommendations for future work.

Chapter Two: Carrier Tracking Loop Review

Since the main focus of this work is carrier phase tracking for earthquake monitoring and other high dynamic applications, this chapter focuses on the principles of carrier phase tracking, tracking errors and signal tracking metrics.

2.1 GNSS Signals

Before describing the operation of carrier tracking loops, a brief description of GNSS signals is needed. This description is for GPS signals. However, with some small differences the concept is the same for all satellite systems (Ward et al 2006, Betz 2015). GPS signals received by a receiver are actually the modulation (combination) of three individual signals. First is the carrier signal. As the name suggests, the carrier signal carries data from satellite to receiver. Modern GPS satellites use three different broadcast frequencies, L1 = 1575.42 MHz, L2 = 1227.60 MHz and L5 = 1176.45 MHz. Depending on receiver architecture and hardware one or more carrier frequencies can be tracked. The frequency plus the induced Doppler frequency, described below, and phase of the carrier signal are tracked using carrier tracking loops.

The second signal is the pseudo-random noise (PRN) signal. The PRN signal is used as a satellite identifier, with each satellite having a different PRN signal. Tracking of the PRN signal, done with delay lock loops (DLLs), provides pseudoranges and time synchronization between receiver time and GPS time. The frequency for a L1 PRN signal is 1.023 MHz.

The third signal is the navigation data. The navigation signal is simply a binary message consisting of 1’s and -1’s. Decoding this binary message provides timing information and the satellites position and velocity, making space based navigation possible. When

a bit transition occurs, the phase of the incoming signal will change by 180°. The frequency of the navigation data is 50 Hz so bit transitions occur every 20 ms. This sets limitations on the design of carrier tracking loops, which will be described later, hence the importance of describing the GNSS signals first.

The three signals can be visualized in Figure 2.1. This figure is not to scale, however is shown for more descriptive representation of GNSS signals.

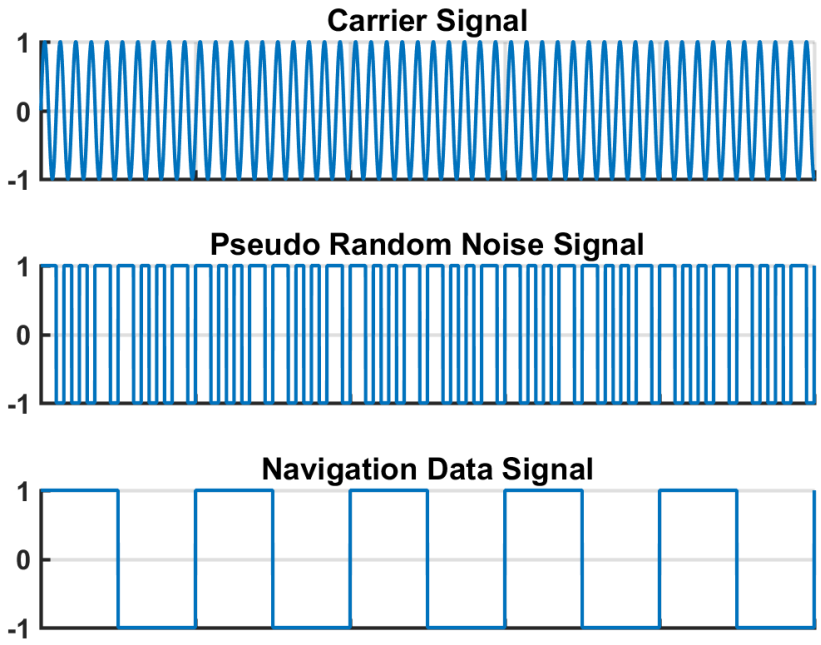

Figure 2.1 Visualization of GPS Signals

It was discussed above that carrier tracking loops are responsible for tracking the carrier frequency plus induced Doppler frequency. The induced Doppler frequency, sometimes referred to as Doppler shift, is primarily caused by the relative motion between a satellite and receiver and is therefore different for each satellite. As GNSS satellites are in motion there will always be a Doppler shift on the broadcast frequency. Because of

this shift, the perceived frequency of the incoming signal will almost never equal the broadcast frequency. The acquisition stage obtains an initial estimate of the Doppler shift. The carrier tracking loop is then responsible for tracking the Doppler shift as it changes over time.

For a static GNSS receiver, satellites located near the horizon will have the largest Doppler shift and satellites near zenith will have minimal Doppler shift. During an earthquake the receiver motion can change rapidly, creating rapid but small Doppler shifts. This effect is the greatest source of tracking error for receivers being used in EMS and high dynamic applications.

The Doppler shift is illustrated in Figure 2.2. It shows the Doppler frequency for a single satellite over time. As the satellite moves over time the Doppler shift changes. Initially there is a positive Doppler shift, causing the incoming frequency to be higher than broadcast frequency. Once the satellite passes over zenith the sign of Doppler shift changes, causing the incoming frequency to be lower than broadcast frequency. When referring to incoming signals or received frequency it will be assumed that Doppler shift is included unless stated otherwise.

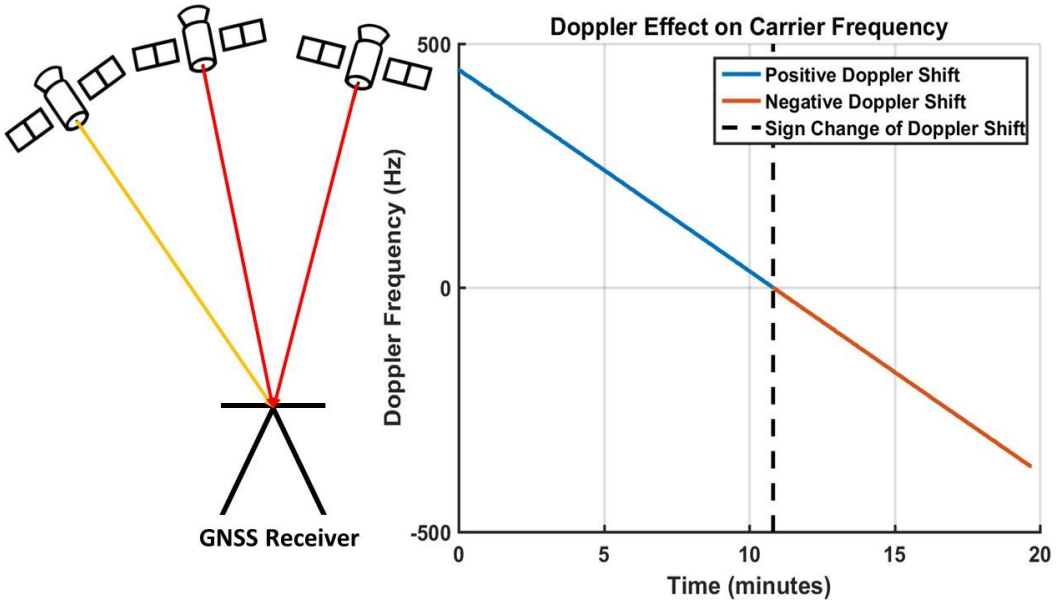

Figure 2.2 Doppler effect on frequency of received signals

In signal processing, signals are often represented by using in-phase (I) and quadrature (Q) notation, especially when dealing with modulated signals like GNSS signals. I/Q data can show the change in phase and frequency of the carrier signal. This concept is visualized in Figure 2.3. A FLL, described in Section 2.3.2.1, ensures that the change of I/Q over time for the local signal matches the change of I/Q for the incoming signal. This means both incoming and local signals are rotating at the same frequency, however there may be a phase error between the two signals. When there is zero phase error, the quadrature component is zero and the in-phase component maximum. This is the objective of a phase lock loop, as described in Section 2.3.2.2. Zero phase error also ensures zero frequency error as both signals are rotating at the same frequency. This is why a PLL is able to provide frequency information and a FLL is unable to provide phase information. This concept is mentioned here for clarity as the rest of this chapter uses I/Q notation. It is important to remember that when a navigation bit transition

occurs, the phase angle for the incoming signal I/Q data will change by 180°. The FLL or PLL must adapt for these changes.

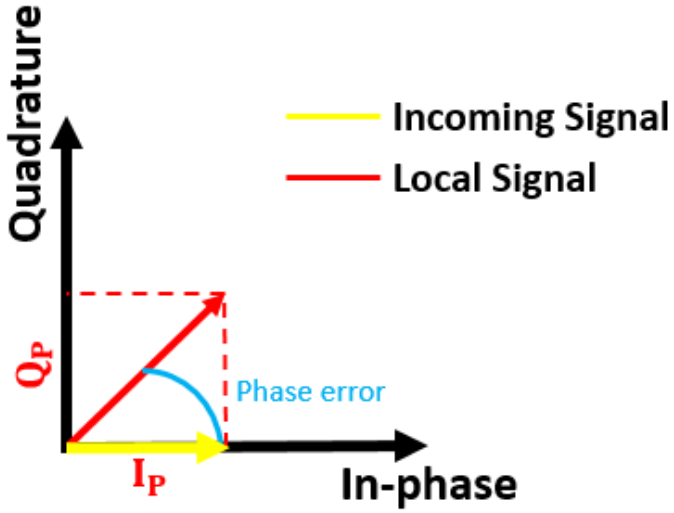

Figure 2.3 In-phase and Quadrature visualization

2.2 Preliminary Steps

The first step a receiver must complete before proceeding to carrier tracking is acquisition of the incoming signal. This is not the topic of this research and will not be discussed further, although it is important to mention that acquisition almost always occurs before carrier tracking; this is the case of EMS since receivers are permanently on. The acquisition stage provides the tracking loops with coarse estimates of the Doppler frequency and time offset between the satellite and receiver clocks. More specifically, it is the code phase that is being estimated, which is related to the timing offset. The receiver may go directly to the tracking stage if the Doppler and time offset are well known, which can occur if loss of lock has recently happened. This code phase is refined using DLLs and is commonly referred to as code tracking. Carrier tracking

loops refine the estimate of the Doppler frequency, and sometimes estimate the phase of the signal, described in more detail in Section 2.3. Although code tracking and DLLs are not the focus of this research, it is mentioned here since a typical receiver implementation has the carrier tracking loops aiding the DLLs, as described in Section 2.3.2.3. Aiding the DLLs places all the dynamic stress onto the carrier tracking loops. This makes carrier tracking loops the weakest link at the tracking level and successful carrier tracking a vital task for a receiver. As well, phase tracking can not be accomplished without code tracking. There are several additional steps a receiver must complete before acquisition and tracking. These steps are amplifying the signal, down conversion to an intermediate frequency and analog to digital conversion (Braash & Van Dierendonck 1999, Betz 2015).

2.3 Carrier Tracking Loops

The fundamental task of a carrier tracking loop is to provide an output signal, referred to as the local signal, that is equal in frequency and phase to the incoming signal. When the local signal is synchronized with the incoming signal, the phase and frequency error between both is zero. This state is typically referred to as locked state and it is in this state that the highest accuracy carrier phase measurements are obtained. This section describes how carrier tracking loops achieve this state. A high level diagram of a carrier tracking loop is shown in Figure 2.4.

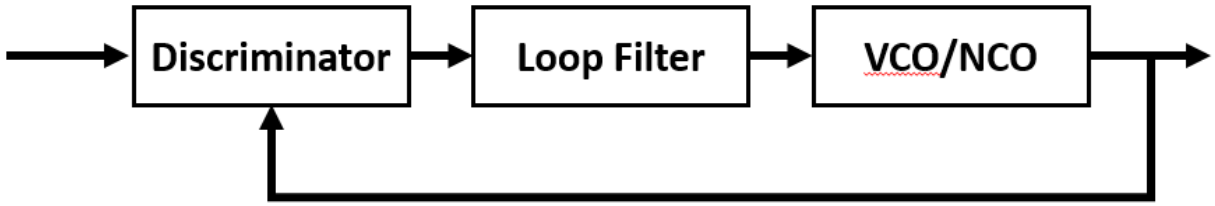

Figure 2.4 Basic Carrier Tracking Loop Design

A GNSS receiver uses a different carrier tracking loop for every satellite and frequency (L1, L2 or L5) being tracked. All tracking loops are operating in parallel. The number of tracking loops being used, sometimes referred to as channels, is dependent on the receiver hardware and architecture. This research uses a scalar based architecture; each channel is independent with no information being shared between channels. The majority of the discussion in this section refers to the singular form of carrier tracking loops and its components. However, it is important for the reader to remember there are multiple carrier tracking loops operating in parallel.

2.3.1 Numerically Controlled Oscillator

A carrier tracking loop is best explained by starting from the output of the voltage controlled oscillator (VCO) or numerically controlled oscillator (NCO). The oscillating frequency of a VCO is controlled and changed by altering the amplitude of the input voltage. Most modern receivers are being implemented in the digital domain, transitioning from the analog domain. A VCO in the digital domain is therefore called a NCO. NCOs are used to tune the frequency of the local signal to match the incoming signal. The oscillating frequency of a NCO is controlled by using past and present phase or frequency errors and estimate the phase/frequency for the next update interval

(Kazemi et al 2009, Kazemi 2010). The local signal is generated from the NCO with initial frequency being initialized from the coarse Doppler shift estimate obtained from acquisition. The local signal is passed back to the discriminator in a close loop process, as shown in Figure 2.4.

2.3.2 Carrier tracking loop discriminator

The discriminator simply finds the error between the local and incoming signal. Output of the discriminator is either the frequency or phase error between the local and incoming signal, depending on implementation. The discriminator defines the type of carrier tracking loop, namely a frequency or phase tracking loop.

2.3.2.1 Frequency Lock Loops

Frequency lock loops (FLLs) track the frequency of incoming signals. FLLs are typically used in the initial tracking stages when performing bit synchronization as it is easier to maintain frequency lock, and are less sensitive when I/Q signals overlap navigation data bit transitions. The objective of a FLL is to track the incoming frequency, so the phase will typically rotate with respect to the incoming signal. Once frequency lock has occurred the phase stops rotating. This makes navigation data demodulation difficult in a FLL since the I components may not be at maximum. Navigation data demodulation is possible when using a FLL, through a process called differential demodulation. However, FLL data detection has a much higher bit and word error rate compared to PLLs (Ward et al 2006). Discriminators used in a FLL require I/Q samples from two different instances. Under high dynamics when the frequency is changing rapidly the time between samples should be minimal to avoid loss of lock or false locks.

FLLs are unable to provide carrier phase measurements as the phase of the incoming signal is unknown. However, they still have a use in high accuracy and high dynamic applications. Under high dynamics, when the Doppler frequency is changing rapidly, a FLL is more successful than a PLL to track frequency. The use of FLLs in interference conditions (multipath or ionosphere scintillation) is also extremely useful (Lin et al 2014, Ward 1998). Because of these useful traits, a FLL is can be used in conjunction with PLLs, in a tracking loop design commonly referred to as FLL-assisted-PLL (Ward 1998). This design is explained in more detail in Section 2.3.2.3.

2.3.2.2 Phase Lock Loops and Costas Loops

As the objective of a FLL is to track the frequency of the incoming signal, the objective of a phase lock loop (PLL) or Costa Loop (CL) is to track the phase of the incoming signal. There is a distinct difference between a conventional PLL and a CL, which is the discriminator used. Both are tracking the phase of the incoming signal. However, a CL is unaffected by the navigation data modulation while a PLL is affected. PLL and CL discriminators are listed in Table 2.1 (Ward et al 2006). The distinction between a CL and a PLL is made here for completeness. In most receivers the phase tracking loops will switch between discriminators, depending on multiple factors (for example low signal power or navigation bit synchronization). As such, in this research the term PLL refers to any type of phase tracking loop.

Navigation data demodulation is easier and more successful when using a PLL compared to a FLL, assuming successful phase tracking. A PLL is able to provide the precise carrier phase measurements required for EMS. The frequency of the incoming signal is also provided when using a PLL.

Table 2.1 Comparison of discriminators and output phase errors for Phase Lock Loops and Costas Loops

Phase Lock Loop Discriminators		Costas Loop Discriminators	
Discriminator	Output Phase Error	Discriminator	Output Phase Error
$\mathrm{ATAN2}(Q_P, I_P)$	ϕ	$Q_P \times I_P$	$\sin 2\phi$
$\frac{Q_P}{\mathrm{Average}\left(\sqrt{I_P^2+Q_P^2}\right)}$	$\sin\phi$	$Q_P \times \mathrm{Sign}(I_P)$	$\sin\phi$
		$\frac{Q_P}{I_P}$	$\tan\phi$
		$\mathrm{ATAN}\left(\frac{Q_P}{I_P}\right)$	ϕ

2.3.2.3 Carrier Tracking Loop Aiding

Since carrier tracking loops (both FLLs and PLLs) are able to track the frequency of the incoming signal, this information can be used to aid the other tracking loops. Two commonly used aiding implementations are FLL or PLL-assisted-DLL and FLL-assisted-PLL.

Aiding the DLLs with the frequency information from a carrier tracking loop makes the carrier tracking loop responsible for handling any dynamic stress experienced. This allows the DLLs to use narrower tracking bandwidths and narrower chip spacing (Ward et al 2006), generating more precise pseudoranges. DLL aiding can be done with the frequency information by either a FLL or PLL, both are used in this research and are

referred to as FLL-assisted-DLL and PLL-assisted-DLL respectively. Carrier aiding is almost always done as the jitter is orders of magnitude less noisy than the code loop noise. This is why carrier tracking loops are commonly referred to as the weakest link within the receiver and makes carrier tracking one of the most important tasks for a receiver. As aiding the DLLs removes almost all of the line-of-sight (LOS) dynamics, the DLLs only track the dynamics of the ionospheric delay (Ward et al 2006).

Assisting the PLL with information from the FLL is similar to carrier tracking loops aiding the DLLs. As will be shown in Section 2.4.1 narrowing the tracking loop bandwidth reduces thermal noise. However, in Section 2.4.2 it will be shown that increasing the bandwidth is better under dynamic stress. A FLL-assisted-PLL attempts to overcome this contradiction. Using a FLL to estimate the frequency of the incoming signal, this estimate can be provided to the PLL. This places the dynamic stress on the FLL as it should, allowing the PLL bandwidth to be narrowed. There are limitations and drawbacks to using the FLL-assisted-PLL. If the dynamics are large and the FLL loses frequency lock, phase lock will likely be lost as well. As well, the carrier phase measurements from a FLL-Assisted-PLL will be noisier than the measurements from a PLL. Even a well designed FLL-assisted-PLL will be significantly less accurate than a pure PLL in high dynamics (Ward 1998). As the focus of this research is to achieve the highest accuracy possible for EMS and high dynamic applications this implementation is not used in this research.

2.3.3 Loop Filter

The objective of the loop filter is to reduce noise in the discriminator output and respond to changes in signal parameters induced by changing dynamics. Two parameters define

the loop filter, namely tracking bandwidth and loop order. These two parameters also determine the loop filters response to signal dynamics. The design of digital loop filters is well established and uses knowledge from design approaches in analog loop filters (Ward et al 2006, Betz 2015, Van Dierendonck 1995). The output of the loop filter is then passed into the NCO as shown in Figure 2.4.

The loop order determines the steady state error and sensitivity to dynamics experienced. First, second and third order loops are common loop orders in GNSS receivers and are sensitive to velocity, acceleration and jerk stress, respectively. In this research a third order loop is used. A third order loop is chosen as it is insensitive to the accelerations experienced during an earthquake. The loop order has no influence on noise performance.

The loop bandwidth is essentially a low pass filter, ignoring frequencies outside the loop bandwidth. The response to signal dynamics is inversely proportional to the loop bandwidth, wider tracking bandwidths are better for dynamic applications. The noise of the filter however is proportional to the loop bandwidth, narrower bandwidths being better for reducing noise and jitter. This creates a design contradiction for receivers being used in dynamic applications that need to be both accurate and reliable.

2.3.4 Damping Ratio and Settling Time

The carrier tracking loops operate in a closed loop process, as shown in Figure 2.4. The time it takes for a tracking loop to reach the desired value (zero phase/frequency error) is referred to as the settling time and is controlled by two parameters, namely tracking loop bandwidth and damping ratio. Figure 2.5 shows the effect of tracking bandwidth and damping ratio on the loop settling time. As can be seen in the figure, larger

damping ratios and tracking bandwidths have shorter settling times. This means they pull-in (converge) to the correct value faster. It will be shown in Chapter 4 the effect that settling time has on adaptive carrier tracking loop performance.

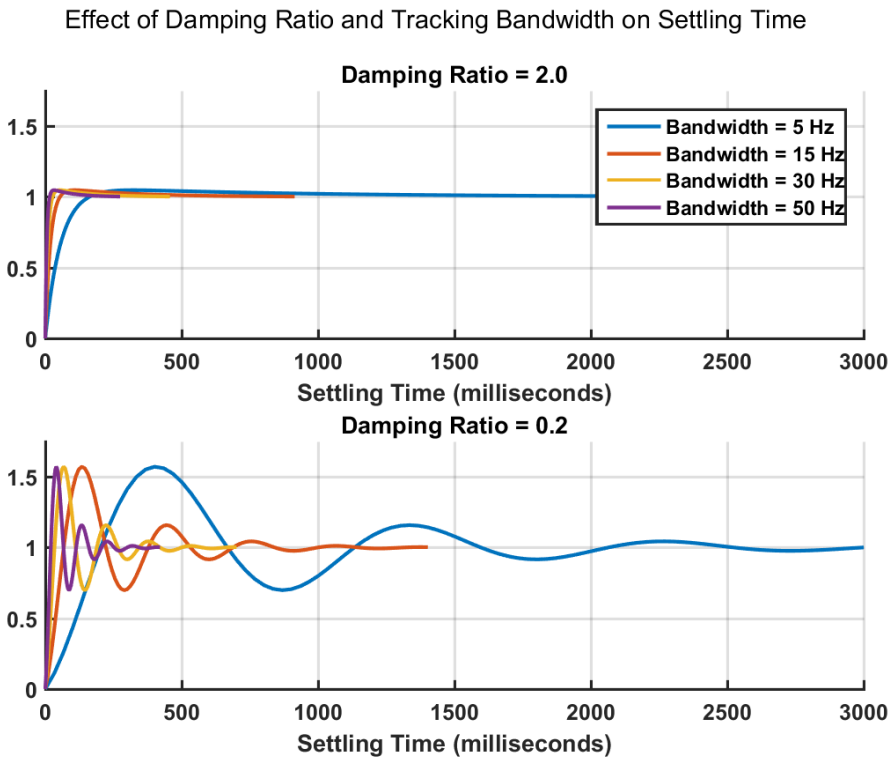

Figure 2.5 Effect of damping ratio and tracking bandwidth on loop settling time

2.4 Carrier Tracking Loop Errors

For GNSS receivers to be useful for EMS precise carrier phase measurements are needed. The errors in the carrier tracking loops will determine how precise the carrier phase measurements will be. This section outlines the dominant error sources affecting carrier phase tracking performance.

2.4.1 Phase Jitter

Phase jitter, which encompasses thermal noise, vibration and Allan deviation are the most common error sources affecting carrier tracking loop performance. Typically, thermal noise is treated as the only source of phase jitter as vibration and Allan deviation errors are often negligible. Thermal noise, in unit of degrees, can be computed as (Ward et al 2006)

$$\sigma_{noise} = \frac{360}{2\pi}\sqrt{\frac{B_n}{C/N_0}\left(1+\frac{1}{2TC/N_0}\right)} \tag{2.1}$$

where:

B_n is the tracking bandwidth (Hz)

T is the integration time (seconds)

C/N_0 is the carrier-to-noise ratio (Hz)

Narrowing B_n and increasing T will reduce the noise in the carrier tracking loops. Reducing the noise is central for earthquake detection since the noise sets the minimum detectable motion threshold and motion smaller than the noise cannot be easily detected. As well, from Equation (2.1) it is clear that the thermal noise is dependent on the C/N_0. Signals with higher C/N_0 will have lower thermal noise. The carrier-to-noise ratio is explained in Section 2.5.3. Figure 2.5 shows the thermal noise, calculated using Equation (2.1), for various tracking bandwidths and carrier-to-noise ratios. As can be seen in this figure, increasing the tracking bandwidth increases the thermal noise and stronger signals have lower thermal noise.

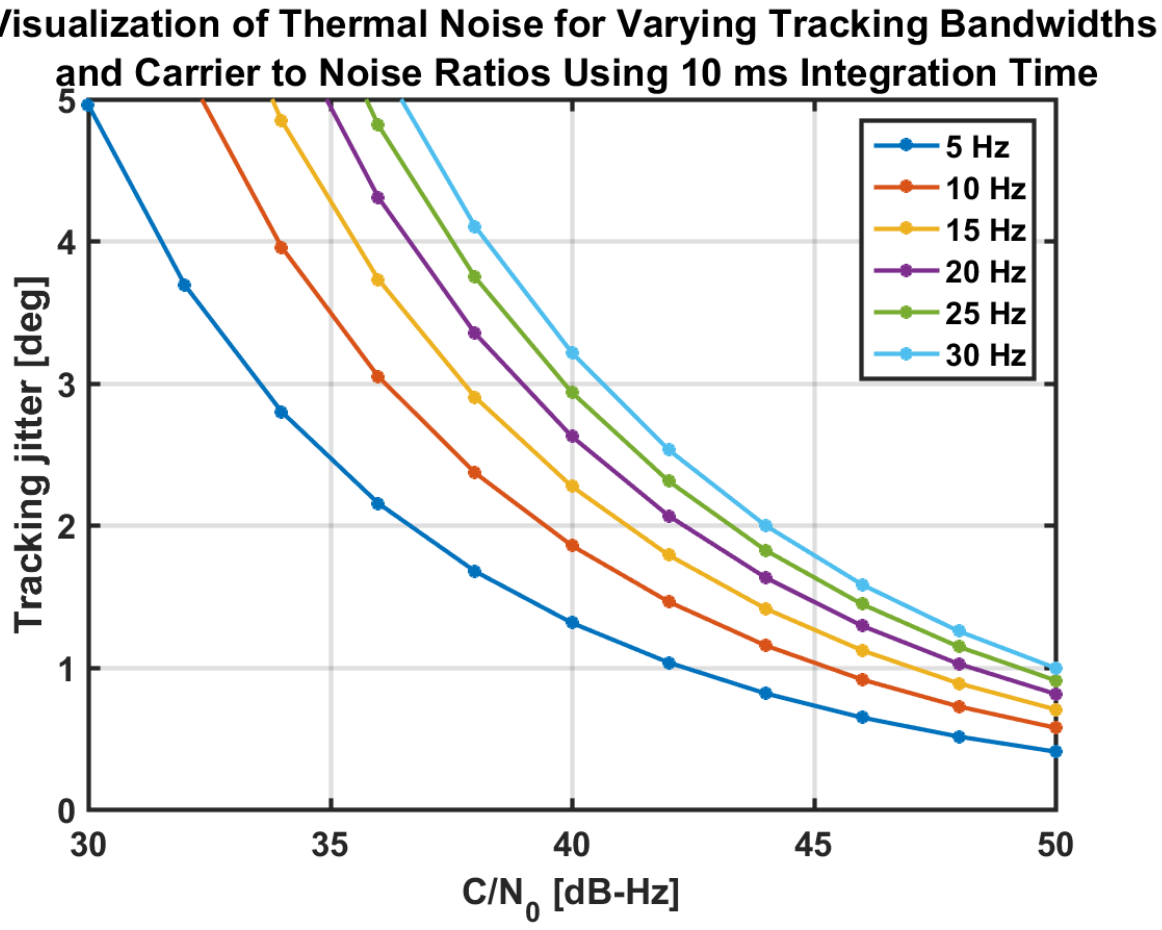

Figure 2.6 Thermal noise as a function of tracking bandwidth and carrier-to-noise ratio using an integration of 10 ms

Measuring vibration induced phase noise is a complex problem. Vibration phase noise, in degrees, can be computed from (Ward et al 2006) as

$$\sigma_{vibration} = \frac{360 f_L}{2\pi} \sqrt{\int_{f\,min}^{f\,max} S_v^2(f_m) \frac{P(f_m)}{f_m^2}\, df_m} \tag{2.2}$$

where σ_v is the 1-sigma vibration induced clock phase noise, f_L is the L-band input frequency (Hz), $S_v^2(f_m)$ is the oscillator vibration sensitivity of $\Delta f/f_L$ per g as a function of f_m, f_m is the random vibration modulation frequency (Hz) and $P(f_m)$ is the power curve of

the random vibration as a function of $f_m(G^2/Hz)$. Vibrations or accelerations on the oscillator induced from an earthquake will affect the carrier tracking performance. However, a carrier tracking loop cannot distinguish between LOS dynamics and the frequency change caused by vibrations and accelerations induced on the oscillator. Since the error is equal in all tracking channels and not geometry dependent, it can be considered part of the receiver clock error. Haberling (2015) showed that the influence of vibration and acceleration on the position solution is minimal. It should be noted that typical receivers used in EMS (geodetic grade receivers) use high quality oscillators which are less sensitive to vibrations than lower quality ones.

2.4.2 Dynamic Stress

Dynamic stress characterizes the transient response of a carrier tracking loop to a non-continuous input signal, for example a step, acceleration or jerk of input phase. As discussed in Section 2.3.3, the dynamic stress tolerance of a carrier tracking loop is dependent on the loop order. This is why third order carrier tracking loops, which are sensitive to jerk, are used here. The dynamic stress for a third order loop can be calculated using (Ward et al 2006)

$$\theta_{dynamic} = 0.4828 \frac{d^3R/dt^3}{B_n^3} \tag{2.3}$$

where d^3R/dt^3 is the maximum LOS jerk dynamics ($°/s^3$). Equation (2.3) demonstrates that increasing the tracking loop bandwidth greatly reduces the dynamic stress. Figure 2.6 visualizes how increasing the tracking loop bandwidth can greatly reduce the dynamic stress error. In the figure, 10 g/s was the maximum dynamic stress used for clarity. However, jerks of 30 g/s in an earthquake have been measured (Tong et al

2005) and the dynamics for the 2011 Tohoku earthquake used in this research have been estimated to be over 50 g/s, as will be seen in Chapter 4.

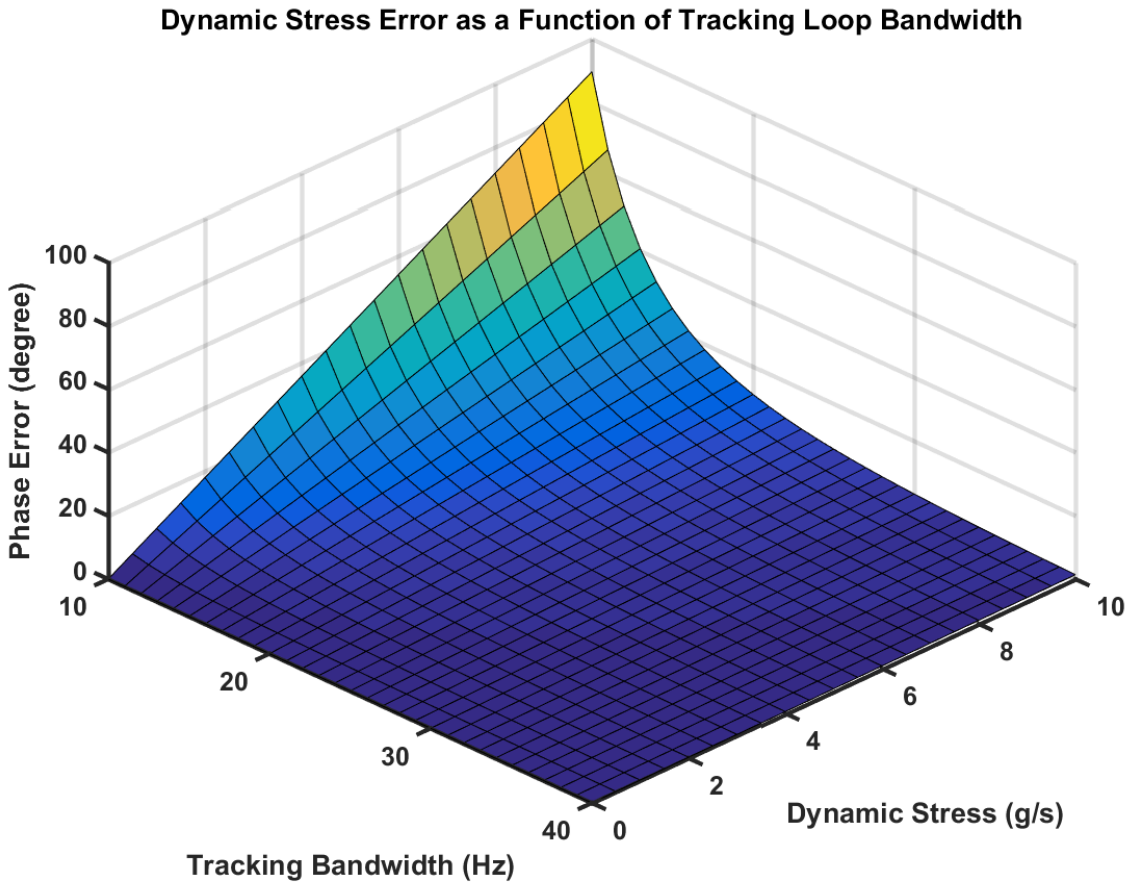

Figure 2.7 Dynamic stress error as a function of tracking bandwidth and line of sight dynamics

2.4.3 Multipath

Multipath is not typically considered an error when discussing carrier tracking loops. However, its effects can affect carrier tracking loop performance and is included here. As well, the affects of multipath that are seen in the position solution are from effects within the tracking loops. This is why multipath is included as a tracking loop error.

Multipath affects both pseudoranges and carrier phase measurements however this research is more concerned with carrier phase multipath.

Multipath is typically defined as the reception of a signal that does not arrive at the receiver through direct LOS. Nearby obstacles (buildings or trees for example) can create reflected signals, which arrive at the receiver combined with direct LOS signals. This affect will cause errors in the final position solution. Differential processing techniques, like those used in EMS, will remove and mitigate most GNSS errors. Multipath though is location dependent making it impossible to remove using a differential method. This makes multipath one of the larger error sources for high accuracy applications and EMS. Reflected signals will always be longer than the direct signal and will typically have reduced signal power compared to direct signals. The reduction of signal power is dependent on the number of reflections and the reflecting surface.

Carrier phase multipath is visualized in Figure 2.7. The direct signal will have zero phase error, assuming successful phase tracking and the reflected signal will have a different phase angle. The received signal will be the combination of both direct and reflected ones. In this figure only one reflection is occurring, however the principle is the same for multiple reflections.

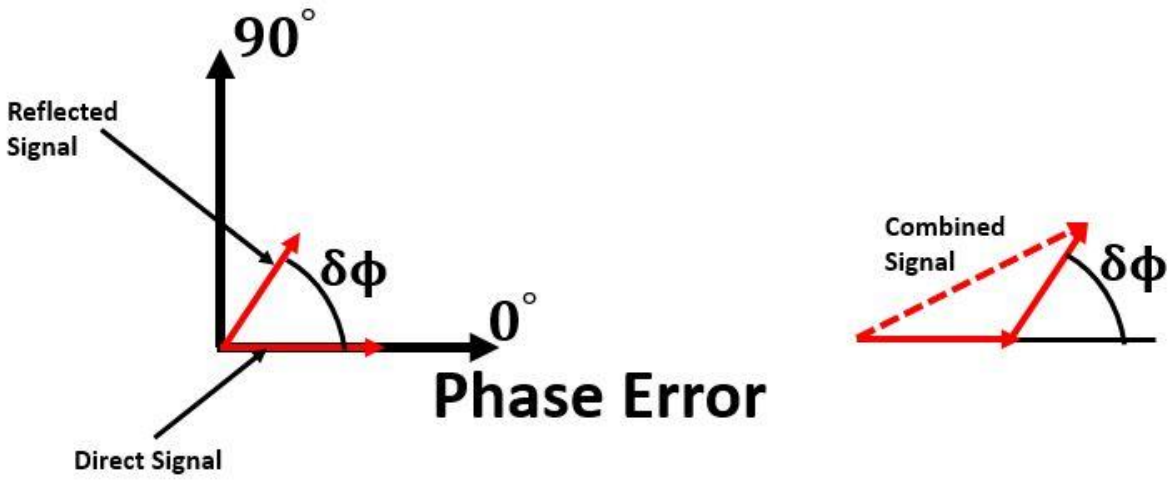

Figure 2.8 Carrier phase multipath visualization

The combined signal can be calculated by

$$\text{Combined Signal} = \sqrt{1+\alpha^2+2\alpha\cos\delta\phi} \tag{2.4}$$

$$\text{phase error} = \Phi = \tan^{-1}\left(\frac{\alpha\sin\delta\phi}{1+\alpha\cos\delta\phi}\right) \tag{2.5}$$

where α is the reflection coefficient. The theoretical maximum phase error is ¼ cycle or 90°, assuming a perfect reflector (α=1) and a phase error (δϕ) of 180°. However, this situation would result in a zero amplitude signal resulting in no signal to track.

As shown in Figure 2.8 the composite signal has a phase shift compared to the direct signal. The NCO generated carrier phase will then lock onto to the composite signal phase resulting in a phase measurement error (Ray et al 2000). This results in systematic errors in the measurements. Multipath signals are sinusoidal in nature and can be detected in the carrier phase residuals, as will be shown in Chapter 5.

Carrier phase multipath is not largely dependent on tracking loop bandwidth or integration times. However, it is dependent on the delay lock loops shown by Ray (2000). Some possible solutions to help minimize carrier phase multipath include removing satellites with low elevation angles, antenna location and antenna type (e.g. vertical response pattern, 3D chokerings).

2.5 Quality Control Parameters for Carrier Tracking Loops

To assess the quality of signal tracking some metrics are required. The most common metrics used by a GNSS receiver are the phase lock indicator, frequency lock indicator and carrier-to-noise ratio. These three metrics are explained below.

There will be an individual phase lock indicator, frequency lock indicator and carrier-to-noise ratio for every satellite and carrier frequency being tracked.

2.5.1 Phase Lock Indicator

The phase lock indicator (PLI) is a useful metric on the quality of phase tracking. The PLI can be calculated as (Van Dierendonck 1995)

$$PLI = \cos(2\delta\phi) \tag{2.6}$$

where $\delta\phi$ is the phase error from the discriminator. When the phase error is zero, the PLI will be 1, indicating successful phase tracking. Equation (2.6) is useful for analysis purposes and can also be calculated using the following:

$$PLI = \frac{I^2-Q^2}{I^2+Q^2} \tag{2.7}$$

which is equivalent to Equation (2.6) (Van Dierendonck 1995). Equation (2.7) can be interpreted as follows: when the receiver is successfully performing carrier tracking the I component of the prompt correlator is maximum and the Q component is minimum.

Figure 2.8 shows the PLI value for phase errors from 0 to 90 degrees. These results were obtained using Equation (2.6). It is clear that as the phase error starts to increase the PLI decreases. This attribute is important in the adaptive carrier tracking loop implementation described in Chapter 3. The term phase lock indicator is sometimes named phase lock detector in other literature.

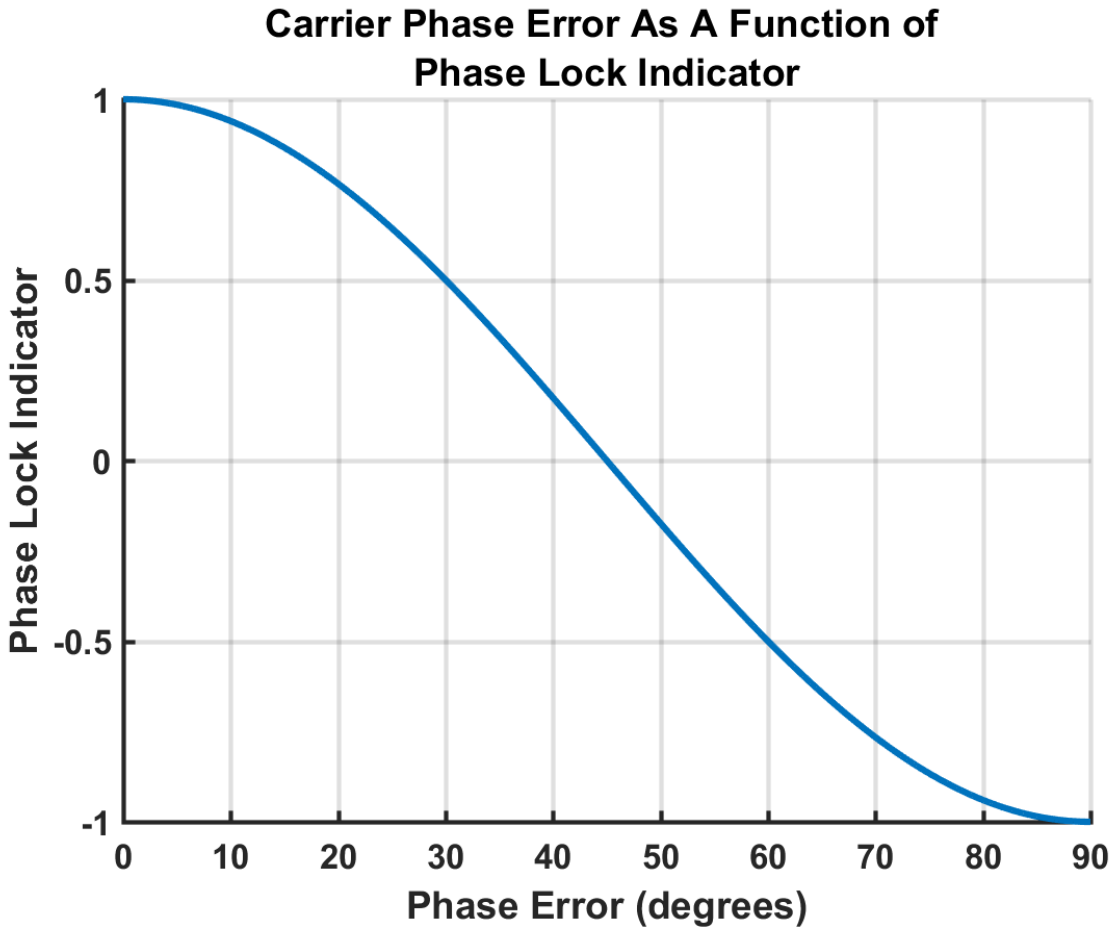

Figure 2.9 Phase lock indicator as a function of phase error

2.5.2 Frequency Lock Indicator

The frequency lock indicator (FLI) is in principle obtained by differentiating the phase error between two epochs. Therefore, correlation values (I and Q) from two epochs are required to estimate the FLI. The FLI can be calculated as (Mongrédien et al 2006)

$$\text{FLI} = \frac{\left(\text{cross}^2\text{-dot}^2\right)}{\text{cross}^2\text{+dot}^2} \tag{2.8}$$
$$\text{cross} = I_{k-1}\cdot Q_k - I_k\cdot Q_{k-1}$$
$$\text{dot} = I_{k-1}I_k + Q_{k-1}\cdot Q_k$$

A general rule of thumb for choosing the detection threshold for the frequency loss of lock is $|\delta f| > \frac{1}{4T}$, where T is the integration time in seconds (Van Dierendonck 1995).

Mongrédien et al (2006) showed that Equation (2.8) can be approximated by $\cos(4\pi\cdot\delta f\cdot T)$. Using this approximation, FLI values were calculated for frequency errors ranging from 0 to 100 Hz and for integration times of 1, 5, 10 and 20 ms. The results can be seen in Figure 2.9, which shows that shorter integration times are able to maintain frequency lock for relatively larger frequency errors. Receivers primarily tracking carrier phase (using a PLL) do not necessarily require FLIs due to frequency lock being determined by the PLI.

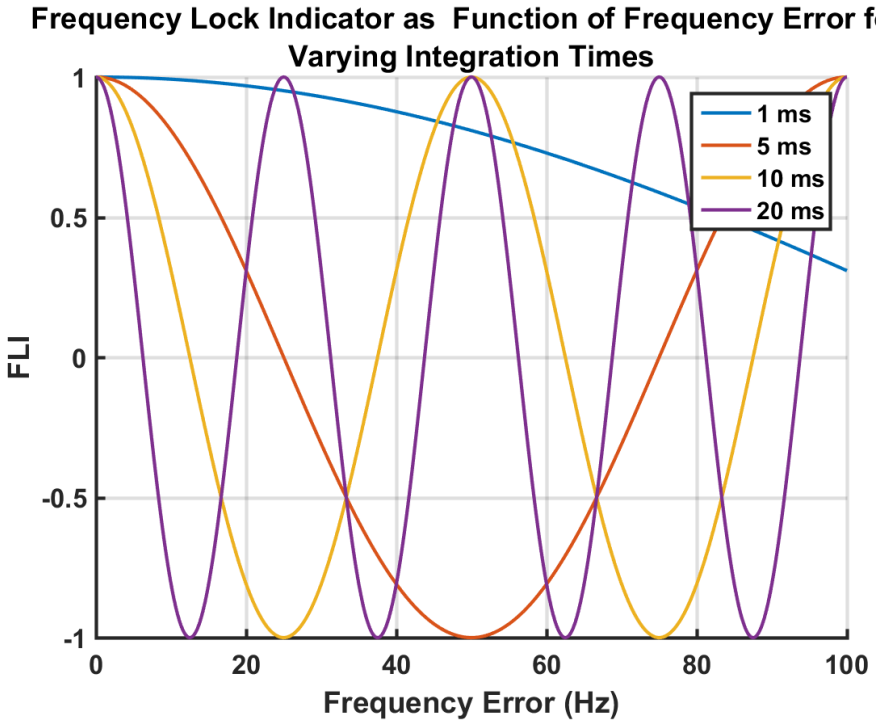

Figure 2.10 Frequency lock indicator as a function of frequency error and integration time

2.5.3 Carrier-to-Noise Ratio

The carrier-to-noise ratio (C/N_0), typically measured in units of dB-Hz (decibel-Hertz), is the ratio of received carrier power to the power spectral density of the noise. It is one of the most useful and important quality metrics used in a receiver (Misra & Enge 2011). According to Muthuraman & Borio (2010) the most widely used C/N_0 estimator uses 1 ms of correlator outputs to compute the narrow band power (NBP) over the data bit period of 20 ms. The NBP and WBP for the m^{th} data bit period can be estimated by (Van Dierendonck 1995)

$$NBP_m = \left(\sum_{k=1}^{K=20} I_k\right)_m^2 + \left(\sum_{k=1}^{K=20} Q_k\right)_m^2 \quad (2.9)$$

$$WBP_m = \left(\sum_{k=1}^{K=20} \left(I_k^2 + Q_k^2 \right) \right)_m \tag{2.10}$$

The ratio (NP) of NBP and WBP and mean of the ratio can be computed by

$$NP_m = \frac{NBP_m}{WBP_m} \tag{2.11}$$

$$\mu_{NP} = \frac{1}{M} \sum_{m=1}^{M} NP_m \tag{2.12}$$

The C/N_0 in dB-Hz can than be estimated using

$$C/N_0 = 10 \log_{10} \left(\frac{1}{T} \frac{\mu - 1}{20 - \mu} \right) \tag{2.13}$$

It is well known that C/N_0 ratios for GPS range between 35 and 50 dB-Hz for an antenna in an open sky environment.

2.5.4 Other Metrics

There are some other common metrics used to determine successful signal tracking that are mentioned here for completeness. False lock can be detected with a discrepancy between carrier and code Doppler. As well, parity can be used as a general phase lock indicator. Large carrier phase tracking errors or cycle slips can cause bit sign errors. More information on these metrics can be found in (Ward et al 2006, Van Dierendonck 1995).

2.6 Carrier Tracking Loop Design

As mentioned earlier, pre-detection integration time, tracking loop bandwidth, discriminator and loop order are what defines a carrier tracking loop. This section outlines major design criteria required when designing carrier tracking loops. As well, some common implementation methods are discussed.

2.6.1 Design Criteria

Most tracking loop filters are now implemented in the digital domain, adapted from analog filtering. In order to achieve the desired tracking loop bandwidth chosen by the designer, the product of B_nT (bandwidth and integration time) should be very small, well below unity ($B_nT \ll 1$). When this criterion is not met the true noise bandwidth will be larger than desired and eventually the loop will become unstable (Stephens & Thomas 1995).

When the navigation data bits are unknown, the pre-detection integration time should be small and the selection of discriminator should take this into consideration. If the pre-detection integration time overlaps a data bit transition, the results will be degraded and in the worst case the signal will be cancelled completely.

As discussed in Section 2.4, phase jitter and dynamic stress are the two major error sources affecting carrier tracking loop performance. The tracking loop thresholds for a PLL are (Ward et al 2006)

$$3\sigma_{PLL} = 3\sigma_{jitter} + \theta_{dynamic} \leq 45^\circ \qquad (2.14)$$

where $\theta_{dynamic}$ is the dynamic stress (Equation 2.3) and σ_{jitter} is the combined jitter from thermal noise (Equation 2.1), vibration and Allan deviation (Equation 2.2). Assuming a

third order PLL and the vibration and Allan deviation are negligible, substituting Equation (2.3) and Equation (2.1) into Equation (2.14) gives

$$\sigma_{PLL} = 3\left(\frac{360}{2\pi}\sqrt{\frac{B_n}{C/N_0}\left(1+\frac{1}{2TC/N_0}\right)}\right) + \left(0.4828\ \frac{d^3R/dt^3}{B_n^3}\right) \leq 45^\circ \tag{2.15}$$

Depending on the C/N_0 ratio, increasing the tracking loop bandwidth increases the thermal noise and jitter above the threshold in Equation (2.15). This must be considered when adapting the bandwidth to deal with dynamic stress. Equation (2.14) implies that the dynamic stress error, as per Equation (2.3), can be thought of as a bias. Therefore, to determine the three sigma tracking threshold the phase jitter, Equation (2.1), is multiplied by three.

2.6.2 Conventional Implementation Techniques

The first step of a carrier tracking loop design is typically to use a FLL. This is done since a FLL can quickly lock onto the frequency of incoming signal frequency compared to a PLL. Once frequency lock has occurred, the next step is to determine the navigation data bit. This is typically done by switching from FLL to a PLL using a Costas discriminator or a PLL using a short integration time. Once the navigation data bits have been estimated, the integration time can be increased and the transition to a pure PLL can be done. If the carrier-to-noise ratio is high and the PLI is near 1, indicating successful tracking, the tracking loop bandwidth can be narrowed to reduce thermal noise. The transition between tracking states is discussed in Chapter 3, which describes the adaptive tracking loops implemented in this research.

2.7 Summary

This chapter discussed the GNSS signal structure, signal notation and preliminary steps a receiver must complete before proceeding to carrier tracking.

For a better understanding of the tracking results provided in subsequent chapters, the operation and design of carrier tracking loops was also discussed. Furthermore, the major error sources affecting carrier tracking performance and quality control metrics were summarized. Lastly, design criteria and some conventional implementation methods were presented.

Chapter Three: Adaptive Carrier Tracking Loops

In this chapter, an adaptive carrier tracking loops is designed. First, problems associated with adapting the carrier tracking loop parameters are described. Second, the adaptive carrier tracking loop for EMS is proposed. Last a method for estimating the phase jitter in real time is described.

3.1 Limitations of Adaptive Tracking Loops

Unaided tracking loops have no information whether an earthquake is being experienced or is going to occur. Choosing a narrow bandwidth during an earthquake can cause loss of lock while choosing a wide bandwidth when static increases loop filter noise. Therefore, decision logic and thresholds are needed for choosing appropriate tracking parameters.

As discussed in Section 2.6.1 the product of bandwidth and integration time must be small to maintain loop stability. This criterion must be considered when adapting the tracking loops. As well, for a particular C/N_0 the tracking bandwidth and integration time can only be increased to a certain point before the loop becomes unstable. Both of these effects can be seen in Figure 3.1 where a PLL is simulated using SATLSim (Borio et al 2011). A tracking bandwidth of 25 Hz and integration time of 10 ms was used, resulting in $B_NT = 0.25$. Due to B_NT not being small, the actual noise bandwidth of the filter is 54 Hz. As B_NT increases the actual noise bandwidth increases. Also shown is the loop instability as the C/N_0 decreases. The C/N_0 that causes loop instability will be different for every tracking bandwidth and integration time combination. Once the C/N_0 is less than 30 dB-Hz using a tracking bandwidth of 25 Hz and integration time of 10 ms, the loop becomes unstable. Also noticeable in the figure is the loop instability point

occurring when the tracking jitter exceeds 15°, as expected from Equation (2.14) and Equation (2.15). Narrowing the bandwidth will allow tracking at lower C/N_0, at the expense of tracking performance during dynamic periods.

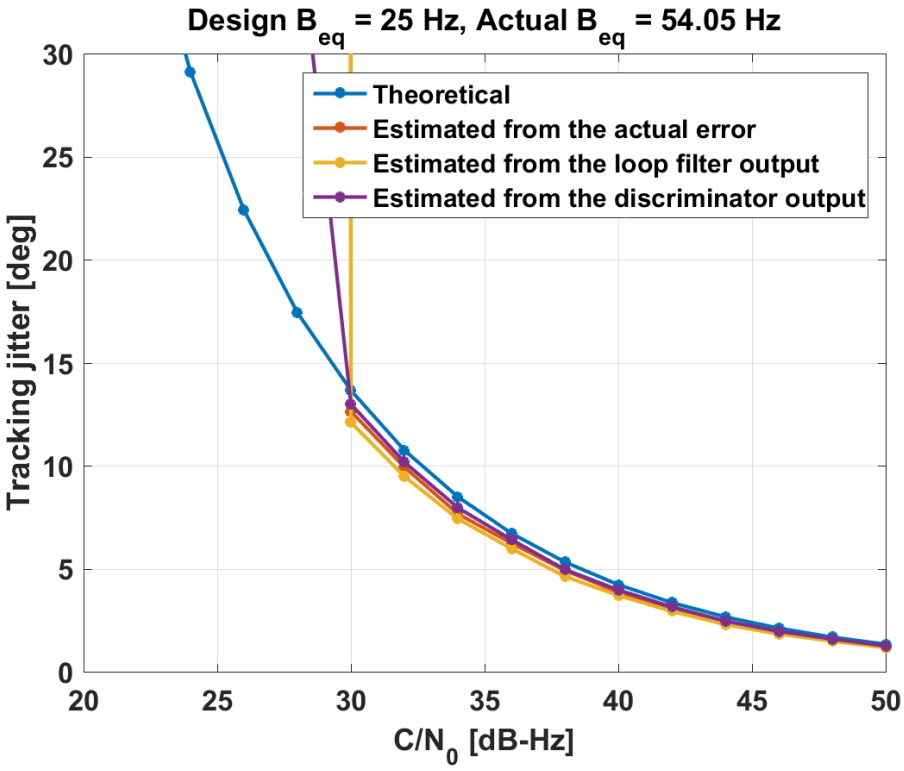

Figure 3.1 Visualization of limitations on tracking bandwidth and integration time

Adapting the tracking loop parameters will change the phase jitter, as expected. This change, if not accounted for, will also affect the position solution. In the latter each phase measurement is assigned a weight. This weight depends on the precision of the phase measurement, which is the phase jitter in Equation (2.14) and (2.15). Using a fixed precision value in the position solution can lead to either optimistic or pessimistic measurement precision. When adapting the tracking loop parameters there should be a

method to estimate the phase jitter, which can then be provided to the position solution, as explained in Section 3.2.4.

When adapting the tracking loop, the settling time must be considered. As discussed in Section 2.3.4 the settling time determines how fast the tracking loop converges to the correct solution. If the settling time of the tracking loop is ignored the tracking loop will be constantly be in transition and never reach steady state operation; this effect will be shown and discussed further in Chapter 4. The selection of the settling time creates a design contradiction on an adaptive carrier track loop. Longer settling times allows the tracking loop to converge, at the expense of possibly losing lock if dynamics occurs during this time. Shorter settling times are better at adapting under dynamic stress, at the expense of an unnecessary tracking state change.

3.2 Proposed Adaptive Carrier Tracking Loop

3.2.1 Carrier tracking loop setup

The proposed adaptive carrier tracking loop (ACTL) consists of 12 different tracking loop filters and switches between these filters. These 12 loop filters are referred to as tracking states and denoted as S_i, where i is the tracking loop filter (1 to 12). The 12 loop filter parameters and discriminators implemented are outlined in Table 3.1

Table 3.1 Adaptive tracking loop parameters

Tracking State (S_i)	Tracking Loop(s)	Bandwidth (B_n)	Integration time (T)	Loop Order
1	FLL/DLL	FLL = 8 Hz, DLL = 1.5 Hz	1 ms	2/2
2	FLL assisted DLL	FLL = 6 Hz, DLL = 1.0 Hz	1 ms	2/1
3	PLL assisted DLL	PLL = 5 Hz, DLL = 0.5 Hz	10 ms	3/1
4	PLL assisted DLL	PLL = 10 Hz, DLL = 0.5 Hz	10 ms	3/1
5	PLL assisted DLL	PLL = 15 Hz, DLL = 0.5 Hz	10 ms	3/1
6	PLL assisted DLL	PLL = 20 Hz, DLL = 0.5 Hz	5 ms	3/1
7	PLL assisted DLL	PLL = 25 Hz, DLL = 0.5 Hz	5 ms	3/1
8	PLL assisted DLL	PLL = 30 Hz, DLL = 0.5 Hz	5 ms	3/1
9	PLL assisted DLL	PLL = 35 Hz, DLL = 0.5 Hz	5 ms	3/1
10	PLL assisted DLL	PLL = 40 Hz, DLL = 0.5 Hz	1 ms	3/1
11	PLL assisted DLL	PLL = 45 Hz, DLL = 0.5 Hz	1 ms	3/1
12	PLL assisted DLL	PLL = 50 Hz, DLL = 0.5 Hz	1 ms	3/1

The tracking loops in Table 3.1 are numbered in the order of tracking stages, assuming the receiver is static and then experiences some form of dynamics. This implementation is convenient for adapting the phase tracking loops. If the bandwidth needs to be increased, the tracking state is incremented by 1 until the widest bandwidth is reached. Likewise, if the bandwidth needs to be decreased, the tracking state is reduced by 1 until the narrowest bandwidth is reached. The selection of the loop bandwidth and integration times were chosen to ensure loop stability, $B_nT \ll 1$. It is well known that 18 Hz is the maximum tracking bandwidth that can be used with an integration time of 20 ms without risking loop stability (Ward et al 2006). This combination has a B_nT value of

0.36 and was used as the benchmark when designing the tracking loops in Table 3.1 Moreover, all tracking loops have a B_nT product below 0.36. The DLL bandwidth selected in Table 3.1 could be narrowed further as the PLL is responsible for any dynamic stress experienced and the DLL is only responsible for tracking the ionosphere.

In Figure 3.3 the thermal noise increase is shown for tracking states 4 to 12 compared to tracking state 3, which is the narrowest tracking bandwidth and would have the lowest thermal noise. As can be seen in this figure, all tracking states have comparable thermal noise when the C/N_0 is greater than 35 dB-Hz. Therefore, with high signal strength there is minimal noise increase when increasing the tracking bandwidth. As well, all tracking states are stable when the C/N_0 is greater than 35 dB-Hz. This means that when the C/N_0 is greater than 35 dB-Hz the tracking state can be increased without risking loop stability. It is well known that the C/N_0 ranges between 35 and 50 dB-Hz for a GPS L1 signal with an antenna in open sky. For all these reasons the proposed ACTL is separated into two branches: non-ideal environments ($C/N_0 < 35$ dB-Hz) and ideal environments ($C/N_0 > 35$ dB-Hz), each being discussed in Section 3.2.3.2 and Section 3.2.3.3, respectively.

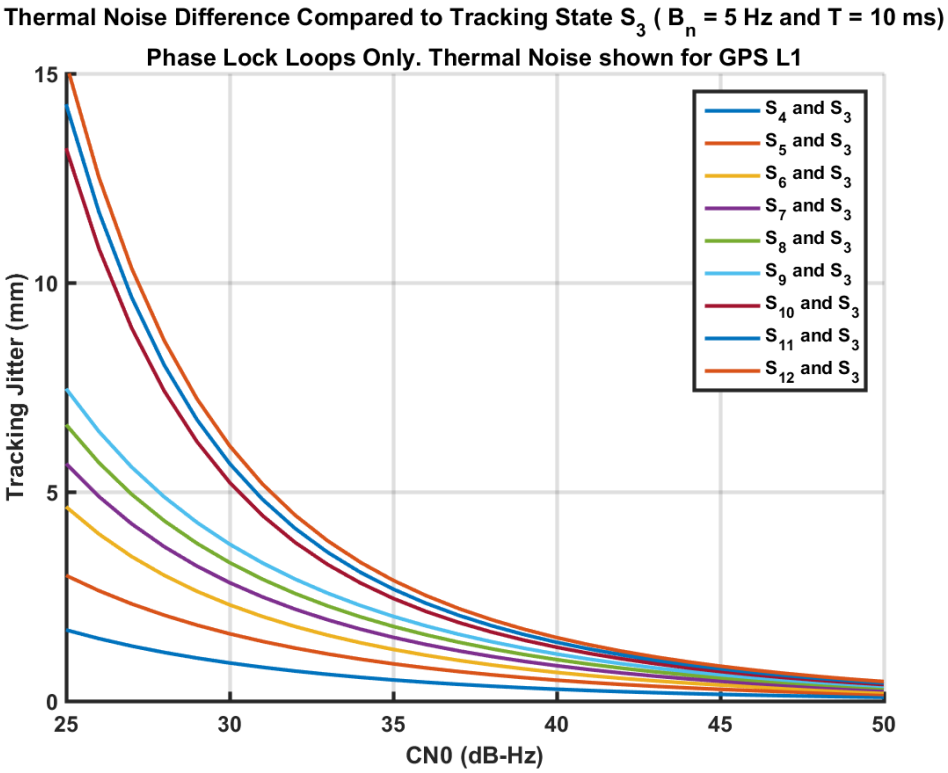

Figure 3.2 Differences in thermal noise for implemented tracking states

In this research a settling time of 0.03 seconds was used for each tracking state. This value was chosen so each tracking state had sufficient time to recover, however short enough if any larger dynamics are experienced. The effect of settling time on tracking performance will be shown in Chapter 4.

3.2.2 Initial Tracking Stages

The initial tracking stages for the ACTL are similar to the steps described in Section 2.6.2. A flow chart for the decision logic of the ACTL can be seen in Figure 3.3. Initially the tracking loop starts with a DLL and wide tracking bandwidth FLL. The FLL will switch to a PLL once the FLI is above 0.90 and has maintained frequency tracking for a minimum of ten seconds. From Figure 2.9, a FLI of 0.90 corresponds to only a few Hz of

frequency error. If at any time during the 10 second window the FLI drops below 0.90, the timer is reset. This is done to ensure successful frequency tracking before moving to a PLL. A drop in FLI in the initial tracking stages is usually an indicator of false lock. If the FLI and time criteria is met, the tracking loop will change to a PLL.

3.2.3 Tracking in Phase Lock Loops

3.2.3.1 Bit Sync and Initial Phase Tracking

Once the tracking loop has transitioned from FLL to PLL the phase and navigation data bits must be determined. Wider tracking bandwidths are ideal for quick phase pull-in. Shorter integration times are preferred for determining the navigation data bit to avoid bit transitions. For these reasons, the initial PLL tracking loop uses a bandwidth of 25 Hz and integration time of 5 ms ($S_i = 7$). There are two exceptions implemented in the ACTL. First, if all other satellites currently being tracked are using larger tracking bandwidths, the initial PLL will choose the largest bandwidth, denoted as S_{max} in Figure 3.3. The assumption here is that the receiver is currently undergoing some dynamics. This situation would occur if a new satellite comes into view during a dynamic period. All other satellites being tracked would have adapted their tracking loops to account for these dynamics. For example, if GPS PRN 20 comes into view and all other satellites being tracked are in tracking state nine, it is likely that dynamics are being experienced so PRN 20 will start in tracking state nine. The second exception is if the data bit or phase is not determined within five seconds after switching to PLL, a wider tracking bandwidth and shorter integration time will be chosen. Once the navigation data bit is known and successful phase tracking has occurred, the main part of the adaptive

tracking loop starts. If a satellite goes out of view or loses lock, the entire process is restarted, reverting back to tracking state one.

3.2.3.2 Tracking in Non-Ideal Environments

Once bit sync and successful phase tracking has occurred, several tests are conducted. The first test is whether the C/N_0 is greater than 35 dB-Hz. As mentioned earlier, if the signal power is less than 35 dB-Hz the decision logic changes to the non-ideal environment tracking branch, which uses lower thresholds to determine whether to change the tracking state. The non-ideal environment branch was implemented under the assumption that it is better to have a carrier phase measurement with more noise (lower C/N_0) but not as precise (low PLI) rather than no phase measurement at all. The phase measurement should be weighted appropriately in the position solution, as discussed in Section 3.3.4.

In the non-ideal environment branch, the tracking state will not be increased until the PLI is less than 0.79. The value of 0.79 was chosen as it corresponds to 1 cm for GPS L1. Loop stability must be ensured before increasing the tracking state. The loop stability is checked by computing the theoretical jitter (Equation 2.1) for the next tracking state (denoted as J_{i+1}). If the theoretical jitter is less than 15° (Equation 2.15) the tracking state is increased, otherwise the current tracking state is maintained until loss of lock occurs. Loss of lock is declared when the PLI is below 0.0. When loss of lock occurs the tracking strategy reverts back to FLL-assisted-DLL. From Equation (2.15) total loss of lock will occur when the phase error is greater than 45°, which corresponds to a PLI of 0. If at any time the PLI has been greater than 0.95 for more than 10 seconds, the tracking state is decreased. A PLI value of 0.95 corresponds to 0.5 cm of

phase error for a GPS L1 phase measurement. The time criterion is added to avoid prematurely narrowing the tracking bandwidth.

3.2.3.3 Tracking in Ideal Environments

If the C/N_0 of the received signal is greater than 35 dB-Hz, higher thresholds and constraints are used. First, if successful phase tracking occurs (PLI > 0.975) and the amount of time spent in this state is greater than ten seconds (denoted as $t_{tracker}$), the tracking loop bandwidth can be decreased. The time criterion is added to avoid prematurely narrowing the tracking bandwidth. The dynamics during an earthquake change rapidly, e.g. there can be short periods of no dynamics between periods of high dynamics. This is the reason for including a time criterion on successful phase tracking. A PLI value of 0.975 corresponds to 0.3 cm of error for a GPS L1 phase measurement. As seen in Figure 3.2 the change of thermal noise when increasing the tracking state is under 0.5 cm, for C/N_0 greater than 35 dB-Hz. Once there is 0.5 cm of phase error (PLI of 0.95), it is better to increase the tracking state to reduce the phase error with minimal increase of thermal noise.

If phase tracking is deteriorating (PLI < 0.90) the C/N_0 is tested. If the C/N_0 is remaining constant, the likely cause for the PLI to drop is dynamics stress. In this situation the tracking state is increased to attempt successful phase tracking recovery. As will be shown in Chapter 4, the C/N_0 will remain constant when under dynamic stress, assuming no other errors. All implemented tracking states shown in Table 3.1 are stable for C/N_0 above 35 dB-Hz. This means the tracking state can be increased without risking stability.

When the PLI is dropping and the C/N_0 is also decreasing, it could be from either multipath, ionospheric scintillation or both, along with possible dynamics. The C/N_0 decrease is determined by comparing the long term average to a short term average. If the two averages are different by more than 1 dB-Hz, a change in C/N_0 is declared. When this situation occurs a lower PLI threshold is chosen before choosing to increase the tracking state compared to the constant C/N_0 scenario. As discussed in Section 2.4.3 carrier phase multipath is best mitigated using narrower tracking bandwidths. If the C/N_0 is decreasing due to multipath effects, the tracking bandwidth should be increased at a slower rate. As well, multipath is cyclical and can occur randomly (random obstruction or near by obstacle), hence increasing the bandwidth prematurely would not be ideal. If a change in C/N_0 is detected, the ACTL uses a lower threshold when deciding to increase the tracking state. In this situation, when the PLI is below 0.55 the ACTL will then increase the tracking state. A PLI of 0.55 corresponds to 1.5 cm on GPS L1. If a change in C/N_0 is declared, a flag is set and the ACTL will remain using these thresholds for 30 seconds.

For a static receiver in open sky conditions, the ideal tracking state (S_3) would be reached in about 30 seconds, assuming no false locks. The tracking loop will remain in this state until the PLI < 0.90. If at any time the tracking state is maximum (S_{12}), it will remain in this state until either loss of lock or successful phase tracking has occurred. When loss of lock (PLI < 0) is declared the tracking loop reverts back to FLL assisted DLL.

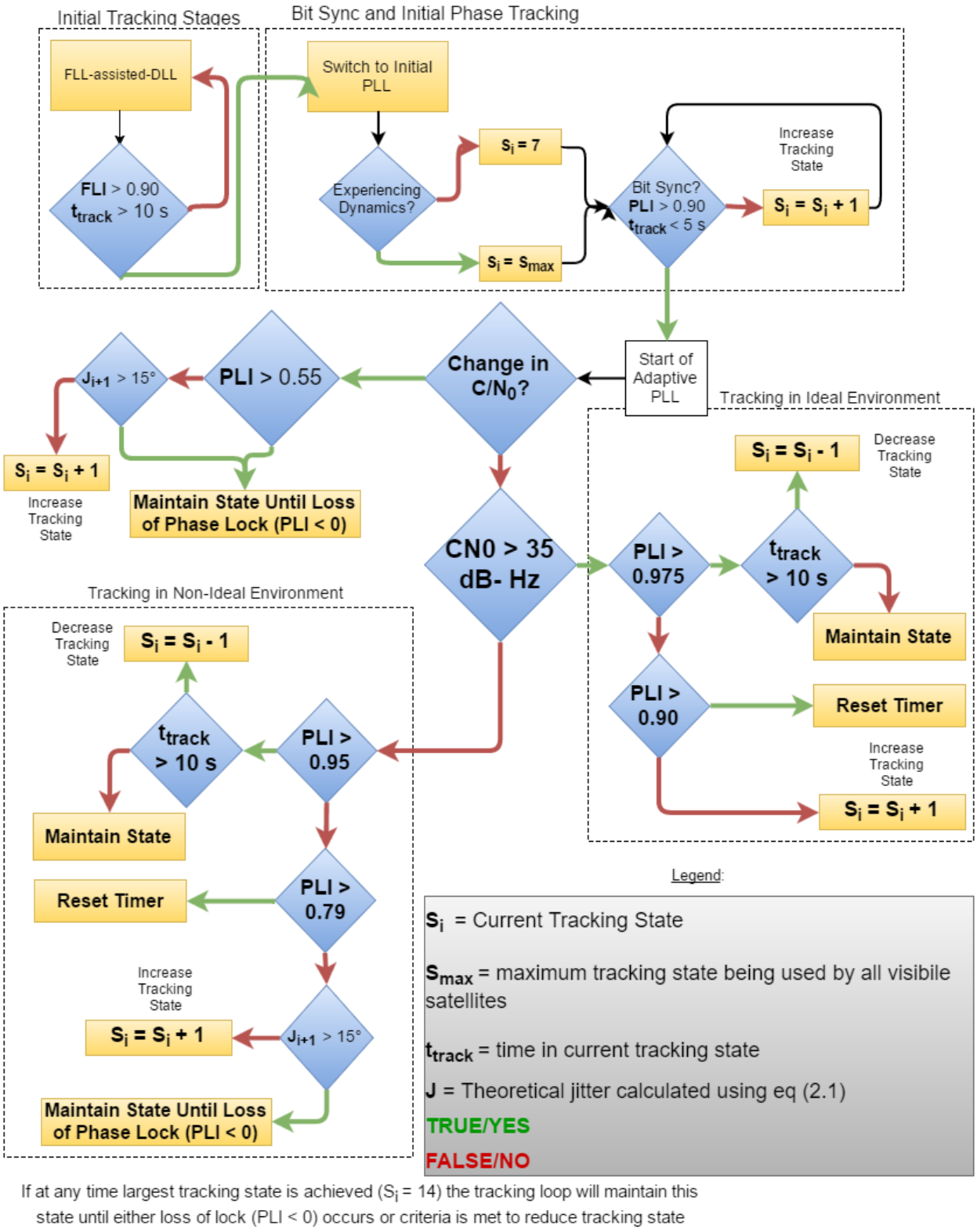

Figure 3.3 Flow chart of decision logic for adaptive carrier tracking loop

3.2.4 Estimating Phase Jitter

The tracking jitter is the standard deviation of the residual tracking error. Jitter can be estimated from the loop filter output or the discriminator output. In hardware receivers the discriminator output is not typically made accessible, unlike the case of a software receiver. Using the standard deviation of the discriminator output will provide a reliable and accurate estimation of the jitter. The discriminator output, which has been passed through the loop filter and NCO (Section 2.3), will account for the tracking bandwidth and integration time of the filter, as well the C/N_0. In Figure 3.1 the estimated phase jitter using the discriminator output is shown in purple. As can be seen, the estimated phase jitter matches well with the theoretical jitter (calculated using Equation 2.1) and the actual jitter (shown in red). To estimate the jitter in real time a moving window of 10 samples was used. This means the estimated jitter is the standard deviation of the last 10 discriminator outputs. In case of a tracking state change the window is completely reset. This was done for two reasons. First was to save computer memory because storing large numbers of samples in memory for each satellite and signal being tracked can lead to computer memory issues. Second and most important was the loop update rate and output data rate used; the loop update rate for GSNRx is 1000 Hz and the measurement output data rate used was 100 Hz. This means there were 10 loop updates between each measurement output.

3.3 Summary

This chapter described the implementation of the new adaptive carrier tracking loop for EMS. Decision logic when adapting the carrier tracking loops was discussed, along with

the thresholds used at each step. Performance of the new adaptive carrier tracking loop will be discussed in Chapter 4 and 5.

Chapter Four: Earthquake Simulation

In this chapter an earthquake simulation is described. The results are separated into two sections: a 10-minute static period before the start of the earthquake followed by five minutes of dynamics induced by the earthquake. Each of these sections is separated into two sub-sections: position and tracking domain. The equipment used and experiment setup will also be discussed.

4.1 Experiment Setup

In order to recreate the complex and dynamic motion of an earthquake a simulation was created. Acceleration data from the 2011 Japanese Tohoku (magnitude 9.0) Earthquake was obtained (K-NET 2015). The acceleration data was collected at 100 Hz and available in the North, East and Vertical directions. The data was integrated once to obtain velocity variations and a second time to obtain position displacements. To remove any drifts and biases caused from the integration, the software SeismoSpect (SeismoSoft 2015) was used. The position, velocity and acceleration data were then used to create a motion file. There was a 10-minute static period before the start of the earthquake and the quake duration itself was five minutes. This motion file could then be used in a GNSS hardware simulator to accurately recreate the motion of a GNSS antenna during the earthquake. In this research a SPIRENT GSS770 simulator was used. The front-end used was a NovAtel Firehose front-end with a 10 MHz bandwidth and 4-bit quantization. The simulated GNSS signals from the hardware simulator were passed through the front-end to convert the signals to the digital domain; the digital data could then be processed by GSNRx, which is capable of tracking multiple constellations and multiple frequencies; in this research only GPS L1 data was used. A NovAtel OEM

628 hardware receiver was used for comparison purposes and the tracking loop parameters are unknown. The front-end components for both the OEM 628 and Firehose front-end are comparable, making signal tracking the most significant difference between GSNRx and the NovAtel OEM 628. The testing conditions are identical for both receivers as the simulated data was collected at the same time. No atmospheric or multipath errors were simulated so dynamic stress and noise were the only error sources.

To fully assess the performance of the adaptive carrier tracking loop discussed in Chapter 3, four different simulations were created. The first two simulations are the 2011 Tohoku Earthquake dynamics in (a) an ideal environment ($C/N_0 > 35$ dB-Hz) and (b) non-ideal environment ($C/N_0 < 35$ dB-Hz). The other two simulations are the 2011 Tohoku Earthquake dynamics multiplied by 10, in both ideal and non-ideal environments. These represent a worst case scenario that may never occur in practice, yet it provides a useful insight into the processes at play. These dynamics were obtained by first scaling the acceleration displacements and then performing the integration to obtain position and velocity displacements.

In each scenario tracking bandwidths of 5, 10, 15, 20, 25, 30, 35, 40, 45 and 50 Hz along with integration times of 1, 5 and 10 ms were tested. All combinations were implemented in GSNRx, unless the B_nT product was larger than 0.45 as this led to loop instability as discussed in Section 2.6.1.

The dynamics in all three dimensions for both original and 10x simulations can be seen in Figures 4.1 and 4.2 [Note the difference in scale on the Y-axis]. In these figures the jerk (measured in g/s) was calculated using the change of acceleration over time. To

create the ideal and non-ideal environments, the C/N_0 was lowered at the 5-minute mark every 15 seconds until the desired C/N_0 was reached. Figure 4.3 shows the C/N_0 for both ideal and non-ideal environment simulations.

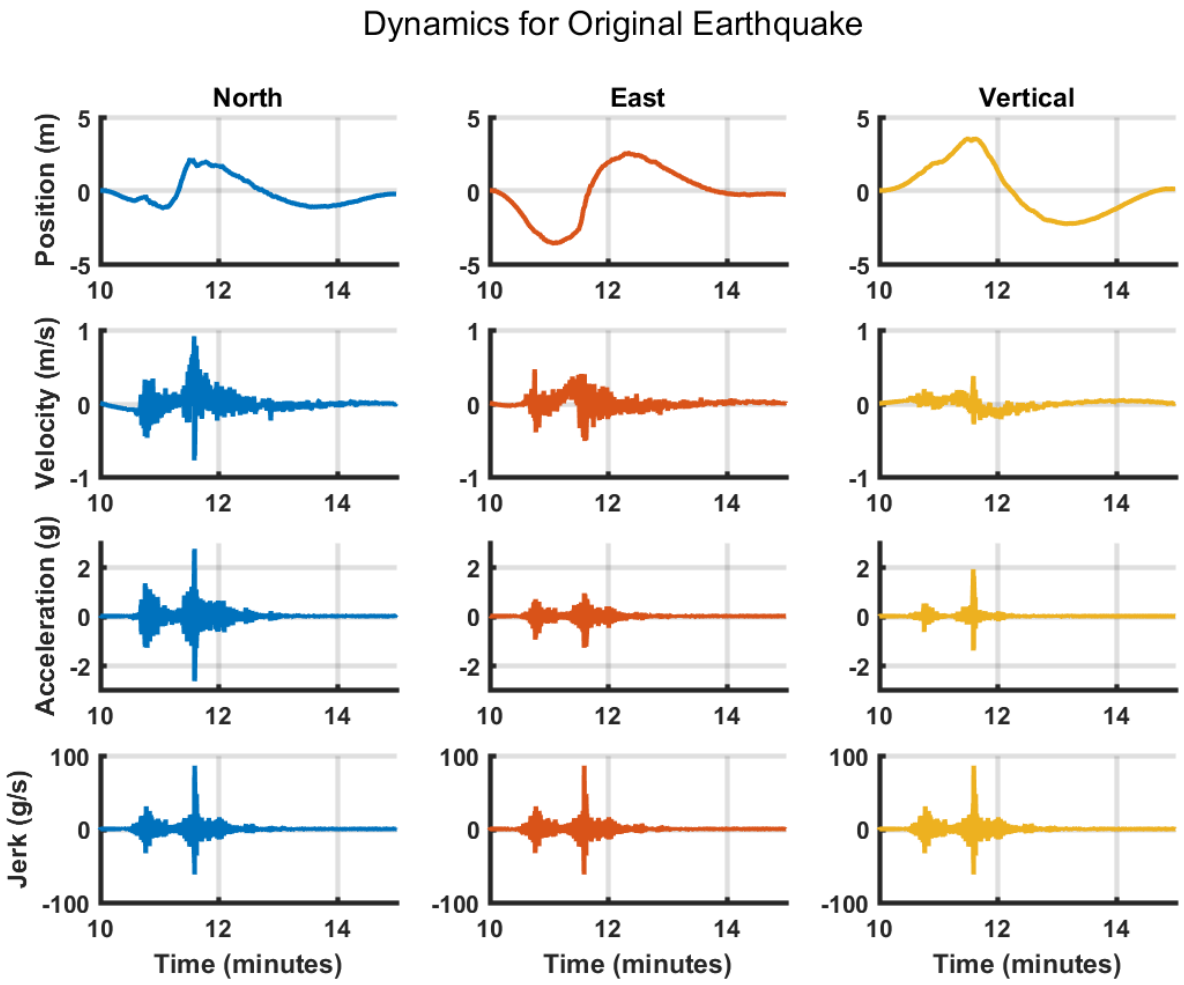

Figure 4.1 Three-dimensional dynamics for the original 2011 M9.0 Tohoku Earthquake

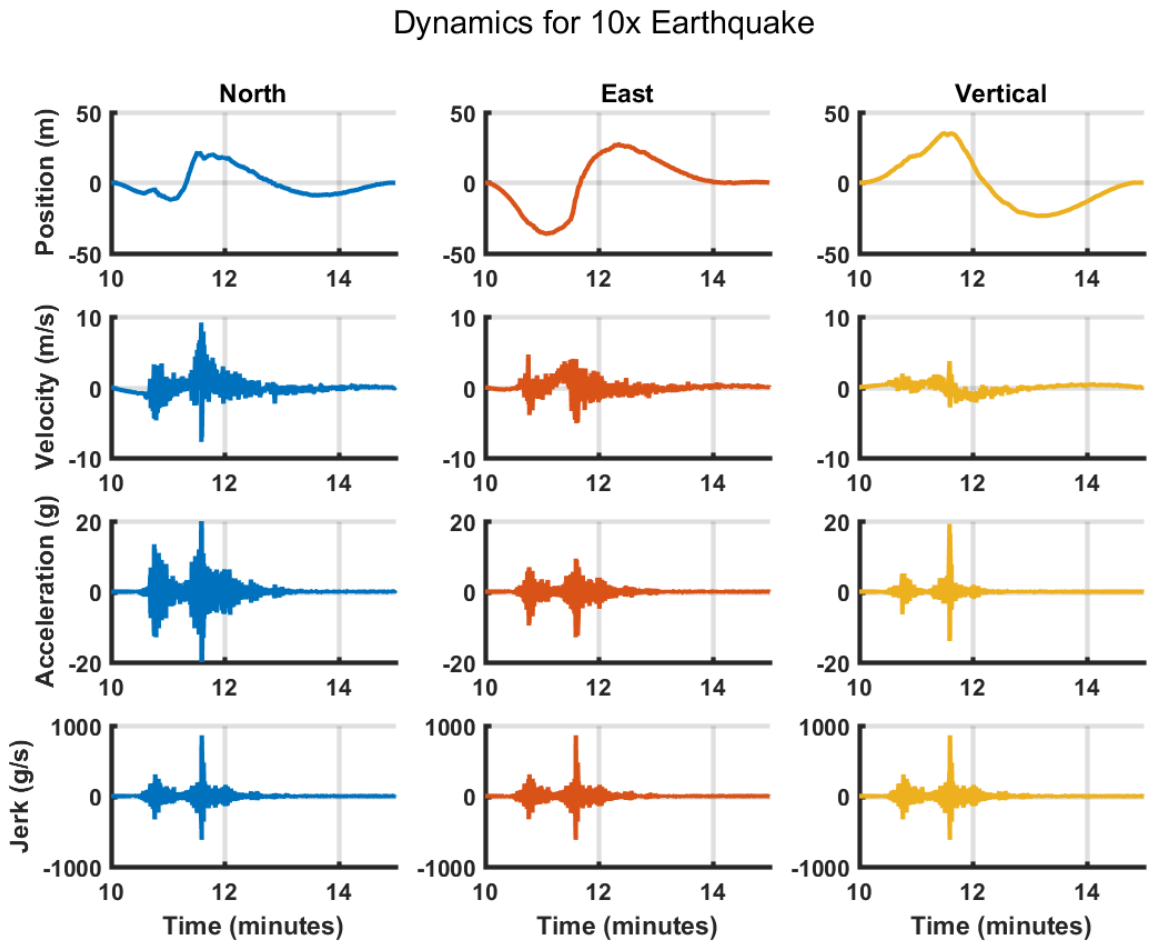

Figure 4.2 Three-dimensional dynamics for the 2011 Tohoku Earthquake scaled by a factor of 10

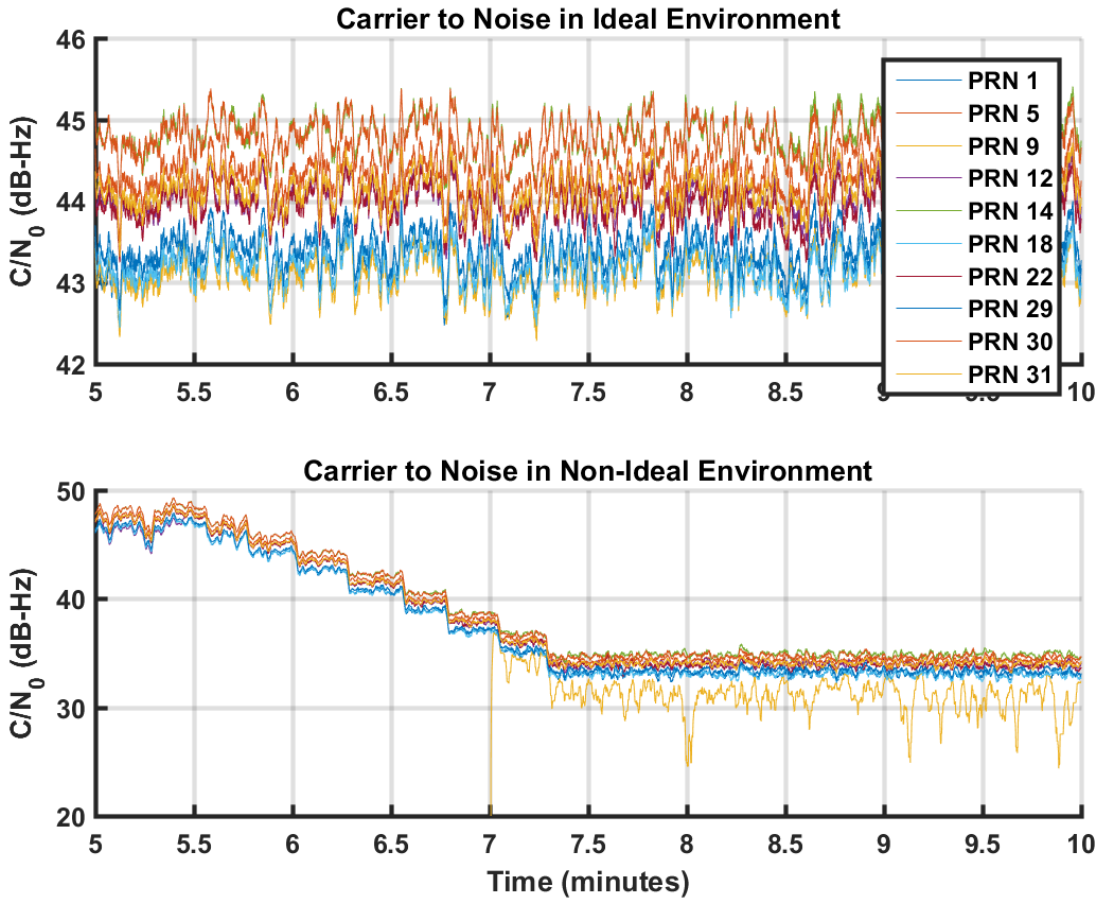

Figure 4.3 Carrier-to-noise ratio comparison for ideal and non-ideal environments

4.2 Position Solution

This research is primarily focused on assessing the tracking performance of carrier tracking loops and proposing an adaptive tracking EMS. Since the objective of a GNSS receiver is to provide a position solution (more generally, position, velocity and time), the position solution results were also assessed. As will be seen, the position solution can be used to assess the quality of tracking and the effect of tracking parameters.

It is well known that carrier phase measurements must be used and their ambiguities resolved to integer values to achieve the cm level accuracy required for EMS. This is

commonly done using differential processing techniques. A second NovAtel OEM 628 receiver was simulated as the reference receiver, located 15 km away from earthquake. In this research, PLANSoft (Ong 2010, Lachapelle et al 2010) was used for resolving the carrier phase ambiguities to integer values and computing the differential position solution. A Kalman filter was used to estimate the position solution, however comparisons will be made to the position solution obtained using least squares.

4.3 Static Period Before Earthquake

4.3.1 Position Domain Results

In this section results are shown for the static period prior to the start of the earthquake, which occurs 10 minutes in the simulation. Since both the original and 10x dynamic simulations have identical static periods, only ideal and non-ideal environment results are shown. During this time period, the only error source affecting carrier tracking performance is thermal noise. Tracking loops with longer integration times and narrower tracking bandwidths have the best performance, as expected from Equation (2.1).

Figure 4.4 shows the root-mean-square (RMS) of the position and velocity errors for the static receiver in this ideal environment. Evident in this figure is the effect that tracking parameters have on noise performance. Receivers with narrower tracking bandwidths and longer integration times have the lowest noise. As the tracking bandwidth increases and integration time decreases, the noise increases. For an integration time of 10 ms the noise increase between tracking bandwidths is minimal since the C/N_0 is high, as discussed in Section 3.2.3. Also shown is the noise performance for the ACTL and the NovAtel OEM 628. The two receivers have comparable performance, with the NovAtel having marginally better performance. As expected, the ACTL has identical

performance of the fixed bandwidth and integration time of 5 Hz and 10 ms integration as this combination is the final PLL tracking state (Table 3.1).

Figure 4.5 shows the position and velocity RMS errors for a static receiver in a non-ideal environment. Similar to the results in Figure 4.4, narrower tracking bandwidths and longer integration times are best for reducing the noise. Since the C/N_0 is lower in the non-ideal environment, from Equation 2.1 it is expected that the thermal noise will increase from the ideal to the non-ideal environment. This is evident when comparing Figure 4.4 and 4.5 results. In a non-ideal environment, the ACTL performs marginally better than the OEM 628, the reverse of the results in an ideal environment. Note the different y-axes scale for the RMS velocity error between Figure 4.4 and 4.5. Earthquake detection is the most vital task for EMS. The noise level in the position solution for a static receiver sets the minimum detectable motion threshold, motion smaller than the noise cannot be detected. Earthquake detection when using a GNSS receiver is done by looking for small variations in position and velocity. Therefore, lower noise in the position solution can lead to better earthquake detection.

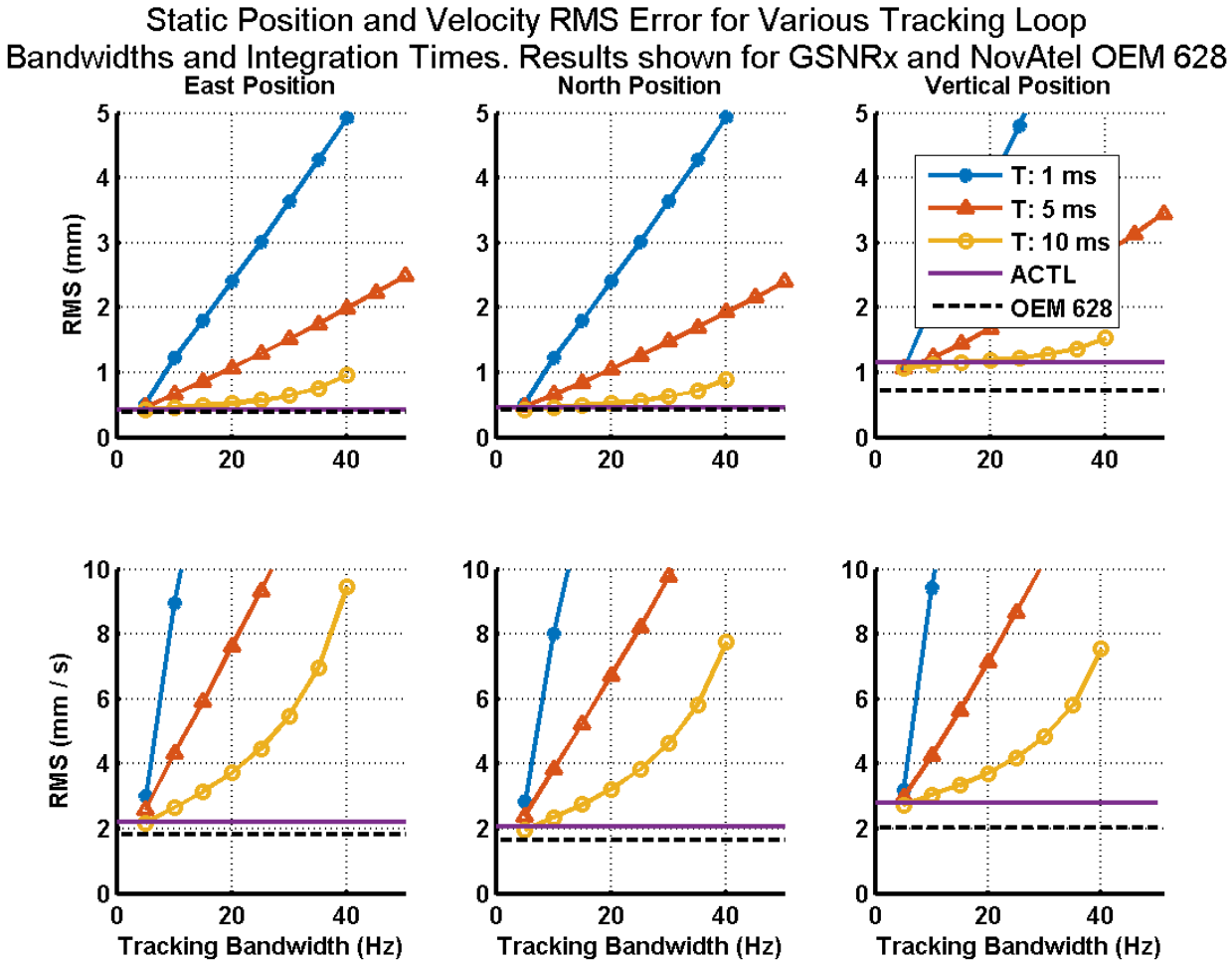

Figure 4.4 Position and velocity RMS errors during static period in an ideal environment prior to simulated earthquake. Results are shown for the ACTL, NovAtel OEM 628 and various tracking loop parameters

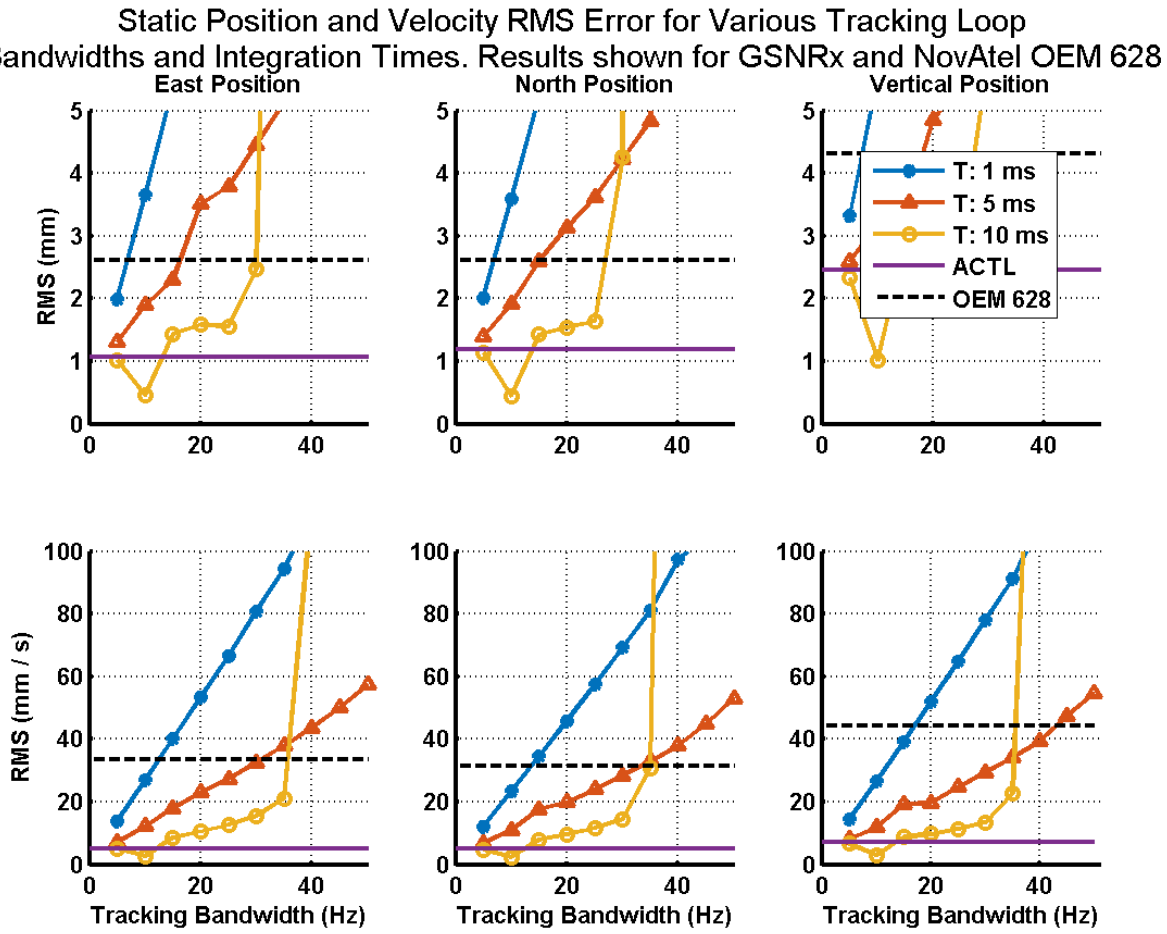

Figure 4.5 Position and velocity RMS errors during static period in a non-ideal environment prior to simulated earthquake. Results are shown for the ACTL, NovAtel OEM 628 and various tracking loop parameters

Figure 4.6 shows the position errors over time for both the ACTL and OEM 628 receivers in both ideal (top row) and non-ideal environments (bottom row). In the ideal environment the performance between the two receivers is comparable. However, in the non-ideal environment it is clear the ACTL outperforms the OEM 628 in term of noise reduction. It is likely that the OEM 628 is using a larger fixed tracking bandwidth compared to the ACTL, hence the noise increase when the C/N_0 decreases.

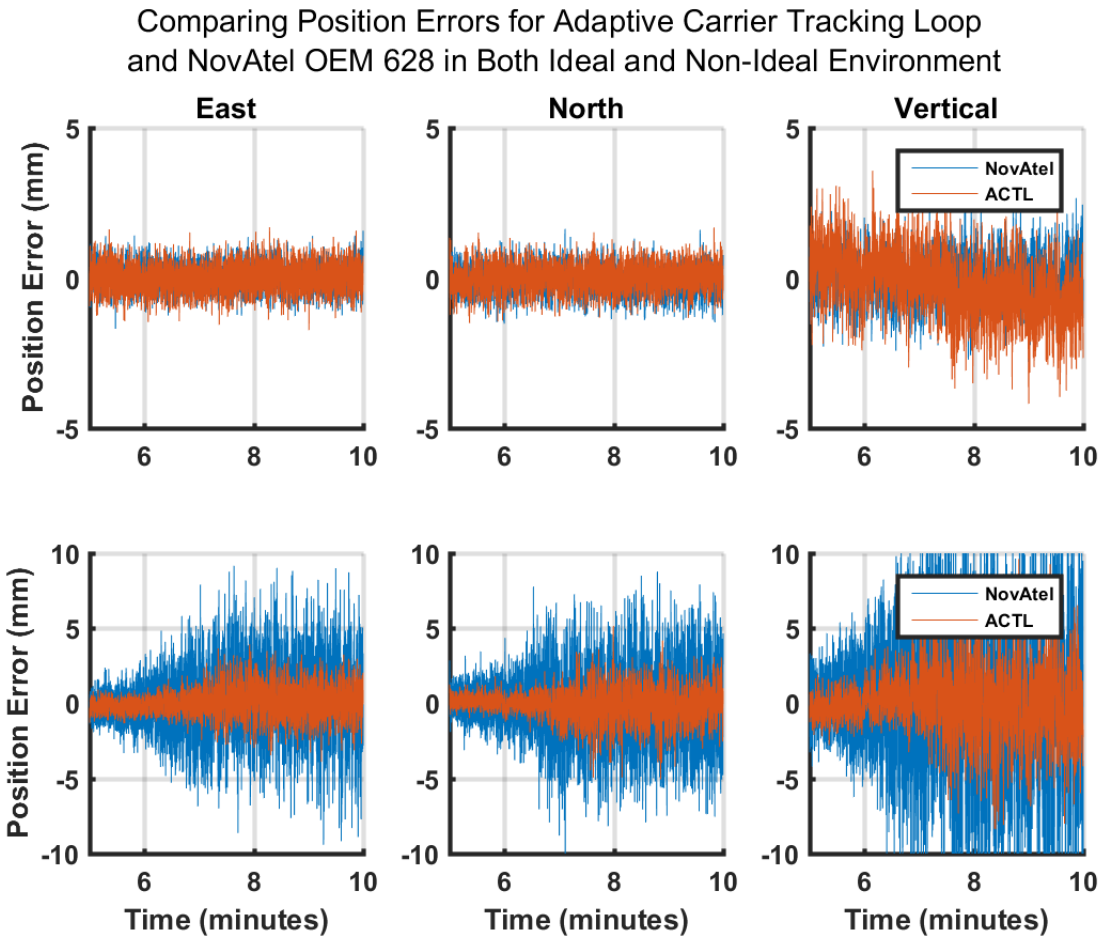

Figure 4.6 Time scale representation of the position errors for the ACTL and NovAtel OEM 628 receivers in both ideal (top row) and non-ideal environments (bottom row)

In Figure 4.7, a time scale representation of the static vertical position errors for the ACTL and NovAtel OEM 628 is shown when using a Kalman filter and epoch-by-epoch Least Squares. Compared to least squares, using a Kalman filter reduces the noise in the position solution. As discussed earlier, reducing the noise is crucial for earthquake detection. It is for this reason the Kalman filter was used. This research is focused on

tracking loop performance, while improving the position solution is considered future work.

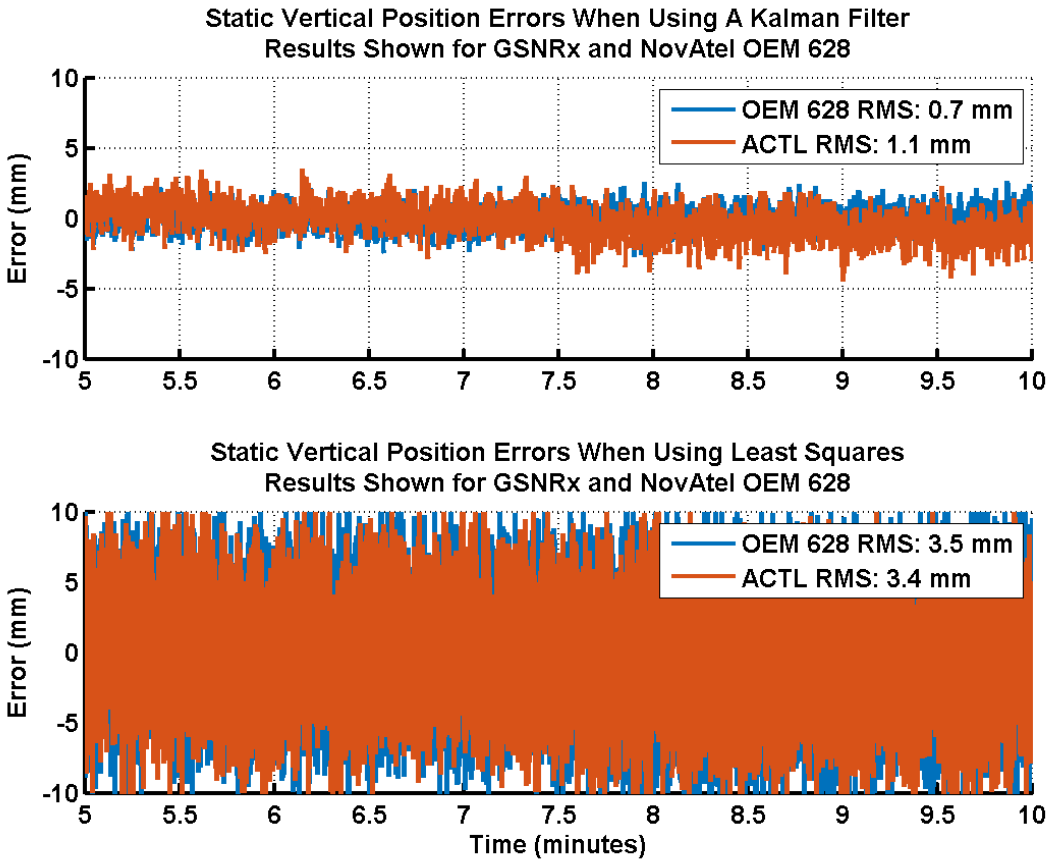

Figure 4.7 Comparison of the position solution obtained using a Kalman filter and epoch-by-epoch least squares

4.3.2 Tracking Domain Results

As discussed in Section 3.2.2, the ACTL will start in FLL-assisted-DLL (S_2) mode for a minimum of 10 seconds before switching to PLL-assisted-DLL (S_7). Once in PLL operation, the ACTL will narrow the tracking bandwidth (decrease tracking state) if phase tracking is successful for a minimum of 10 seconds. These steps can be seen in the top plot of Figure 4.8. It takes approximately 30 seconds for the ACTL to reach the

desired tracking state (S_3). The bottom plot shows the phase discriminator output during the initial tracking stages. During the first 10 seconds the ACTL is in FLL mode so there is no phase discriminator output. The noise from the discriminator output decreases as the tracking state decreases, as expected. The time scale shown (in seconds) does not correspond to the same time scale of the simulation (in minutes). Moreover, this figure shows the initial 35 seconds for every satellite being tracked, but the time they are tracked or come into view during the 15-minute simulation may vary.

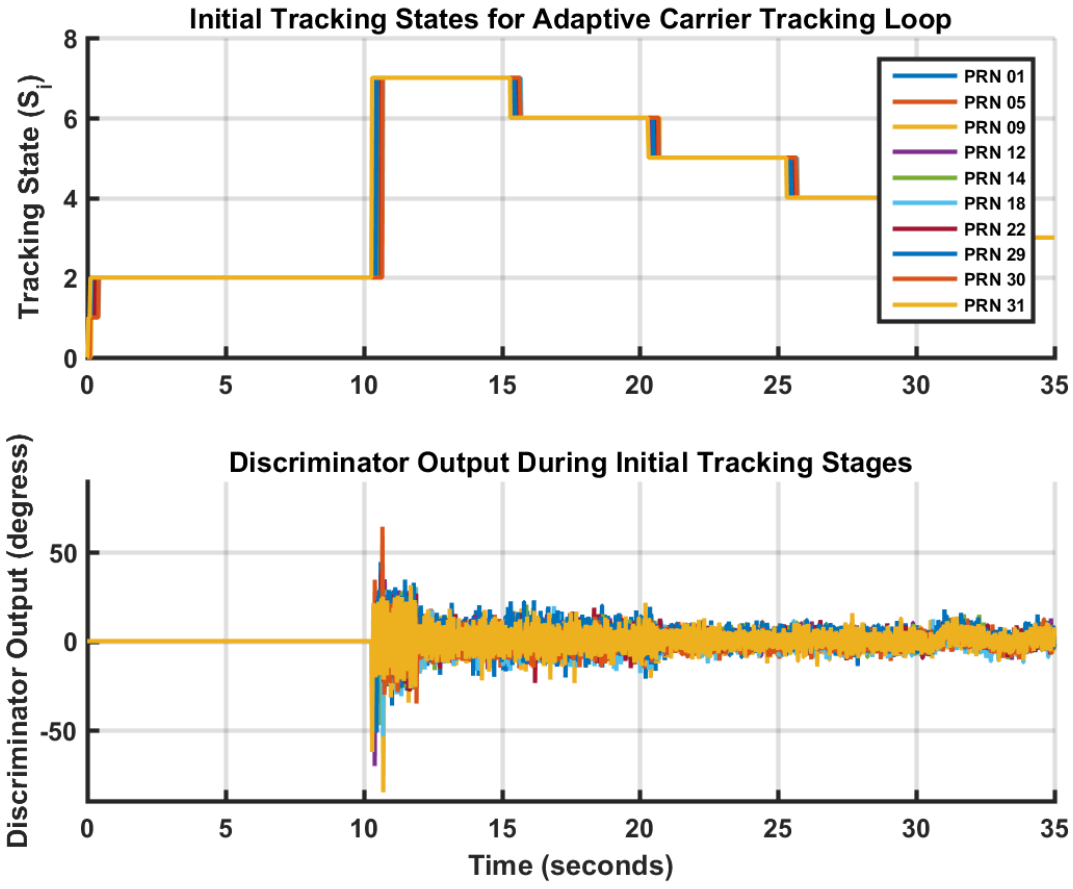

Figure 4.8 Initial tracking states and discriminator output for the ACTL

In Chapter 2 it was discussed how the navigation data bits, phase and phase errors are estimated using I/Q notation. When using a FLL the phase is not estimated, therefore both I and Q could be maximum or minimum. However, once the tracking loop transitions to PLL the phase is estimated and I samples will be maximum and Q will be minimum (Chapter 2). These traits of the FLL and PLL are evident in Figure 4.9. During the initial 10 seconds, the ACTL is using a FLL so the I and Q samples fluctuate between maximum and minimum. During this time, it is difficult to identify navigation data bit transitions. Once the ACTL has transitioned to PLL, the data bit transitions can be identified easier (transitions from positive to negative). This is one of the advantages of using a PLL as compared to a FLL. A FLL is able to determine bit transitions however the results are less accurate/reliable.

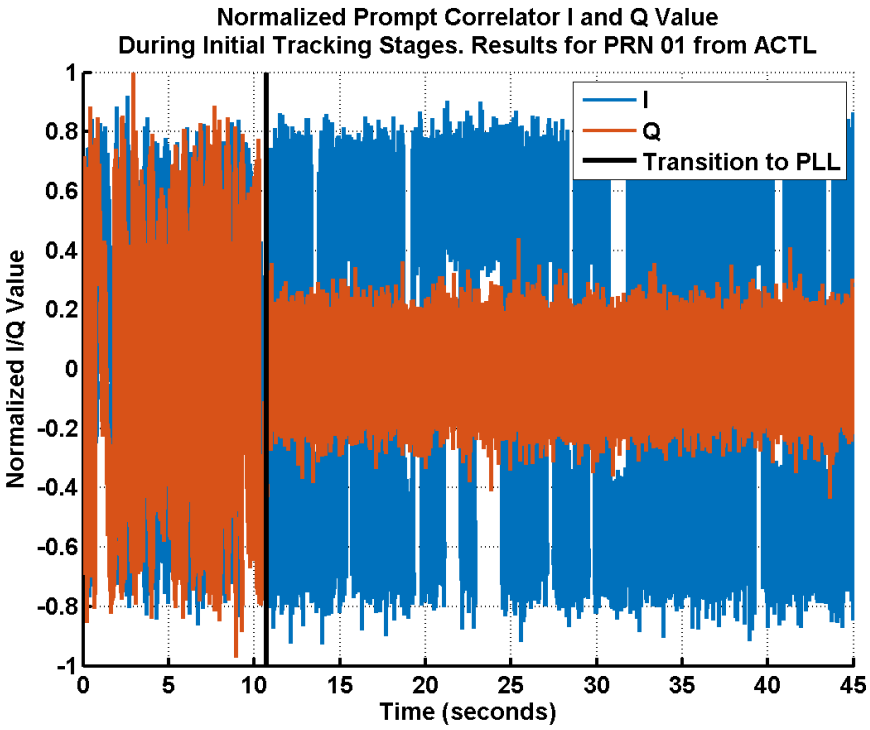

Figure 4.9 I and Q during initial tracking stages

Figure 4.10 compares the phase discriminator outputs in degrees for the ACTL in both ideal and non-ideal environments. When the C/N_0 increases the noise from the discriminator output increases. For both environments, all PRNs are in tracking state S_3. It was discussed in Section 3.2.3 that tracking in the non-ideal environment branch uses lower thresholds. The reasoning for this decision can be seen in Figure 4.10, which shows the PLI in both environments. As the noise increases on the discriminator output, so does the noise on the PLI. Using tighter thresholds in a non-ideal environment may lead to an unnecessary switching of the tracking state. For example, in Figure 4.11 the PLI for PRN 22 in the non-ideal environment drops below the adapting threshold used in the ideal environment (PLI < 0.9). If the same thresholds were used in both environments, the tracking state for PRN 22 would have unnecessarily increased, further increasing the noise. The change of PLI when the C/N_0 decreases in Figure 4.11 was used for detecting multipath in the ACTL, discussed further in Chapter 5.

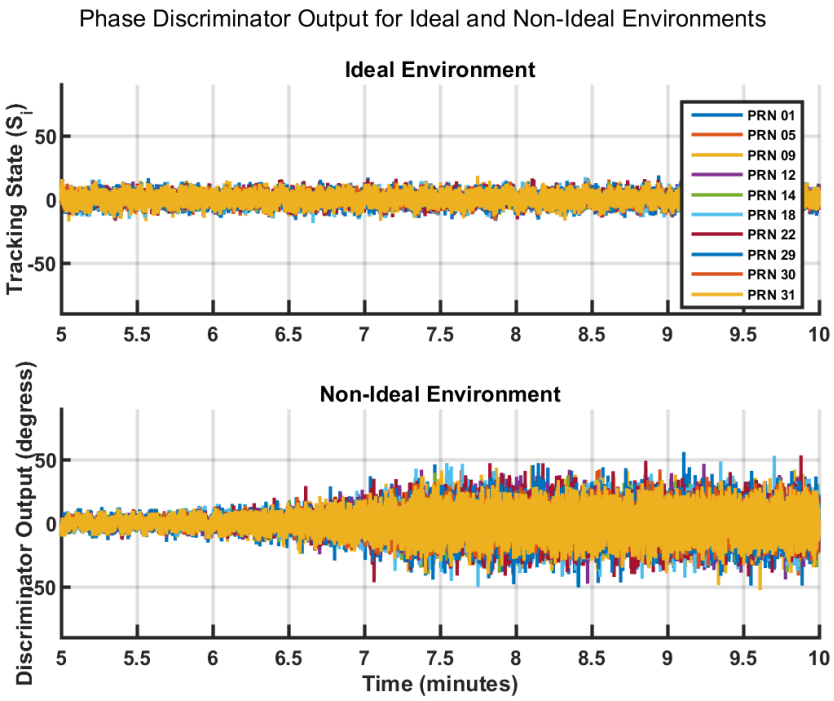

Figure 4.10 Discriminator output in ideal and non-ideal environments.

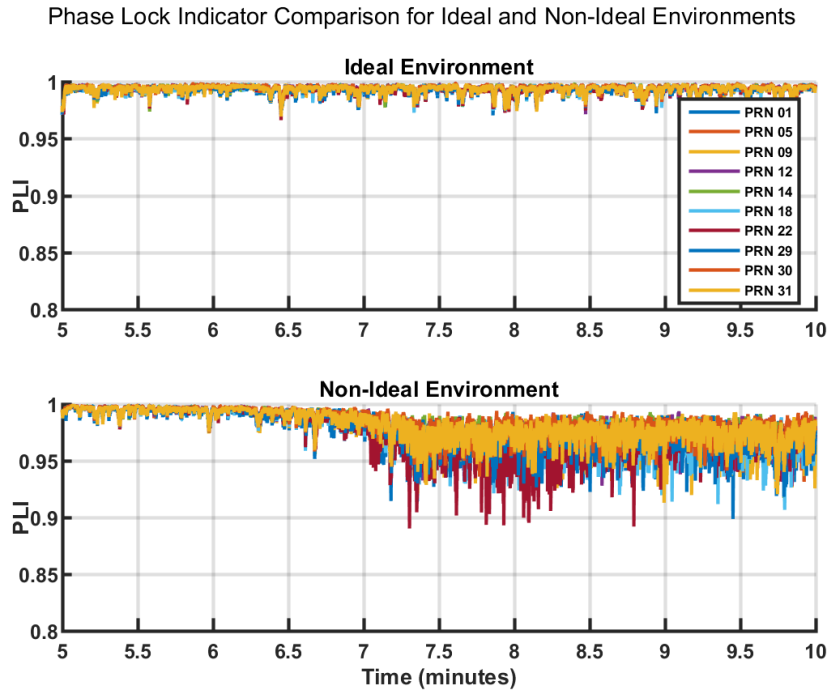

Figure 4.11 Phase Lock Indicator in ideal and non-ideal environments

The estimated phase jitter used in the position solution is shown in the tracking domain section since it is obtained directly from the carrier tracking loops. The NovAtel OEM 628 also provides estimates for the phase jitter. Analyzing the estimates of phase jitter between the receivers can provide an indication of what is happening at the tracking loop level. This is more important for analyzing the OEM 628 since the tracking information provided is limited.

Figure 4.12 shows the estimated phase jitter for the ACTL and OEM 628 receivers in both environments. For clarity the legend was omitted, however the same notation and colours were used as those used in Figure 4.10 and Figure 4.11. The figure shows that the estimated phase jitter decreases during the initial tracking stages (2-minute mark) for the ACTL as the tracking state decreases. The estimated phase jitter increases when the C/N_0 decreases in the non-ideal environment plots. These results show that the implemented method discussed in Section 3.2.4 can provide phase jitter estimates when adapting the tracking loops and the C/N_0 changes. The estimated phase jitter for the ACTL is lower than that of the OEM 628. However, since the methodology for estimating phase jitter in the OEM 628 is unknown, one cannot say if the ACTL is performing better than the OEM 628. A possible reason for the difference is that the OEM 628 is using more pessimistic values than the true estimated jitter. Another possibility for the difference is that the OEM 628 is using different tracking parameters than those of the ACTL. The results of the non-ideal environment shown in Figure 4.6 support this possibility.

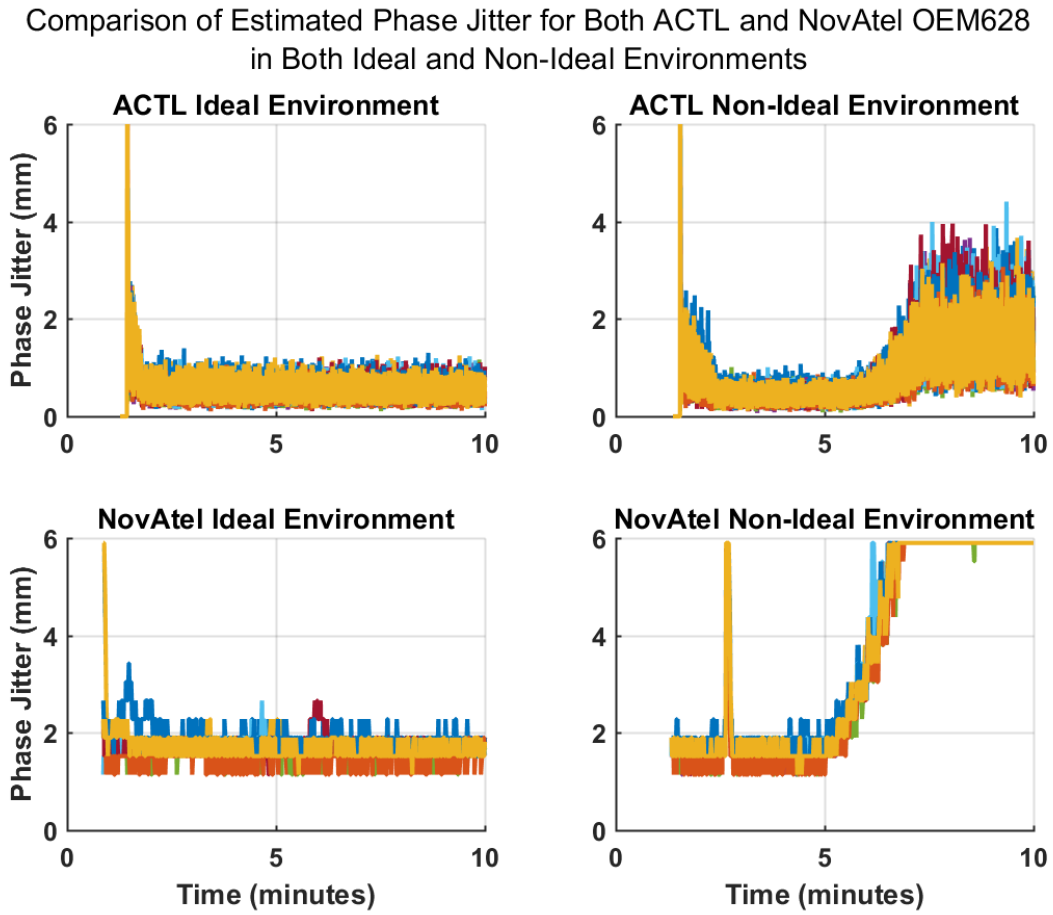

Figure 4.12 Comparison of estimated phase jitter for both ACTL and NovAtel OEM628 in ideal and non-ideal environments

4.4 Earthquake Simulation

4.4.1 Position Domain Results

In Figure 4.13 the position RMS errors and maximum position errors are shown for all receivers tested in an ideal environment and with the original earthquake dynamics. The maximum position errors are the maximum single epoch errors and may occur at different times for each receiver. There is a parabolic trend which suggests that tracking bandwidths of 15 to 30 Hz with a 10 ms integration time is the ideal combination for

EMS. The ACTL results are comparable to the best combination (lowest point on each graph) of tracking bandwidth and integration time. This suggests that the tracking loop parameters and thresholds used for the ACTL are close to ideal and suitable for reducing the noise (RMS errors) and dynamic stress (maximum errors). The results from the ACTL and OEM 628 are also comparable.

In Figure 4.14 the position RMS errors and maximum position errors are shown for all receivers tested in a non-ideal environment and with the original earthquake dynamics. Compared to the results of Figure 4.13, the ACTL results are further from the ideal combination. This suggests that different thresholds could be chosen in the non-ideal tracking environment branch. However, the thresholds and decision logic would only require minor refinement since the results are close to the ideal combination.

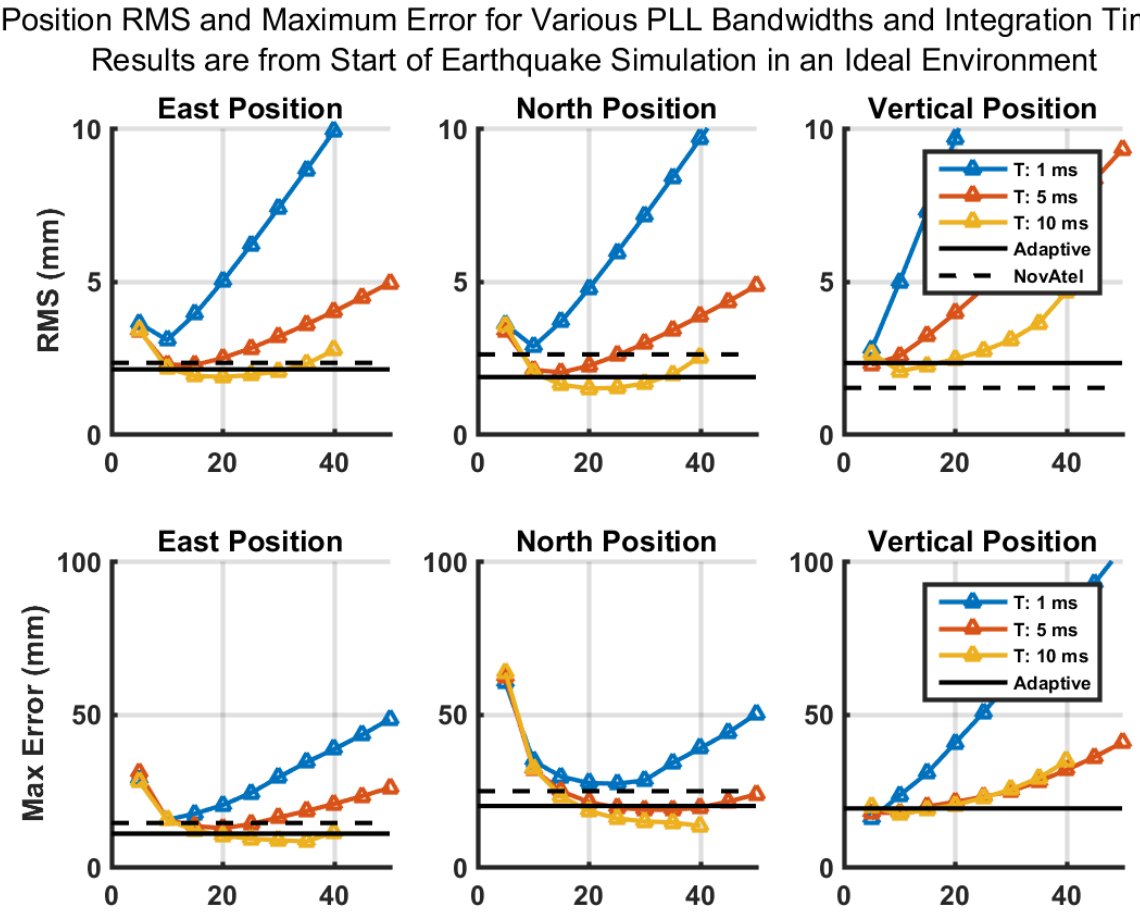

Figure 4.13 Position RMS and maximum errors during the earthquake simulation. Results are shown for the original earthquake dynamics in an ideal environment

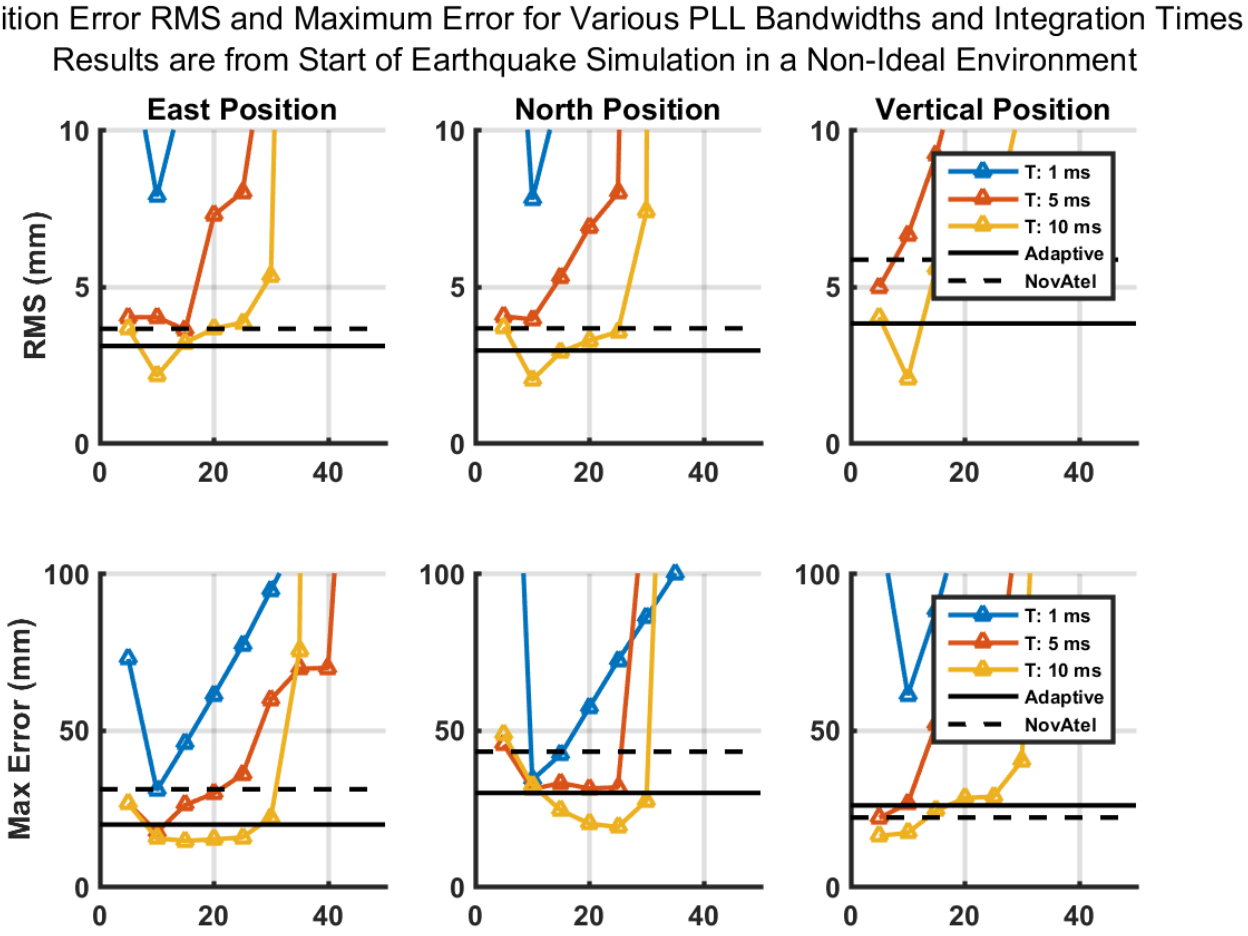

Figure 4.14 Position RMS and maximum errors during the earthquake simulation. Results are shown for the original earthquake dynamics in a non-ideal environment

In Figures 4.15 to Figure 4.18, the time series of position errors in the North direction for all simulations are shown for different tracking loop bandwidths and integration times for the ideal and non-ideal environments. The North direction was chosen as this was the direction with the largest acceleration. The first row in each figure shows the position errors for a fixed tracking bandwidth of 20 Hz and integration times of 1, 5 and 10 ms. The second row in each figure shows the position errors for a fixed integration time of 5

ms and tracking bandwidths of 5, 15, 30 and 50 Hz. It is clear from these figures that increasing the integration time reduces the noise as expected. The noise is also reduced by narrowing the tracking bandwidth. However, narrowing the tracking bandwidth comes at the expense of increased dynamic stress error. This can be seen by the larger position error spikes at 11.5 minutes in Figure 4.15 and Figure 4.16 (the original dynamics) when using a tracking bandwidth of 5 Hz. In Figure 4.17 and Figure 4.18 (the 10x dynamics) larger tracking bandwidths are able to track for longer periods of dynamics stress. In these two figures the tracking bandwidth of 50 Hz was able to track for the duration of the simulation. However, cycle slips were detected and so no fixed solution was provided.

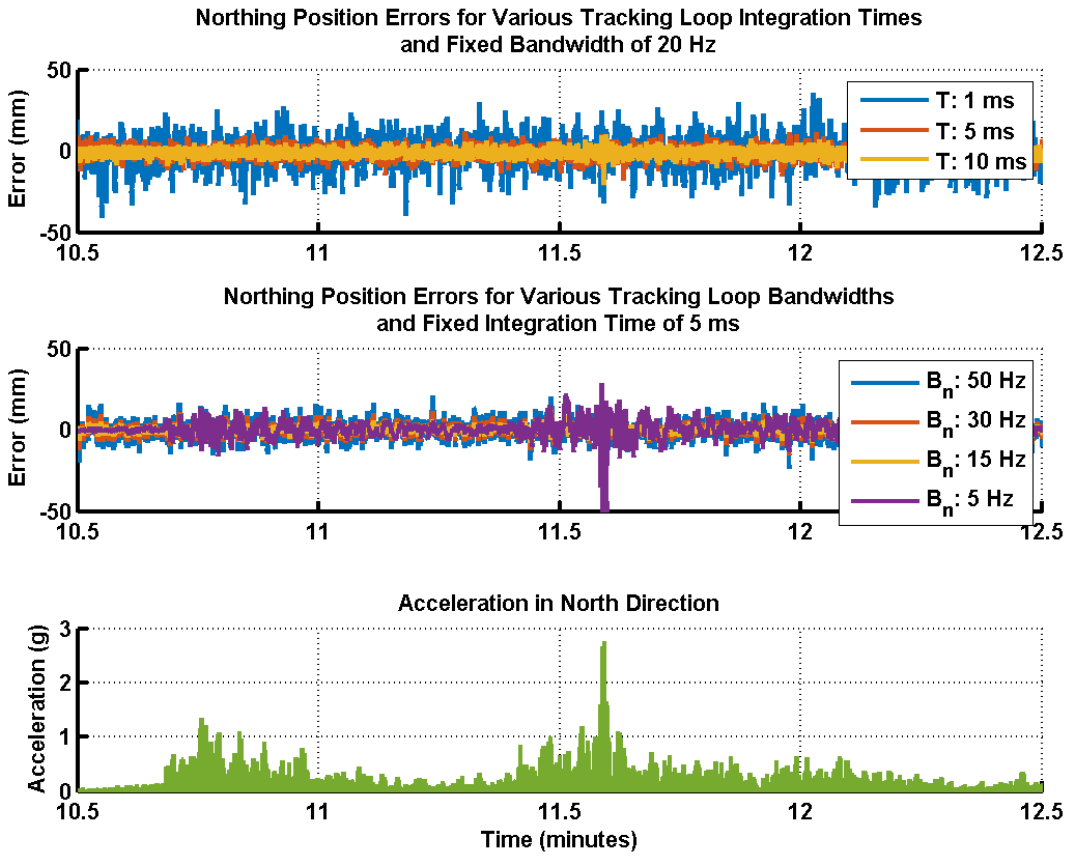

Figure 4.15 Time series of northing position errors for the original dynamics in an ideal environment for different tracking loops

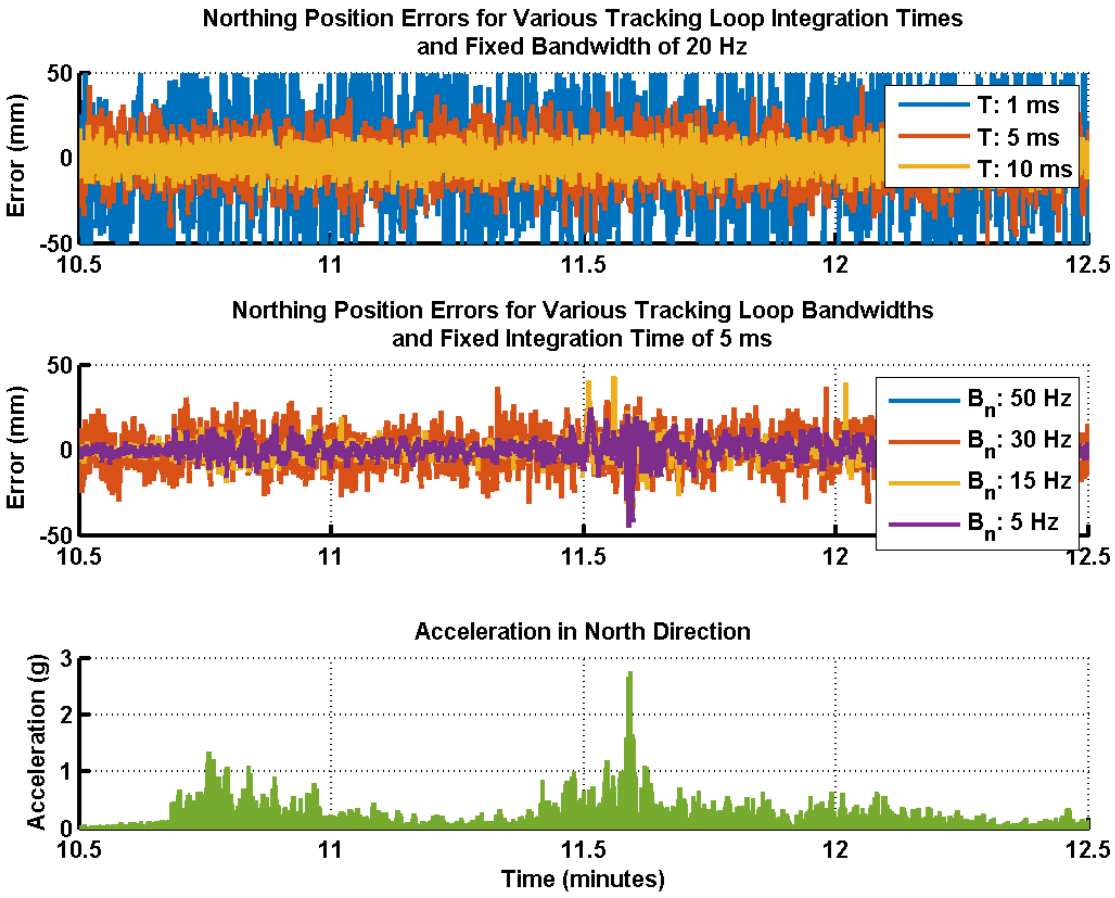

Figure 4.16 Time series of northing position errors for the original dynamics in a non-ideal environment for different tracking loops

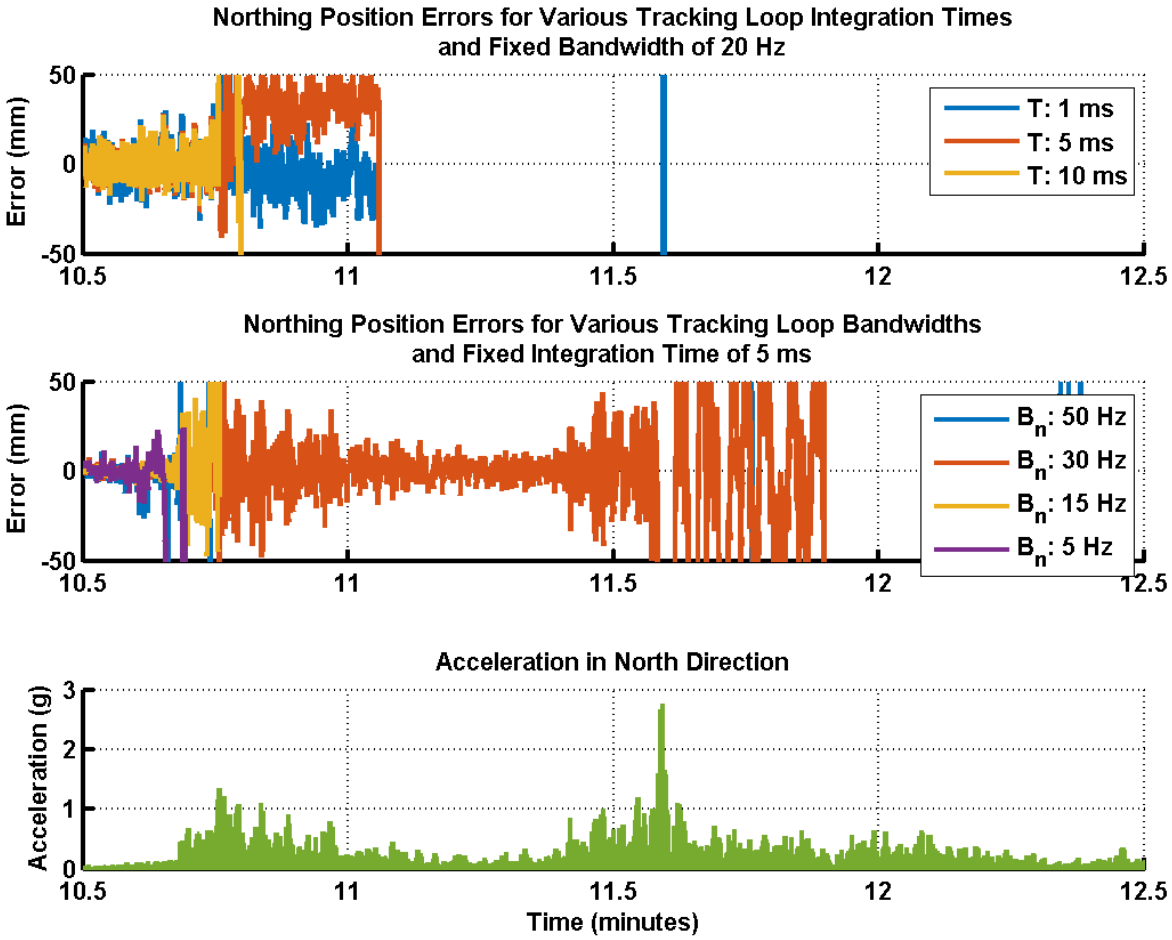

Figure 4.17 Time series of northing position errors for the 10x dynamics in an ideal environment for different tracking loops

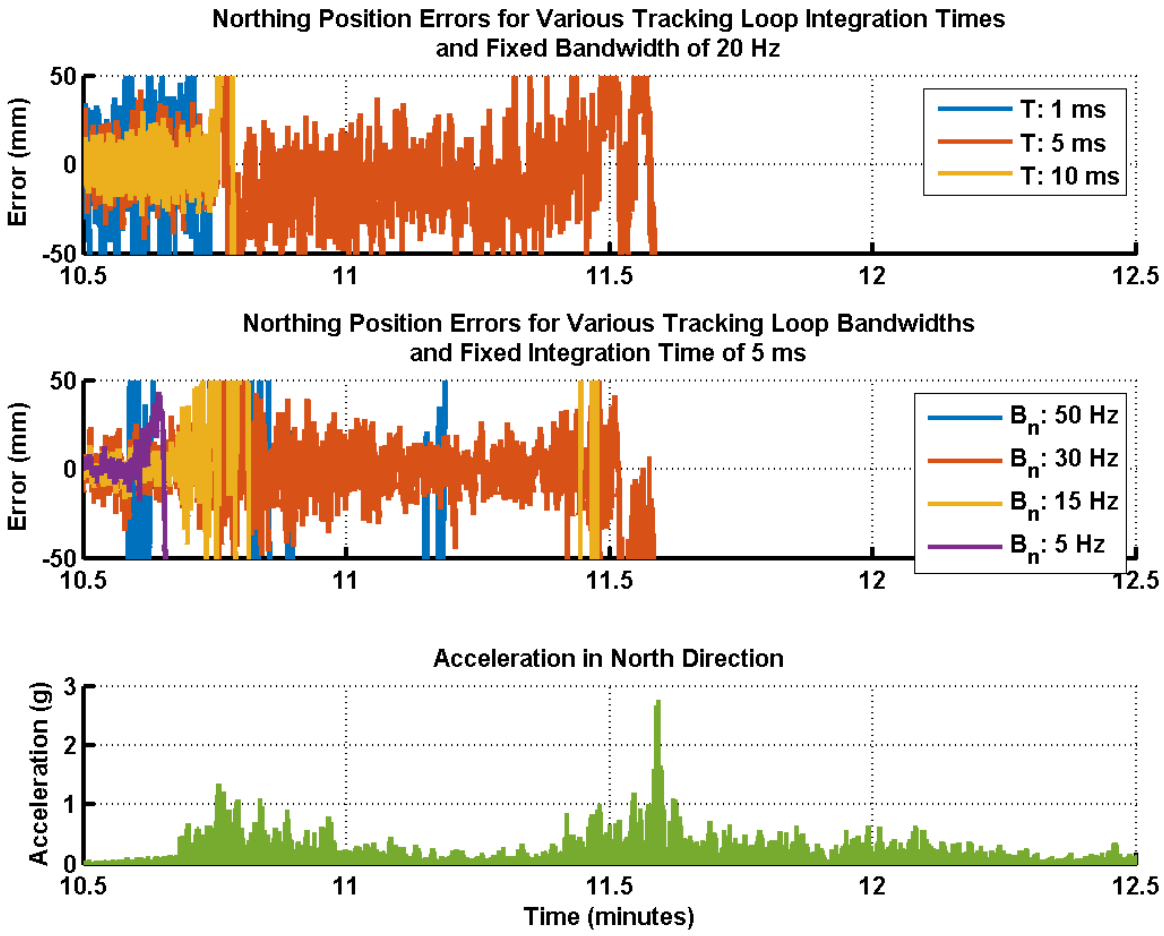

Figure 4.18 Time series of northing position errors for the 10x dynamics in an ideal environment for different tracking loops

In the simulation using the original dynamics scaled by a factor of 10, the tracking loops are pushed to the limit. These simulations were done primarily to analyze tracking performance, although a position solution analysis is also provided for the sake of completion. As in Figures 4.17 and 4.18, all receivers tested had varying tracking performance, losing lock on different satellites and at different times. Almost all receivers tested lost lock directly after the acceleration started, due to the larger

accelerations. This means the position RMS and max errors calculated for each receiver are for different durations, thus not suitable for comparison purposes. Hence, only time series of northing position errors for the ACTL and NovAtel OEM 628 are shown in Figure 4.19. As can be seen in this Figure, the ACTL was able to provide an accurate solution for the full earthquake simulation. The OEM 628 lost lock after the large dynamics. The RMS errors for the OEM 628 were calculated using only times when lock has occurred.

In Figure 4.20 the time series of the position errors in the North direction for the ACTL and NovAtel OEM 628 in the 10x dynamics non-ideal environments is shown. The y-axis scale is now in metres. In this simulation the OEM 628 lost lock once dynamics were experienced. The ACTL is able to provide a position solution for the duration of the simulation However, in this situation, cycle slips were detected on all satellites and all ambiguities were reset. As such, no fixed solution could be computed for the duration of the earthquake.

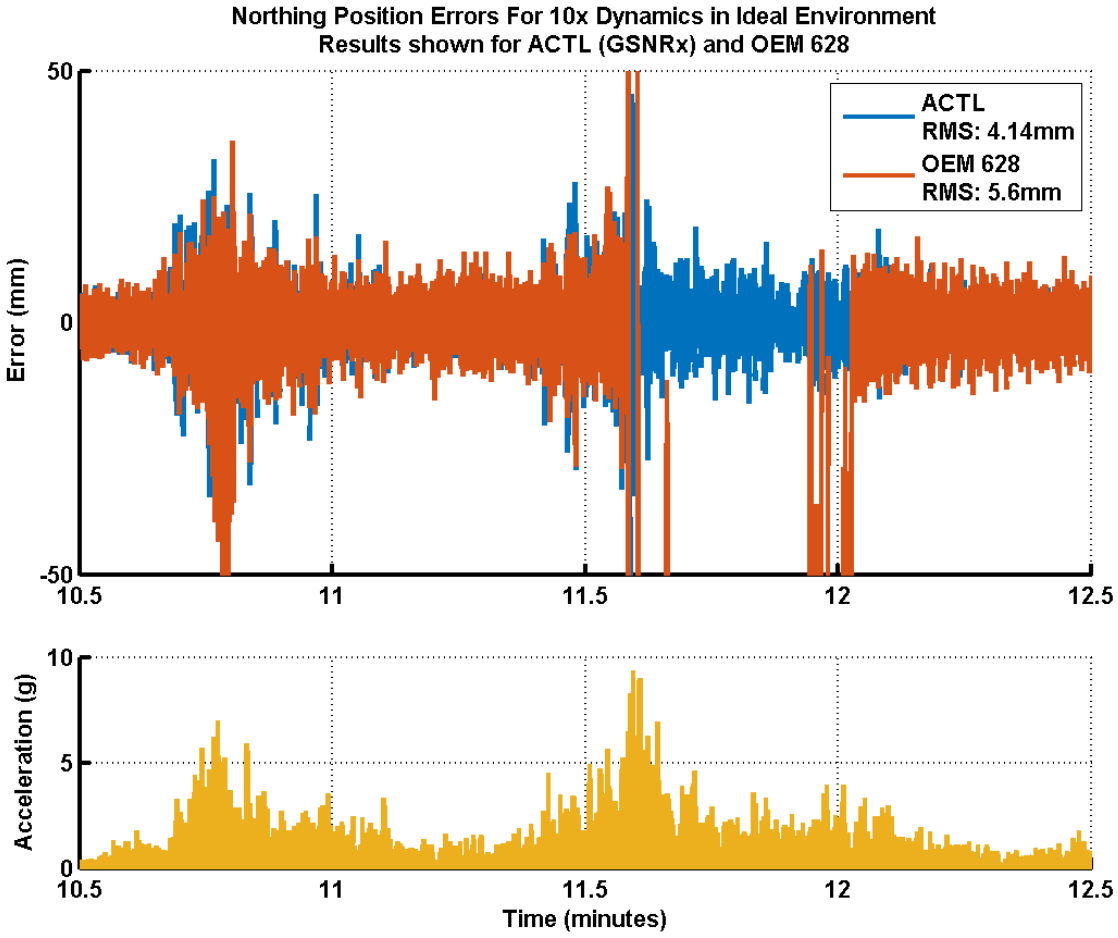

Figure 4.19 Time series of northing position errors for ACTL and NovAtel OEM 628 using 10x dynamics in an ideal environment

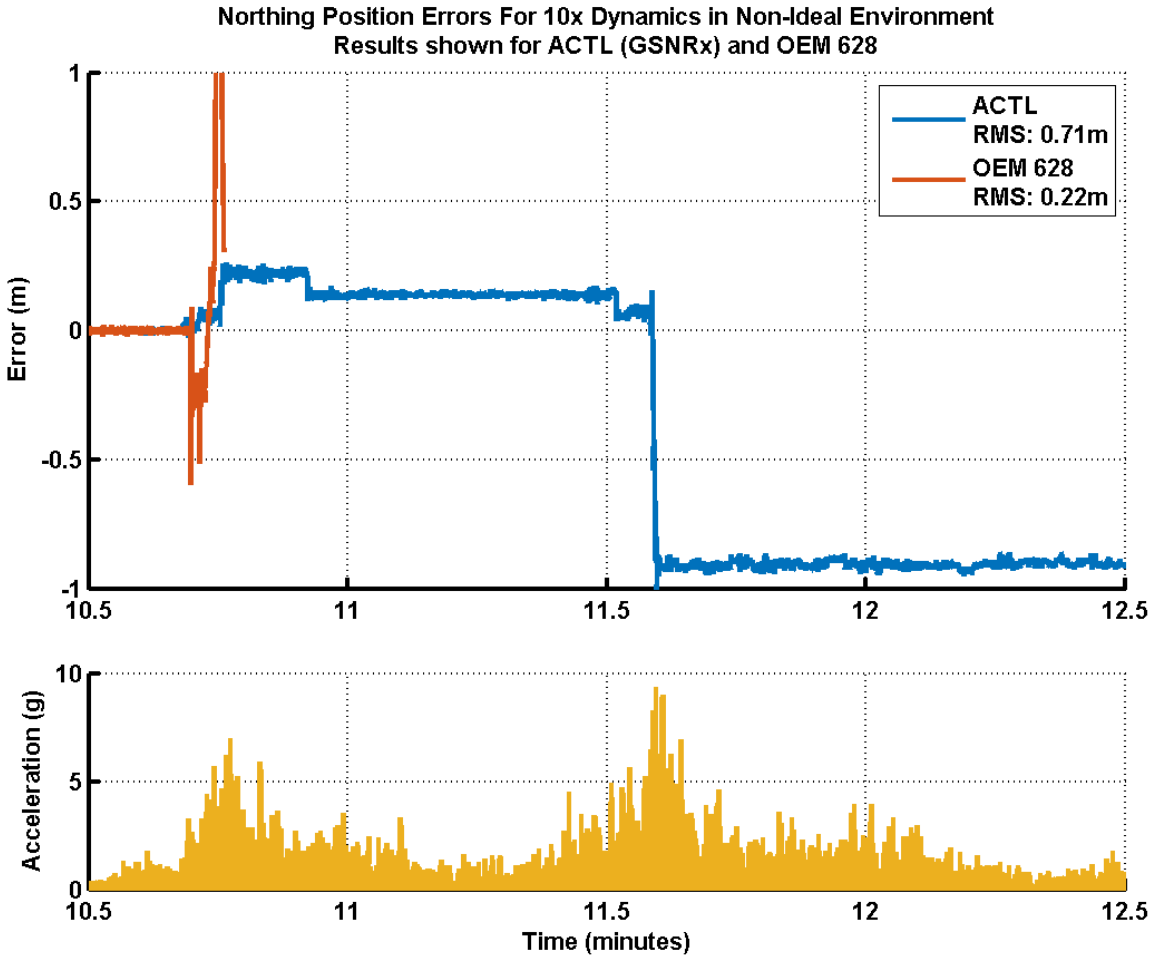

Figure 4.20 Time series of northing position errors for ACTL and NovAtel OEM 628 using 10x dynamics in a non-ideal environment

In Figure 4.21 and Figure 4.22 position solutions obtained using Kalman filtering and epoch-by-epoch least squares is presented for the original and 10x dynamics. The epoch-by-epoch least squares solution is able to provide a more accurate position solution during dynamic periods compared to the Kalman filter solution. As mentioned, this research is focused on tracking performance and improving the position solution is addressed as future work. Improvements in the position solution would include adding

multi-frequency data, cycle slip detection methods and the dynamic model used in the Kalman filter.

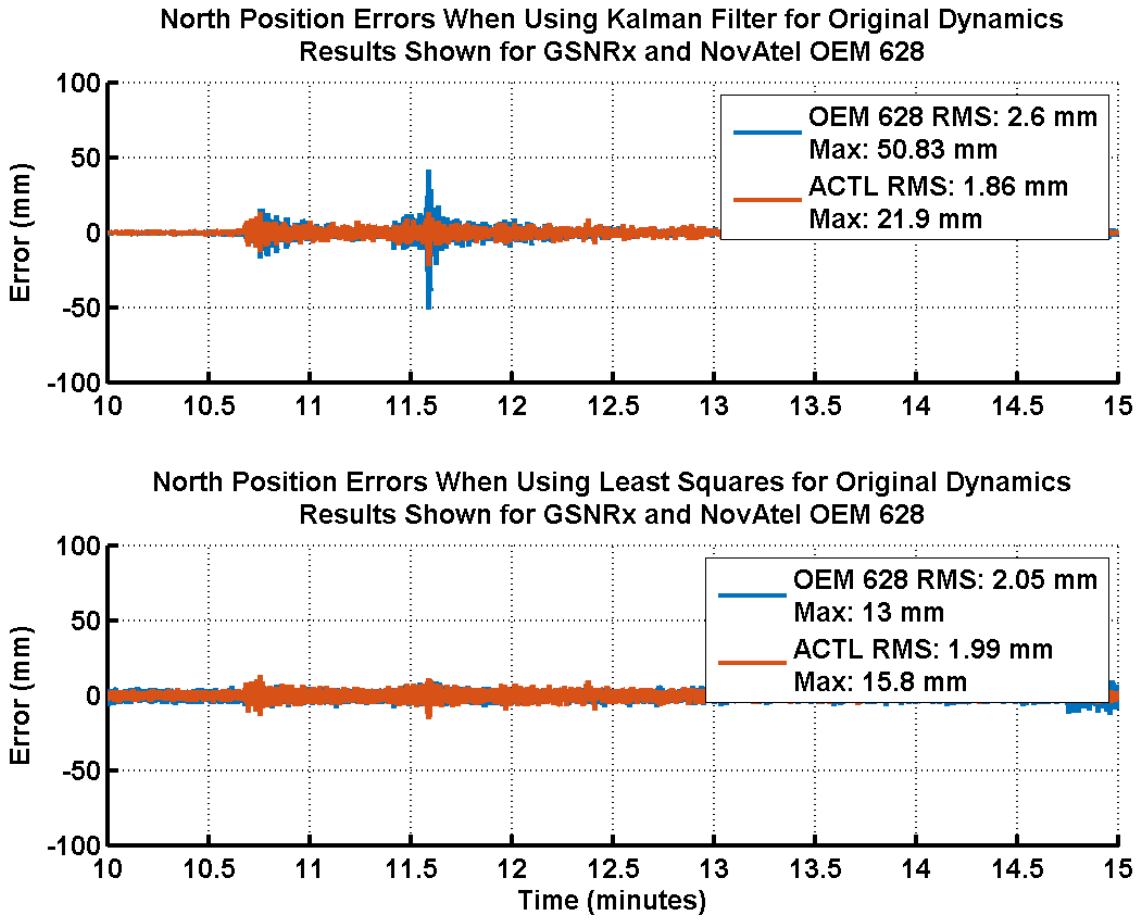

Figure 4.21 Comparison of Least Squares and Kalman Filtering position solution for the Original dynamics

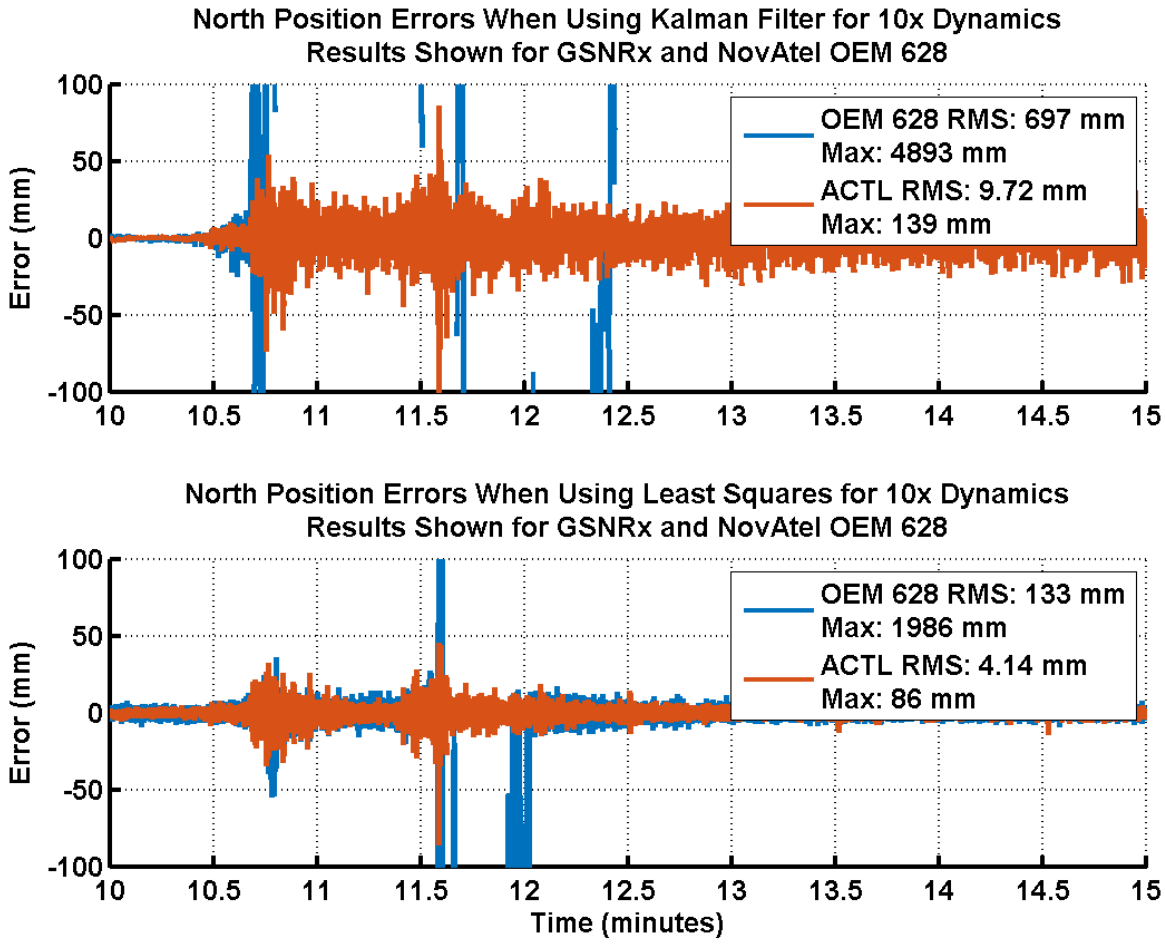

Figure 4.22 Comparison of Least Squares and Kalman Filtering position solution for the 10x dynamics

Figure 4.23 is the estimated position displacement and position errors in the Northing direction for the ACTL and OEM 628 during the peak acceleration period. As can be seen, the position errors for both the ACTL and OEM 628 are sinusoidal. This may be a sign of over filtering as the errors should be random and have noise appearance. Further investigation is required to determine the true cause of these trends.

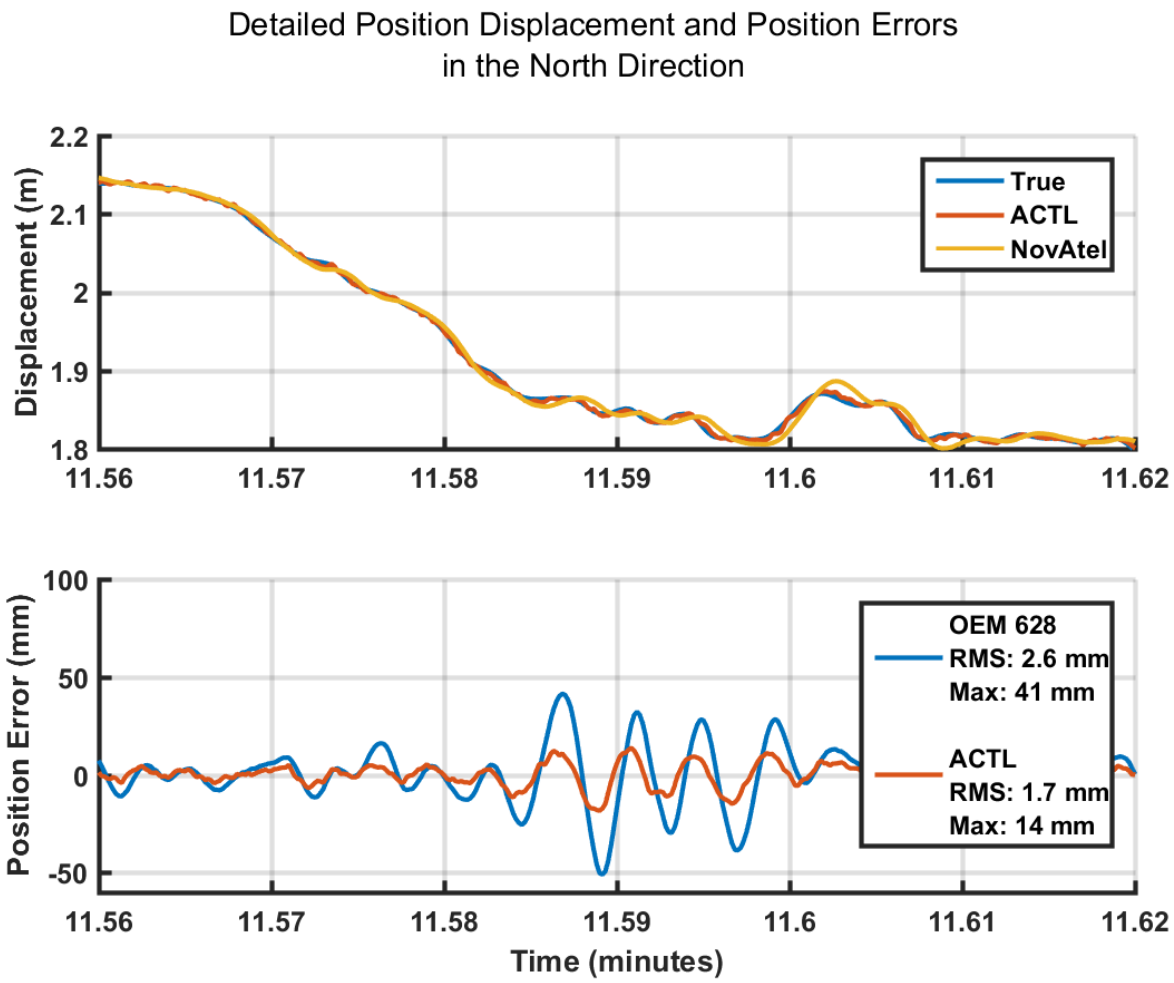

Figure 4.23 Detailed position displacement and position errors in the Northing direction

4.4.2 Tracking Domain Results

The tracking states selected by the ACTL for the original earthquake and 10X dynamics are shown in Figure 4.24 and Figure 4.25, respectively. As can be seen in both figures, the tracking state increases as acceleration increases in order to cope with the dynamic stress experienced by carrier tracking loops. In the non-ideal tracking environment, the

tracking state increases at a slower rate due to the lower thresholds used in the non-ideal tracking branch. The rapid fluctuations in tracking states, more noticeable in Figure 4.25, is caused by the short settling time used. As discussed in Sections 2.3.4 and 3.1, the settling time is not long enough for the next tracking state to converge. A longer settling time could have been selected. Also noticeable in Figure 4.25 is that PRN 18 completely loses lock at 11.5 minutes and regains it at 12.5 minutes. When it regains lock it goes directly to tracking state S_{13} since all other PRNs are already in that state. This is one of the implementation advantages of the ACTL as was discussed in Section 3.2.2.

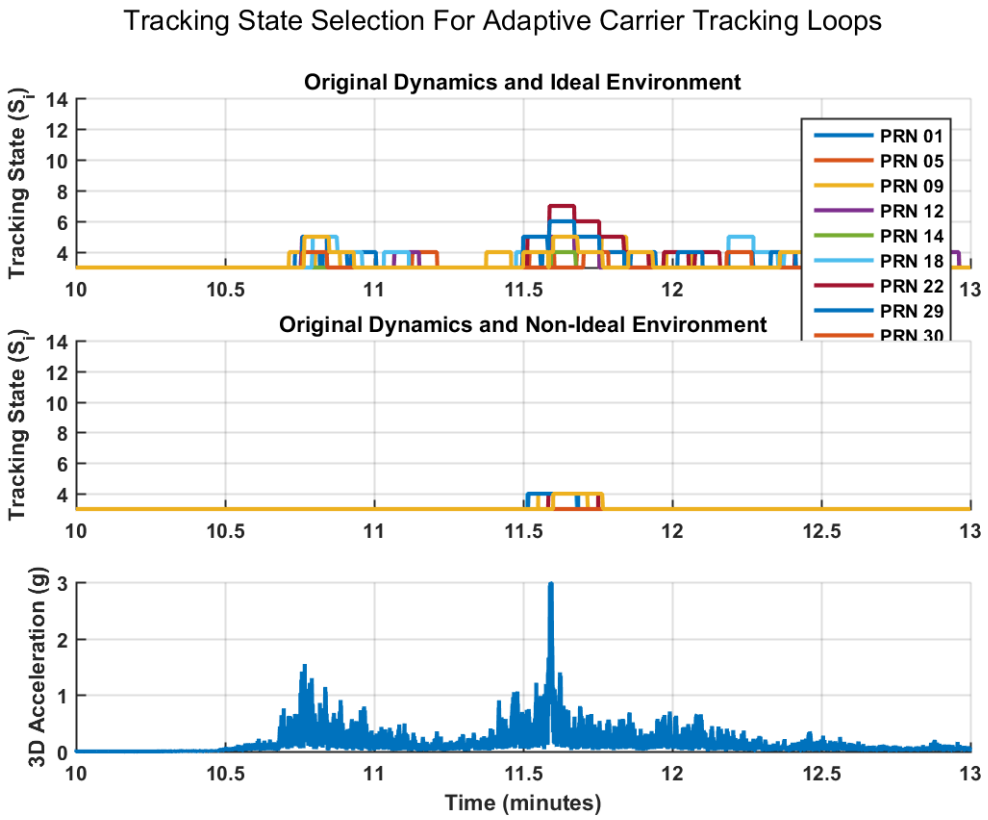

Figure 4.24 Tracking state selection for the original earthquake dynamics in both ideal and non-ideal environments

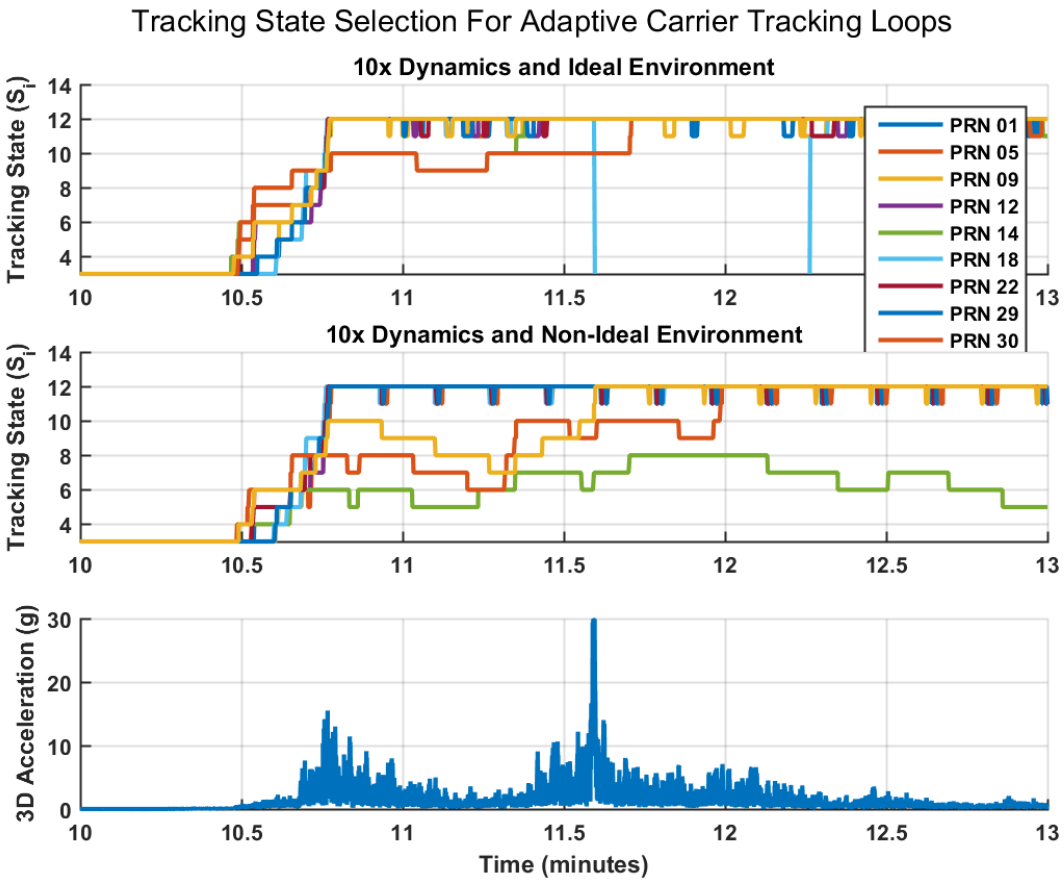

Figure 4.25 Tracking state selection for the 10X earthquake dynamics in both ideal and non-ideal environments

In Figure 4.26 the effect of settling time on adaptive carrier tracking loops is shown. These results are shown for the original earthquake dynamics. The tracking state and PLI are shown for PRNs 5, 18 and 31 and for settling times of 0.0, 0.03 and 0.25 seconds. Ignoring the settling time, settling time of 0, leads to the adaptive tracking loop increasing the tracking state until maximum is reached. This happens because the PLI first drops below threshold. The tracking loop increases the state and at the next loop update there is insufficient time for the new tracking state to attempt recovery, thus the

PLI is still below threshold and the tracking loop increases the tracking state again. This process repeats until the maximum tracking state increases. This situation also occurs when trying to decrease the tracking state. There is an initial drop in PLI when decreasing the tracking state due to the narrowing of the tracking bandwidth. If no settling time is used this drop is detected and the tracking state is increased. To avoid these situations, a settling time must be used. However, if the settling time is long (0.25 seconds), the tracking loop takes longer to adapt to the dynamics causing the PLI to drop further below threshold. As discussed in Section 3.2, 0.03 seconds was used in this research.

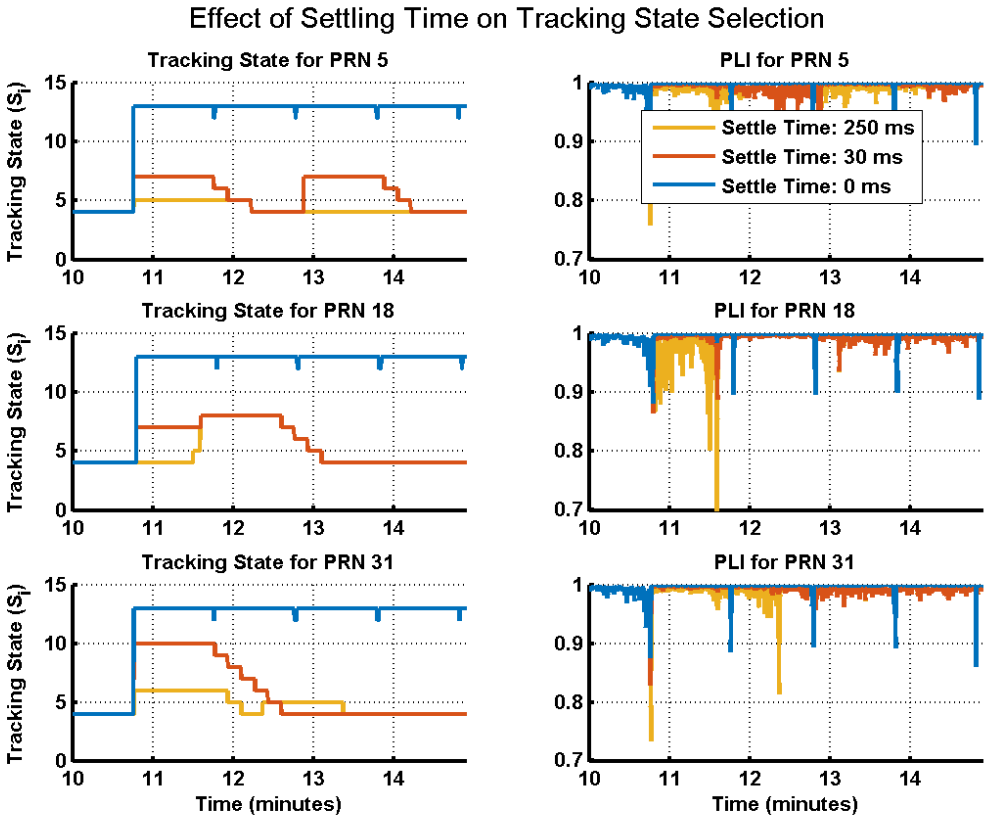

Figure 4.26 Effect of settling time on adaptive carrier tracking loop performance.

4.5 Conclusion/Summary

The performance of the ACTL on tracking performance was evaluated using four different earthquake simulations. It was shown that it is capable of providing reliable tracking performance along with an accurate position solution for both the original earthquake dynamics and the earthquake dynamics scaled by a factor of 10 in an ideal environment. In non-ideal environments the tracking performance were improved by modifying the tracking thresholds and decision logic. The ACTL has comparable performance to the NovAtel OEM 628 during the original earthquake dynamics. However, in the factor of 10 simulations, the ACTL outperformed the OEM 628.

Chapter Five: Effects of Multipath Carrier Phase Tracking

5.1 Multipath Analysis

Using differential processing will eliminate all systematic biases (receiver and satellite clock biases) and mitigate distance dependent errors (atmospheric and orbital errors). Multipath is location dependent and cannot be removed or mitigated through differential processing. Therefore, multipath, is one of the largest error sources affecting a static GNSS receiver when using differential processing. Multipath affects both pseudoranges and carrier phase measurements. This chapter focuses on phase multipath and understanding its effects on phase tracking performance. Understanding how phase multipath affects tracking loop performance is important when designing tracking loops for EMS applications.

5.1.1 Open Sky Test

In an open sky environment, the multipath effects will generally be minimal. Multipath effects will be more visible on satellites with low elevation. For the data set analysed herein, a NovAtel ProPak V3 was used as the reference receiver. The reference receiver location is shown in Figure 5.1, together with the remote unit 500 m away on campus of the University of Calgary. A NovAtel OEM 628 was used as a remote receiver. The observing conditions are assumed to be similar to those encountered for typical EMS applications.

Figure 5.1 Open sky setup. Distance between reference and rover is 500 metres

In Figure 5.2 the PLI, C/N_0 and discriminator output for PRN 20 are shown. PRN 20 has the lowest elevation angle, therefore the effects of multipath will be more visible. As can be seen in the figure, the C/N_0 has a slow cyclic trend. The discriminator trend is harder to detect although there is a slow decrease and increase over time. The above suggests these metrics could be useful in multipath detection and mitigation. In this research, trends in C/N_0 were used, as discussed in Section 3.2. If the C/N_0 is decreasing, it is assumed to be from multipath, therefore lower PLI thresholds are used when adapting the tracking state.

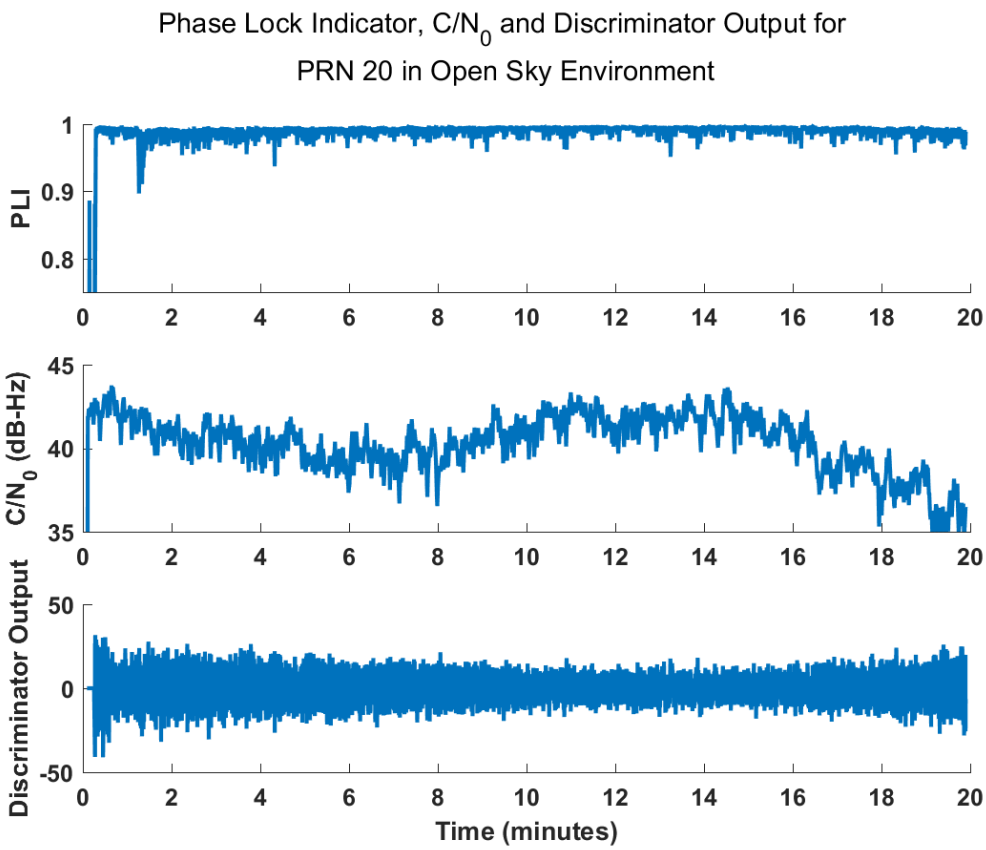

Figure 5.2 PLI, C/N0 and discriminator output for PRN 20 in an open sky environment

The multipath trends are more evident in the phase residuals obtained from the Kalman filter position solution. The double difference phase residuals for the ACTL and OEM 628 are shown in Figure 5.3. In this figure, the cyclic multipath trends are easier to identify and are higher on lower elevation satellites. Applying an elevation mask is a common solution to mitigate the larger multipath trends from low elevation satellites.

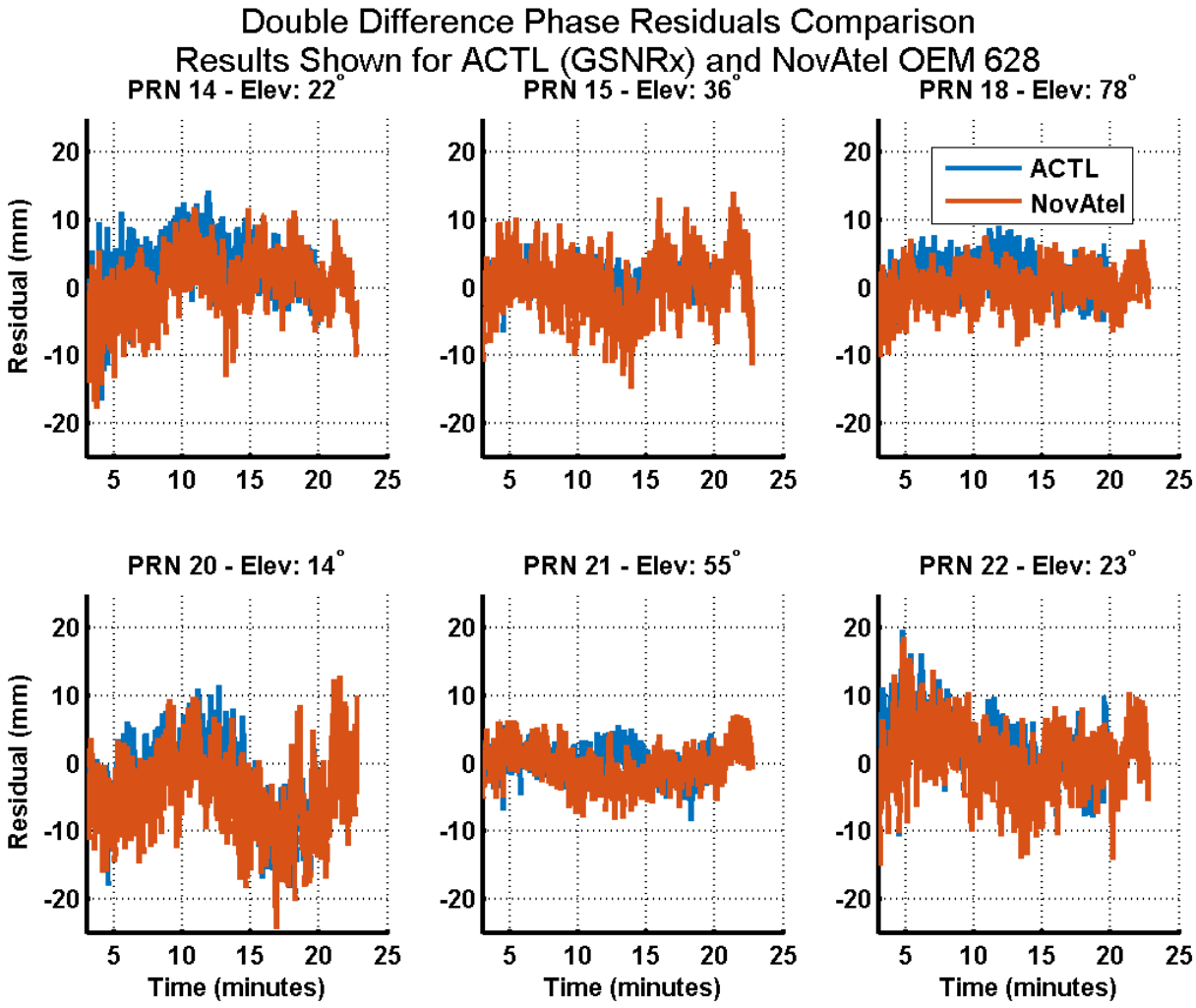

Figure 5.3 Double difference phase residuals in open sky environment. Residuals are shown for both ACTL and OEM 628

The RMS of the double difference phase residuals in Figure 5.3 are provided in Table 5.1. Both the ACTL and OEM 628 have comparable performance. An open sky environment is the expected observing conditions for a receiver being used in EMS.

Figure 5.4 shows the three dimensional position errors for the ACTL and OEM 628 in an open sky environment. Both receivers have comparable performance. These results

show how the cyclic tendencies of multipath can affect the position solution of a static receiver. Understanding how multipath will affect the position solution is important when using a receiver for EMS, especially earthquake detection.

Table 5.1 RMS of double difference phase residuals in open sky environment

PRN	ACTL (GSNRx) RMS (mm)	NovAtel OEM 628 RMS (mm)
14	4.6	5.0
15	4.2	2.2
18	2.8	3.0
20	7.0	6.6
21	2.7	2.3
22	4.9	4.8

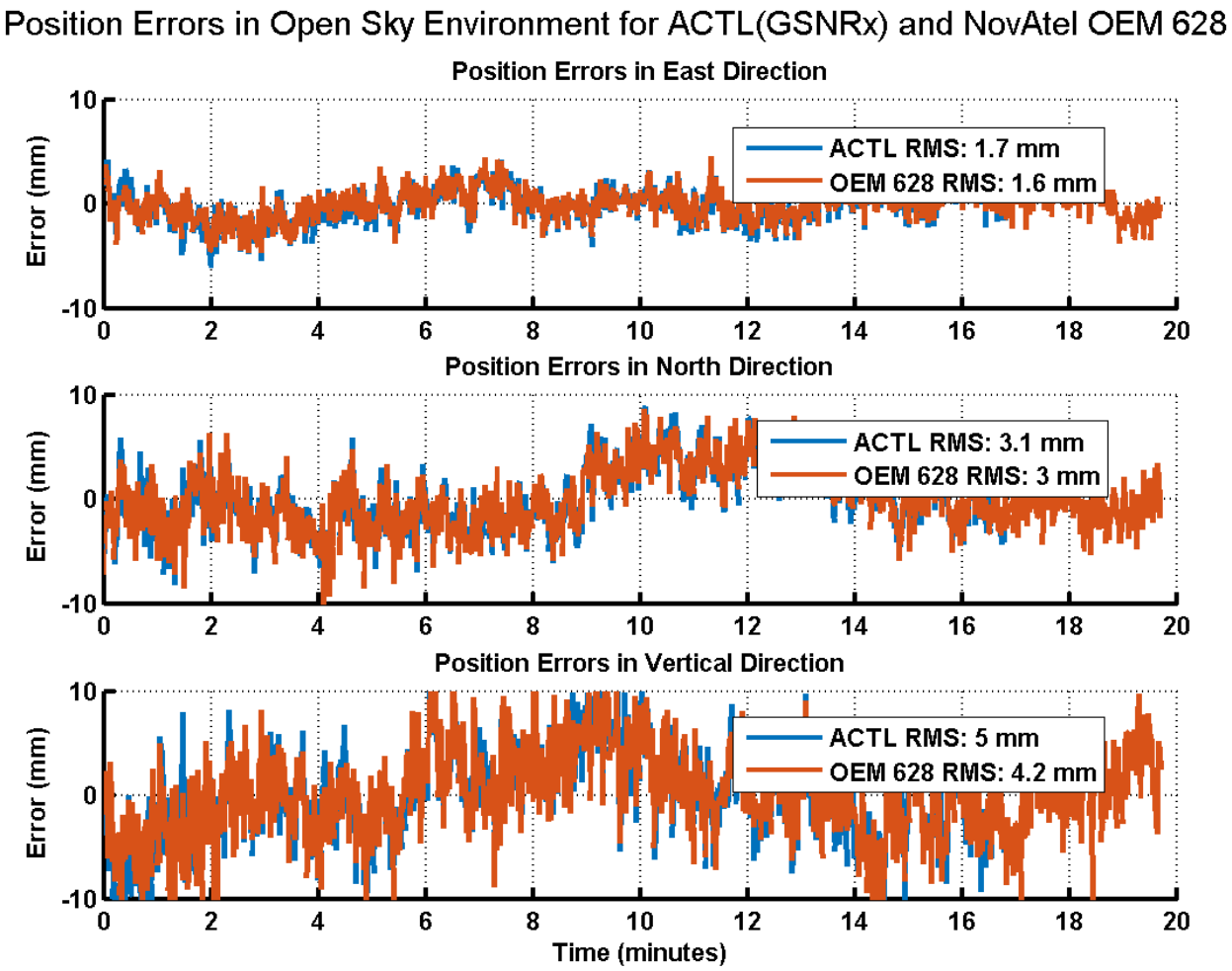

Figure 5.4 Position errors in open sky environment

5.1.2 High Multipath Environment

To assess the effects multipath has on tracking performance, a second data set was collected. In this setup the receiver was placed in a high multipath environment, nearby buildings and trees, as shown in Figure 5.5.

The PLI, tracking state and C/N_0 values for the ACTL are shown in Figure 5.6. In this figure the multipath trends are more evident in the C/N_0 and PLI values. The C/N_0 values ascend and descend in a cyclic manner. When the C/N_0 decreases, it is detected

by the ACTL, as discussed in Section 3.2 and lower thresholds are used when changing the tracking state.

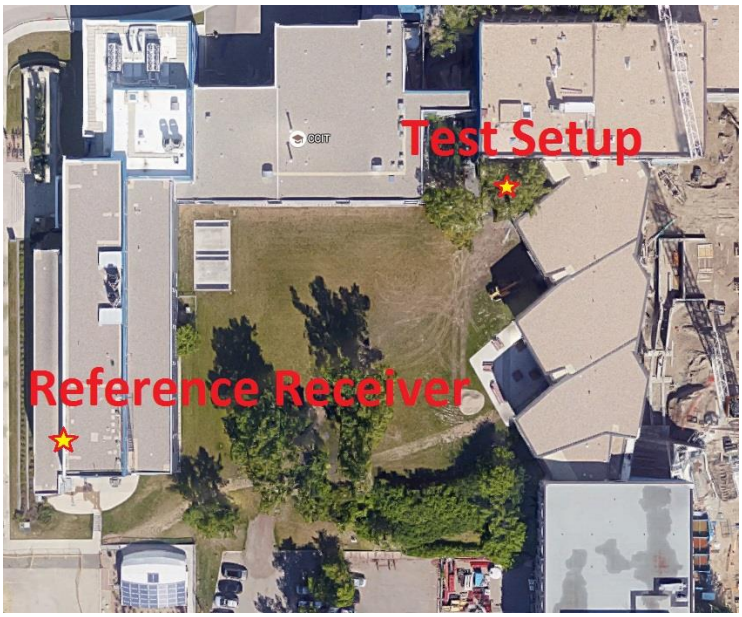

Figure 5.5 High mutipath setup. Reference-remote distance is 80 m

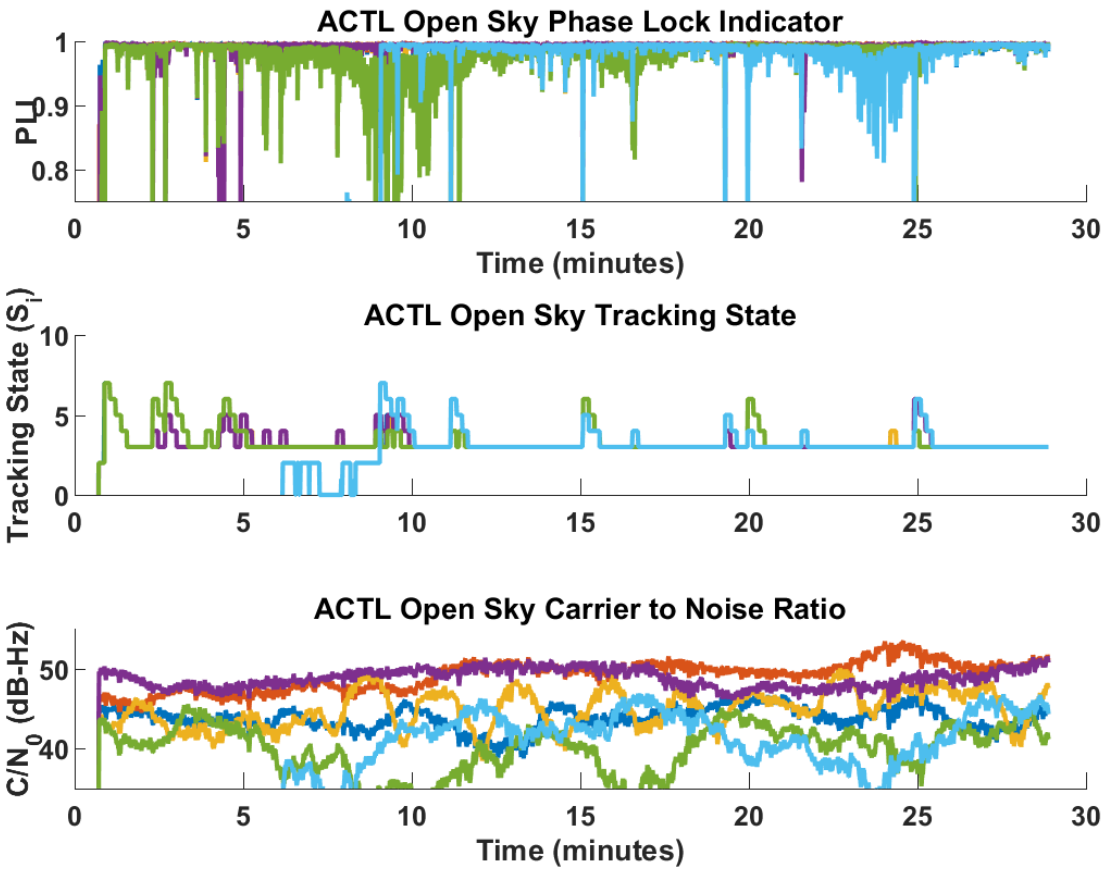

Figure 5.6 The PLI, Tracking State and C/N_0 values for the ACTL in a high multipath environment

In Figure 5.7 the PLI, C/N_0 and discriminator output for the ACTL with a carrier tracking loop using a fixed tracking bandwidth of 15 Hz and integration time of 10 ms are shown for PRN 24, which has the lowest elevation angle and therefore higher multipath effects. There is no distinguishable difference in performance (discriminator output) between the two receivers used. This is expected as tracking loop parameters have little effect on multipath performance. Due to the relatively low frequency of multipath effects, the

effects will pass through the PLLs regardless of the loop filter used. This is why the NovAtel OEM628 and ACTL have similar carrier phase multipath performance.

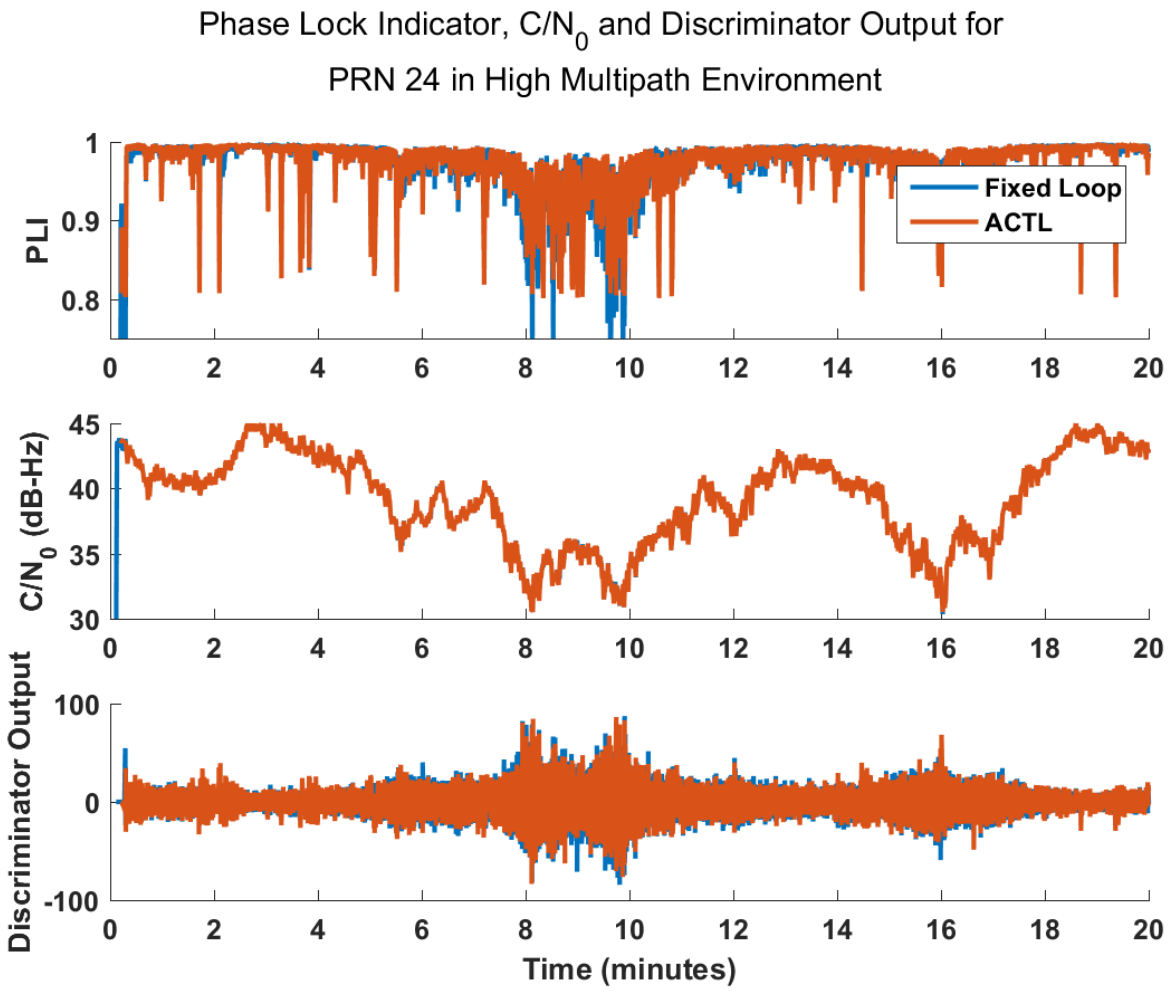

Figure 5.7 Phase lock indicator, C/N0 and discriminator output for PRN 24 in a high multipath environment. Results are shown for a fixed 15 Hz bandwidth PLL and the ACTL

The double difference phase residuals for ACTL and NovAtel OEM 628 are shown in Figure 5.8. The cyclic nature of multipath is evident when looking at the phase residuals. In Table 5.2 the RMS of the residuals of Figure 5.8 are shown. Evident in this

figure is how the residuals are drifting from zero. It was expected the residuals would show cyclic trends similar to the residuals in Figure 5.3 with larger amplitudes. This drift is likely caused from an incorrect ambiguity fix which is a result of poor satellite visibility and satellite geometry due to the experiment location. Multiple data processing options were used to try and overcome this issue. This situation could be mitigated with longer observation time, using measurements on multiple frequencies or multi-constellation data.

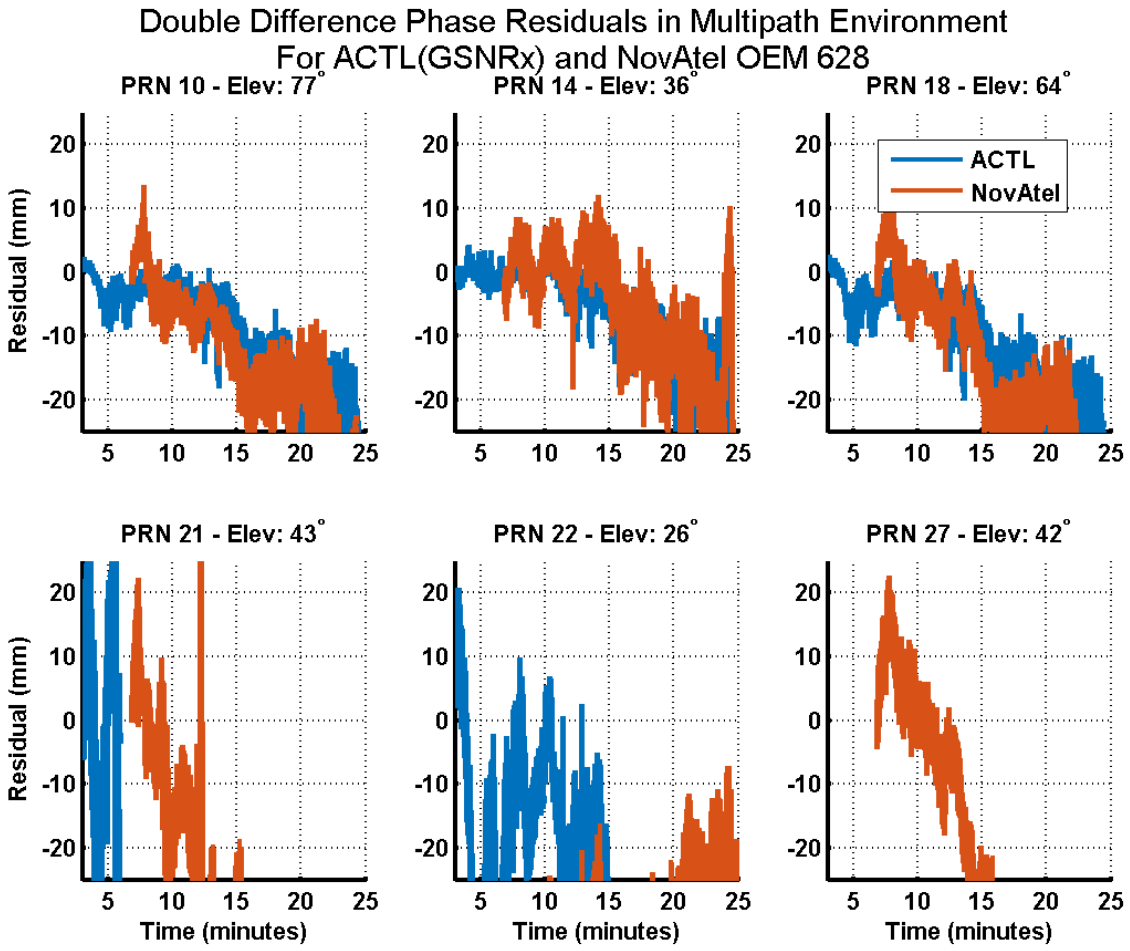

Figure 5.8 Double difference phase residuals for the ACTL and NovAtel OEM 628 in a high multipath environment

Table 5.2 RMS of double difference phase residuals in open sky environment

PRN	ACTL (GSNRx) RMS (mm)	NovAtel OEM 628 RMS (mm)
10	14.1	20.9
14	11.2	14.3
18	14.8	25.9
21	34.4	39.1
22	14.3	27.3
27	N/A	66.8

5.2 Conclusion/Summary

In this chapter the effects of multipath on carrier tracking loop performance was analyzed using two tests, one with low multipath and another with high multipath. Using the PLI, discriminator output and C/N_0 values can be useful tools in detecting multipath. The performance of the ACTL was compared to both a fixed bandwidth tracking loop and NovAtel OEM 628.

Chapter Six: Conclusion and Recommendations

6.1 Conclusion

The performance of GNSS carrier tracking loops for EEWMS applications was evaluated. Using the software defined receiver GSNRx, tracking bandwidths of 5, 10, 15, 20, 30, 40 and 50 Hz with integration times of 1, 5 and 10 ms were tested. Longer integration times and narrow tracking bandwidths are best when in static mode and for earthquake detection due to the reduction of thermal noise. When the tracking loops are under dynamic stress wider bandwidths and shorter integration times might be required. There is an evident optimal tracking bandwidth of 20 Hz and 10 ms integration time is best suited for reducing RMS and maximum errors during an earthquake event. As a consequence, an adaptive carrier tracking loop was designed and tested. Using PLI and C/N_0 values, an approach was shown to overcome the design contradiction of high accuracy and dynamic stress tolerance requirements. The proposed adaptive carrier tracking loop was capable of providing low noise before the start of an earthquake while proving accurate and reliable motion records during the event. The adaptive carrier tracking loop was tested in four different environments. In each environment comparisons were made with an high end hardware geodetic receiver.

- In an ideal environment, both the ACTL method and OEM 628 receiver had comparable performance. During the static period before the earthquake, the OEM 628 had marginally better noise performance, with RMS error differences less than 0.3 mm in each of the three components. During the earthquake the ACTL had marginally better noise performance, with RMS error differences of

less than 0.6 mm in each component; The ACTL method was able to reduce the maximum position errors by 57%, 70% and 19% in the East, North and Vertical components, respectively.

- During the static period in the non-ideal environment, the ACTL had better noise performance, with a 50% improvement in all three directions. During the earthquake period, the ACTL had a 20% improvement over the OEM 628. However, it was found that different thresholds could have been used when adapting the tracking loop in the non-ideal environment. This suggests that further minor improvements could be achieved. The ACTL had a 60% improvement in reducing maximum errors in the East and North component.
- In the ideal environment with 10x dynamics, the ACTL was able to track for the entire high dynamic period, with the OEM 628 unit losing lock after 11.5 minutes.
- In the non-ideal environment with 10x dynamics the OEM 628 lost lock almost immediately after high acceleration was injected (10.5 minutes) while the ACTL was able to track for the full period; the latter resulted however in cycle slips at 10.3 minutes and no fixed position solution could be computed.

The effect of multipath on carrier tracking loop performance was also investigated. Multipath remains one of the largest error sources affecting the carrier phase performance of a receiver in EMS. Tracking loop parameters have little effect on multipath performance due to the short frequency of multipath effects. This is why the ACTL and OEM 628 have similar performance in both open sky and high multipath environments.

6.2 Recommendations

Suggestions for future work are as follows:

1. In this work only the performance of the GPS L1 signal was analyzed. Tracking performance of newer GNSS frequencies (L2 and L5) should also be analyzed and considered when designing a GNSS receiver for EMS. With the addition of pilot channels and longer chipping rates, modern signals use different discriminators and tracking strategies compared to the legacy GPS L1. Multi-constellation performance should also be considered.
2. With the addition of multi-frequency and multi-constellation data, the position solution could be improved. Using multiple frequencies and constellations improves the ambiguity resolution process and cycle slip detection. Also, adding a differential position solution to GSNRx should be done. With the high accuracy of a differential solution available, methods of detecting the earthquake could be implemented. Once an earthquake is detected, the tracking strategy used by the ACTL could be improved. Moreover, once the start of an earthquake is detected the tracking bandwidth can be increased for the impending dynamics.
3. Incorporating an IMU with a GNSS receiver could further improve performance. An IMU directly measures acceleration, which is ideal for earthquake detection.
4. Carrier phase multipath remains one of the largest error source for a static receiver when using differential methods. Improving multipath mitigation and estimation techniques would be beneficial for a GNSS receiver, most important for earthquake detection.

References

Babu, R. and J. Wang (2009). “Ultra-tight GPS/INS/PL integration: a system concept and performance analysis”, *GPS Solutions*, vol 13, no 1, pp 75–82.

Betz, J. W (2015) *Engineering Satellite-Based Navigation and Timing: Global Navigation Satellite Systems, Signals and Receivers*, John Wiley & Sons, Toronto ON

Braash, M. and A.J. Van Dierendonck (1999) “GPS Receiver Architectures and Measurements”, in *Proceedings of the IEEE,* vol 87, no 1, pp 48-64

Crowell, B. W., Y. Bock and D. Melgar (2012). “Real-time inversion of GPS data for finite fault modeling and rapid hazard assessment”, in Geophysical Research Letters, vol 39, May 2015

Crowell, B. W., Y. Bock and M.B. Squibb (2009). “Demonstration of Earthquake Early Warning Using Total Displacement Waveforms from Real-time GPS Networks”, in Seismological Research Letters, vol 80, pp772–782

Gao, G. and G. Lachapelle (2008) “A novel architecture for ultra-tight HSGPS-INS integration”, in Journal of Global Positioning Systems, vol 7, no 1, pp 46-41

Genrich, J. F. and Y. Bock (2006) “Instantaneous geodetic positioning with 10-50 Hz GPS measurements: Noise characteristics and implications for monitoring networks”, in Journal of Geophysical Research, vol 111, pp 1-12

Häberling, S., M. Rothacher, Y. Zhang, J.F. Clinton and A. Geiger (2015) “Assessment of high-rate GPS using a single-axis shake table” in Journal of Geodesy, vol 89, pp 697–709

Haberling, S. (2015). *Theoretical and Practical Aspects of High-Rate GNSS Geodetic Observations*, PhD Thesis, ETH Zurich, Switzerland

Kamel, A. M., D. Borio, J. Nielsen and G. Lachapelle (2011) “Interference mitigation for highly dynamic GPS receivers using intelligent tracking loops”, in *Proceedings of the International Technical Meeting of the Institute of Navigation*, 24-26 January, San Diego CA

Kazemi, P., C. O’Driscoll and G. Lachapelle (2009) “Digital Phase Lock Loop With Frequency Rate Feedback” in *Proceedings of ION GNSS 2009,* 22-25 September, Savannah GA

Kazemi, P. (2010) *Development of New Filter and Tracking Schemes for Weak GPS Signal Tracking,* PhD Thesis, Department of Geomatics Engineering, University of Calgary, Canada, pp 26-54

Lachapelle, G., A. Morrison, R. Ong (2010) “STEALTH™ A GNSS-Based Advanced Device to Train Canadian Olympic Skiers”, in *Geomatica,* vol 64, no 3, pp. 327-335.

Lian, P., G. Lachapelle, and C. Ma (2005) “Improving tracking performance of PLL in high dynamics applications”. in *Proceedings of the International Technical Meeting of the Institute of Navigation*, 24-26 January, San Diego CA

Lin, T., G. Lachapelle and L. Fortes (2014) “GNSS Solutions: How Do Modern GNSS Signal Processing Techniques Deal with Equatorial Ionosphere Scintillation” Inside GNSS, (January/February), 26-34

Lin, T., M. Martin, A. Broumandan, G. Lachapelle (2012) “Demonstration of a high sensitivity GNSS software receiver for indoor positioning”, in *Advances in Space Research*, vol 51, pp. 1035-1045

Mongrédien, M., G. Lachapelle and M.E. Cannon (2006) “Testing GPS L5 Acquisition and Tracking Algorithms Using a Hardware Simulator”, Proceedings of GNSS06 (Forth Worth, 26-29 Sep, Session C6), The Institute of Navigation, 13 pages.

Muthuraman, K., and D. Borio (2010) C/N_0 Estimation for Modernized GNSS Signals: Theoretical Bounds and a Novel Iterative Estimator. NAVIGATION, Journal of The Institute of Navigation, Vol. 57, No. 4, Winter 2010, 309-323.

National Research Institute for Earth Science and Disaster Prevention 2015, *Strong Motion Seismograph Networks (K-NET, KiK-net),* http://www.kyoshin.bosai.go.jp/ , last accessed October 2 2015.

Ong, R. (2010) Reliability of Combined GPS/GLONASS Ambiguity Resolution, MSc Thesis, published as Report No. 20311, Department of Geomatics Engineering, The University of Calgary, Canada

Petovello, M., and G. Lachapelle (2006) "Comparison of Vector-Based Software Receiver Implementations with Application to Ultra-Tight GPS/INS Integration," ION GNSS 2006, Fort Worth TX, 26-29 September 2006 pp. 26–29

Petovello, M.G., C. O'Driscoll, G. Lachapelle, D. Borio, H. Murtaza (2008c) “Architecture and Benefits of an Advanced GNSS Software Receiver”, International Symposium on GPS/GNSS 2008, November 11-14, Tokyo, Japan, 11 pages

Ray, J.K (2000), *Mitigation of GPS Code and Carrier Phase Multipath Effects Using a Multi-Antenna System,* PhD Thesis, Department of Geomatics Engineering, University of Calgary, Canada, pp 56-92

Ray, J.K., M.E. Cannon and P. Fenton (2000) “Mitigation of Carrier Phase Multipath Effects Using Multiple Closely-Spaced Antennas”, in *NAVIGATION, Journal of The Institute of Navigation*, vol 46, no 3, pp 193-201

SeismoSoft.com, Earthquake Engineering Software Solutions 2015. Available from: http://www.seismosoft.com/seismospect, last accessed October 2, 2015.

Simon, D. and H. El-Sherief (1995) “Fuzzy logic for digital phase-locked loop filter design. Fuzzy Systems”, in *IEEE Transactions on Fuzzy Systems*, vol 3, no 2, pp 211–218.

Stephens, S.A and J.B Thomas (1995) “Controlled-Root Formulation for Digital Phase Locked Loops”, in *IEEE Transactions on Aerospace and Electronic Systems*, vol 31, no 1, pp 78-95

Tong, M., G.Q. Wang and G.C. Lee (2005) “Time Derivative of Earthquake Acceleration”, in *Earthquake Engineering and Engineering Vibration,* vol 4, no 1, pp 1-16

Van Dierendonck, A. J. (1995) GPS Receivers. B. Parkinson and J. J. Spilker, Jr., eds., Global Positioning System: Theory and Applications, volume I, chapter 8. American Institute of Aeronautics and Astronautics, Inc., Washington D.C., USA

Wang, X. and S. Song (2015). “Design and realization of adaptive tracking loops for GPS receiver”, in *Aircraft Engineering and Aerospace Technology*, vol 87, no 4, pp 368–375

Ward, P. W. (1998). Performance Comparison between FLL, PLL and a Novel FLL-Assisted-PLL Carrier Tracking Loop Under RF Interference Conditions. In Proceedings of ION GNSS (pp. 783–795).

Ward, P.W., J.W. Betz and C.J. Hegarty (2006) Understanding GPS: Principles and Applications, K. D. Kaplan and C. J. Hegarty, ed., Understanding GPS Principles and Applications, Chapter 5, Artech House

Watson, R., M. Petovello, G. Lachapelle and R. Klukas (2008). “Impact of Oscillator Errors on IMU-Aided GPS Tracking Loop Performance” in *Proceedings of ENC-GNSS 2007*, Geneva Switzerland, 29-31 May 2007

Wright, T. J., N. Houlié, M. Hildyard and T. Iwabuchi (2012). “Real-time, reliable magnitudes for large earthquakes from 1 Hz GPS precise point positioning: The 2011 Tohoku-Oki (Japan) earthquake” in *Geophysical Research Letters*, vol 39, no 12, pp 1-5